2014

Coarsegrained modeling and electrostatics of phospholipid monolayers

Sweta Vangaveti
Iowa State University

Coarsegrained modeling and electrostatics of phospholipid monolayers

by

Sweta Vangaveti

A dissertation submitted to the graduate faculty

in partial fulfillment of the requirements for the degree of

DOCTOR OF PHILOSOPHY

Major: Bioinformatics and Computational Biology

Program of Study Committee:

Alex Travesset, Major Professor

Robert Jernigan

Xueyu Song

Sanjeevi Sivasankar

Marzia Rosati

Iowa State University

Ames, Iowa

2014

DEDICATION

I would like to dedicate this thesis to friends and family for their continued love and support.

TABLE OF CONTENTS

LIST OF TABLES

LIST OF FIGURES

ACKNOWLEDGEMENTS

I would like to take this opportunity to express my thanks to those who helped me with various aspects of conducting research and the writing of this thesis. First and foremost, Dr.Alex Travesset for his constant guidance, patience and support throughout this research and the writing of this thesis. I am grateful to my committee members for their time and encouragement. I would additionally like to thank Dr. Monica H Lamm for providing with the computer facilities required for the completion of this work. Lastly I would like to express my gratitude to my family and friends without whose love and support this work would be difficult to accomplish.

ABSTRACT

The cell membrane, composed primarily of lipids and proteins serves to protect the cell and regulate the traffic of signals and molecules in and out of the cell. This regulation is carried out by a complex network of processes that occur by means of interactions of the membrane components with their surrounding environment. Most of the trafficking functions of the membrane are carried out via micro domains formed within the membrane. These microdomains compartmentalize proteins and lipids that are necessary for carrying out a particular cellular function.

PIP2 (phosphatidylinositol (4,5) bisphosphate) is a phospholipid present in minute quantities ($\approx 0.1\%$) in the cell membrane but involved in a multitude of signaling processes. PIP2 enriched sites are found in the inner leaflet of the cell membrane. The formation of these microdomains serves as a trigger or a starting point of various signaling pathways. Several experiments have identified that the electrostatic interaction of divalent ions (primarily Ca^2+) or proteins with membranes induces clustering of PIP2s. However, there is still a debate in the scientific community regarding the size, time and duration of existence of these microdomains and the underlying mechanism that leads to their formation.

This study is focused on understanding the divalent ion induced clustering of PIP2s, by modeling and analyzing the interactions of charged lipid monolayers with an electrolyte. A simplified single particle model of the phospholipid is first used to understand the properties of the system. It is shown that electrostatic interactions if properly accounted for, are sufficient to explain the behavior of such systems (independent of experimentally determined ion-lipid association constants). Extensive molecular dynamic simulations are then employed to study the interaction of a coarse grained model of a phospholipid monolayer (of phosphatidic acid (PA) , phosphatidyl serine (PS) and PIP2) with electrolytes. The results indicate that the two regions in the system the Stern layer and the diffuse layer can be treated independently within the framework of the

model. This grants flexibility in the amount of detail necessary to describe each layer. In mixed lipid layers of PIP2 and PS, divalent ions exhibit preferential binding to PIP2 clusters. The internal energy values show that a clustered PIP2 configuration in PIP2-PS monolayers is more stable than the corresponding dispersed configuration. The results suggest the inherent presence of PIP2 clusters over a wide range of divalent ion concentrations.

CHAPTER 1. INTRODUCTION

1.1 Introduction

The 'cell theory' defines cells as the basic structural and functional unit of life. Cells typically consist of several subunits or components, called organelles, many of which (including the cell itself), are surrounded by distinct membranes which separate them from their surroundings. These membranes have diverse structure, composition and physical and chemical properties which vary from cell to cell and from organism to organism.

Cell Membranes or plasma membranes form the boundary that separates one cell from another. However these are not merely passive boundaries but active sites for various cellular functions. They participate in a variety of functions ranging from simple ones like maintaining and regulating ion levels inside and outside the cell, to complex interactions with proteins that carry chemical messages in and out of the cell via a process called signal transduction. These membranes are thus vital to cell survival and a comprehensive understanding of membranes and their mechanisms is important for understanding the functioning of cells in general.

Cell membranes have been the subject of numerous studies and increasing evidence about their specific role in carrying out cellular functions has been revealed. Fatal diseases like cancer are associated with malfunctioning of the membrane components [1]. Cell membrane components are known to actively participate in all processes that involve the communication of the cell with its external environment, from triggering cell division, to interaction with important proteins, to preventing a viral infection via antibodies or surface receptors, to signaling cell death [2].

All cellular components work cooperatively to maintain cell homeostasis (equilibrium) which is the basis of cell survival. It is hence essential to understand the interactions between these

cellular components to be able to comprehend different cellular mechanisms. The first logical step would thus be to identify the properties and functions of the cell's individual components – macromolecules like lipids, proteins, DNA, RNA etc. The experimental and computational methods to study the properties of membranes and its constituents are less predictive as compared to those used to study macromolecules like DNA and Proteins. These relatively less explored membrane components – lipids, are the focus of this study.

Owing to their lipids which are mostly acids, cell membranes are negatively charged. The location and concentration of charges plays a significant role in many membrane functions. A number of these functions are carried out primarily by the interaction of membrane constituents with proteins, charged ions and other membranes in its vicinity. Keeping this aspect in mind, this study elaborates the electrostatic interaction of membrane components - phospholipids, with ions.

1.2 Thesis Organization

The first chapter gives some background about cell membranes and its functions, followed by the motivation behind the study and the challenges encountered. Each subsequent chapter is a paper. The second chapter is a paper that analyzes the electrostatic interactions of ions with the membrane using a simple model (a single charge) of the lipid (published). The third chapter extends the analysis further by studying the effects of changing different parameters in the lipid-electrolyte system using molecular dynamic simulations (published). The fourth chapter is a paper that explores the effect of lipid headgroup structure and the lipid composition on the ion distribution (submitted). Finally a comprehensive summary and discussion about the results from the entire study are presented in the last chapter.

1.3 Cell Membrane : Structure and composition

The existence of cell membranes was first proposed in the 1880s to account for the osmotic behavior of plant cells. A few decades later cell membranes were recognized as an envelope vital to cell survival. A bilayer structure for the membranes was observed by Grendel and Gorter

[3], and its association with proteins was confirmed by Danielli and Davson [4]. The most popular model for cell membranes, the fluid mosaic model, was later proposed by Singer and Nicolson in 1972 [5]. They described a cell membrane as a two dimensional viscous fluid made of phospholipid bilayers with randomly distributed proteins both of which are free to diffuse. However, our understanding of the structure of the cell membrane is constantly evolving and the fluid mosaic model currently used differs considerably from the original model. In this new model, membranes are described as two dimensional fluid-fluid systems with considerable lateral organization, as opposed to a homogenous distribution of lipids and proteins proposed in the earlier model. Membrane proteins, we know now, are embedded in, associated with the surface of, or in some cases even covalently bonded to, the membrane [6]. In these lipid bilayers, one of the faces is exposed to the extracellular environment and is called the outer leaflet, while the one which is oriented to the inside of the cell is called the inner leaflet. Cell membranes are asymmetric i.e. the lipid-protein composition of the two leaflets is remarkably different (See Fig. fig:lipid and membrane). This asymmetry plays an important role in the proper functioning of the membrane. Cell membranes are composed of three major classes of molecules: lipids, proteins and sterols. The percentage of each component varies depending on the function and the intracellular and intercellular environment of the cells, e.g. the lipid to protein ratio in myelin sheets present in nerve cell endings is 4:1 (where the membranes function as insulators) while for bacterial cell membranes it is about 1:4. Typically cell membrane thickness is of the order of 6-10 nm, and the lipid density in the cell membranes is of the order of 1.6×10^6 lipids per μm^2. [7].

1.3.1 Lipids

Cellular lipids exhibit a lot of variety in structure and function; however the basic framework is the same. Each lipid consists of a hydrophilic or polar end (referred to as the head group) and a hydrophobic or non-polar end (referred to as the tail). The tail and the head group are both attached to a parent compound (referred to as the backbone). This structure is responsible for the amphiphatic property of the lipids which enables them to cluster together in an aqueous

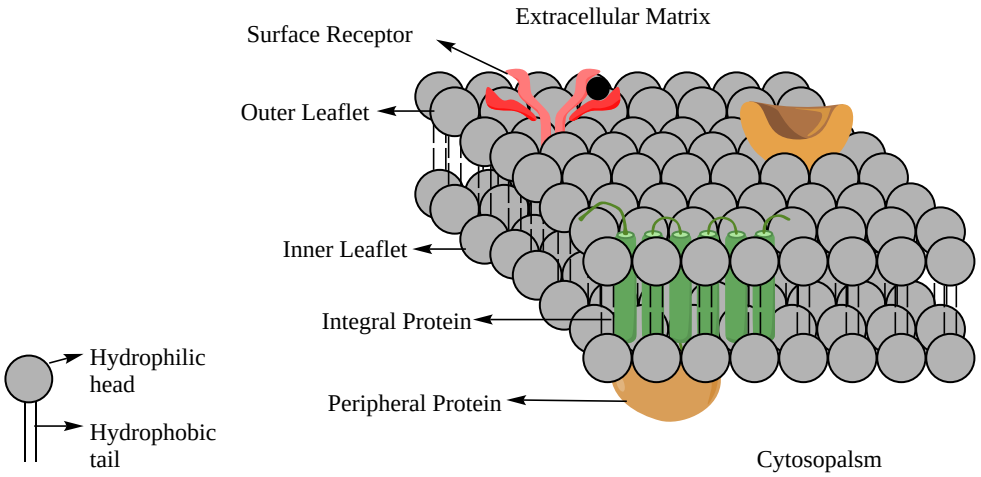

(a) A typical lipid (b) Cell Membrane

Figure 1.1 Diagrammatic representation of an individual lipid and cell membrane

environment forming a bimolecular layer structure. The hydrophobic tails form the inner core while the polar head groups interact with the aqueous environment. (Fig. 1.1).

The tails consist of two hydrocarbon acyl or fatty acid chains, usually with an even number of carbon atoms. These chains may be saturated or unsaturated but are usually linear. The double bonds however introduce a bend in the carbon chains, the presence of which disrupt close packing and affects fluidity of the membrane. The head groups are generally alcohols like serine, choline etc. The backbone usually consists of an alcohol and a phosphate group. Based on their backbone and head groups, membrane lipids can be classified into three major categories: – glycerophospholipids, sphingolipids and glycolipids.[8]

Glycerophospholipids or phosphoglycerides are the most abundant membrane lipids. These lipids contain a glycerol phosphate backbone, were two of the hydroxyl groups in glycerol are attached to the hydrocarbon chains via an ester bond, while the third one is linked to a phosphate which carries the polar head group as shown in Fig. 1.2(a). The head group varies from simple hydrogen atom to complex alcohols like glycerol, choline, serine, ethanolamine and inositols. The simplest phosphoglyceride with hydrogen as the head group is called phosphatidic acid and other phosphoglycerides with a head group instead of hydrogen are named accordingly as phosphatidylcholine, phosphatidylserine and so on. The phosphoinotides which have an

inositol ring with varying number and position of hydroxyl groups are particularly interesting because they make up as small as 0.02% of the membrane lipids but play a very important role in signaling pathways. Phosphatidylcholine is generally found on the outer leaflet while the other phosphoglycerides are generally present in the inner leaflet of the membrane. The relative percentage of each of these lipids is tightly regulated since their concentration affects and controls several membrane functions.

Sphingophospholipids are a class of lipids similar to glycerophospholipids with the phosphate group linked to sphingosine instead of glycerol as the backbone. Sphingomyelin is the only known sphingolipid in which one fatty acid chain is linked to the amine group in sphingosine via an amide bond, while the other fatty acid chain comes from sphingosine itself. The head group in sphingomyelin is a choline group. (Fig. 1.2(b))

Glycolipids are sugar containing lipids. The backbone group in these lipids is also sphingosine, the difference being that the alcohol head group is replaced by a single or multiple sugar residues (Fig. 1.2(c)). Common examples of glycolipids are cerebrosides (with a single glucose molecule) and gangliosides (with multiple sugar residues).

1.3.2 Proteins

Proteins are also an important and integral part of the cell membrane. While lipids provide the basic framework for the membranes, imparting structure and helping in carrying out some of its functions, proteins are primarily concerned with the functionality of the membranes. Some proteins diffuse through the membrane as readily as the surrounding lipids while others are anchored to their positions. The protein content and type vary depending on the function that the membrane or the cell is programmed to perform. Membrane proteins, depending on their location with respect to the membrane are broadly classified into two main categories – Integral and Peripheral proteins.

Integral Proteins are embedded in the membrane, and some even span the entire membrane thickness several times. These proteins, like the lipids, are amphiphatic; the hydrophobic part is bound to the membrane via non-polar interactions with the acyl chains of the lipid, while the hydrophilic part surfaces on one or both sides of the membrane. Their extraction requires the

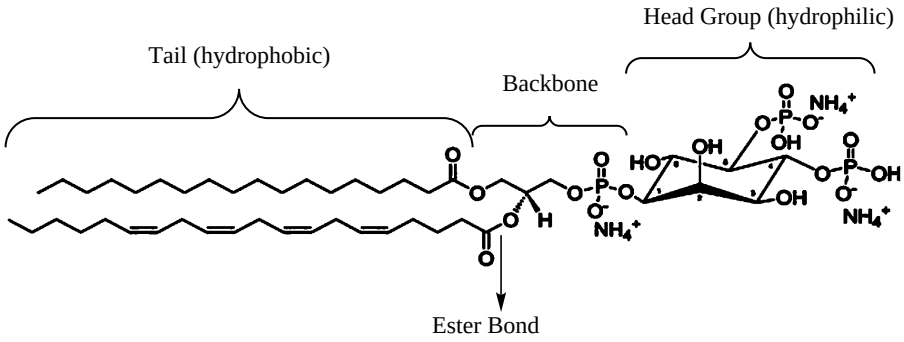

(a) Phosphoglyceride

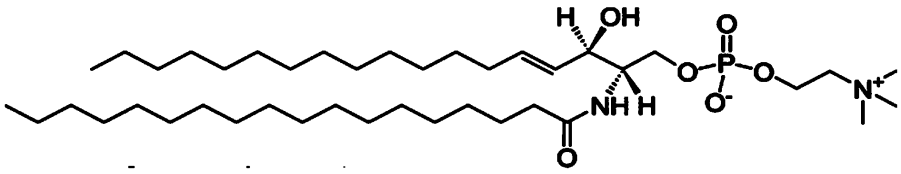

(b) Sphingomyelin

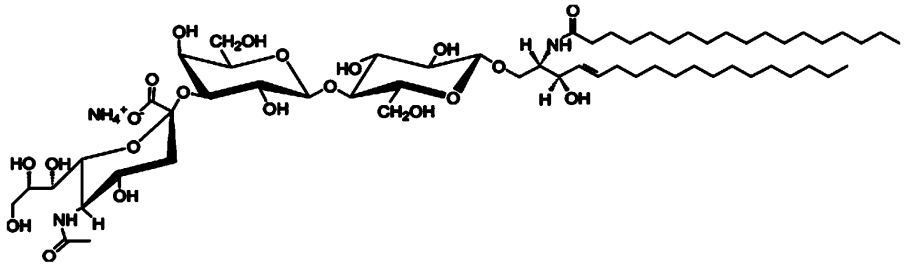

(c) Glycolipid

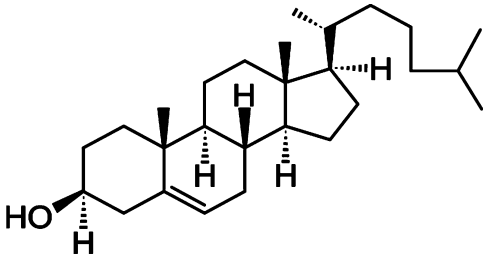

(d) Cholesterol

Figure 1.2 Lipid structures for different classes of lipids and cholesterol (the most common sterol in cell membranes).[Images taken from Avanti Polar Lipids Inc. (http://www.avantilipids.com)]

use of strong detergents that can break down these non-polar interactions. Examples include insulin receptor, Rhodopsin, several ion-channel proteins, receptor proteins etc.

Peripheral Proteins are generally associated with one of the membrane leaflets or with the integral proteins. Electrostatic and hydrogen bond interactions between the amino acid residues on the surface of these proteins, and the charged membrane facilitate the association of these proteins with membrane lipids and integral proteins. Unlike integral proteins, this class of proteins can be easily removed from the membrane by the addition of salt, change in concentration of divalent cations or by varying the pH. Enzymes like lipases, several bacterial and fungal toxins, and proteins containing domains that interact with membrane lipids are few examples of peripheral proteins.

Some proteins are also found to be associated with carbohydrates in the extracellular region. These carbohydrates aid in recognizing foreign bodies, and also help in signal recognition during intracellular communication. Additionally they also prevent the disorientation of the proteins attached to them as the highly hydrophilic sugar residues cannot enter the non-polar hydrophobic core of the membrane, thus restricitng the movement of the protein. These proteins that have one or more sugar residues attached to them are termed **glycoproteins**.

1.3.3 Sterols

These are alcohols with unsaturated, polycyclic alkyl chains. Cholesterol (Fig. 1.2(d)) is an important sterol found in cell membranes of higher organisms. Cholesterol has a large backbone group - a two ring steroid nucleus and is a neutral molecule as opposed to the charged cell membrane components mentioned so far. The steroid ring runs parallel to the acyl chains of the phospholipids, and the hydroxyl group in the molecule forms a bond with the carbonyl group in the phospholipid head groups. Due to this bond and its bulky ring structure, a cholesterol molecule introduces some flexibility in the closely interacting acyl chains of the lipids. However it also blocks the lateral diffusion of the lipids to some extent, modifying the fluidity of the membrane. Large clusters of these molecules are found in the membrane as dynamic micro domains termed as lipid rafts[9]. These rafts have caught the attention of many because they play an important role in several viral infection pathways and immune responses.[10]

1.4 Cell Membrane : Functions

The various membranes in the cell directly or indirectly participate in and regulate most of the cellular processes. The cell membrane is particularly important in this regard as it is the means by which cells communicate with other cells and the extracellular chemical environment. Cell membranes are selectively permeable and thus help to keep a check on the inflow and outflow of molecules in the cell. Several diseases begin with the unchecked entry of a harmful foreign material (like a virus particle) into the cell which can disrupt the cellular machinery. A few of the several functions that make the cell membranes so vital are listed below: [11]

Regulate cell growth and replication -Cell cycle is a series of well controlled steps which lead to cell growth and cell division. A kinase, phosphoinositide-3-kinase (PI3K) is a key player in the cell cycle. This enzyme phosphorylates the inositol ring at the third position in phosphoinositides, which is the first step in recruiting a series of proteins that then carry the signal forward. The PI3K activity in the cell is central to its survival and proliferation. Over activation of PI3K is responsible for unregulated cell growth (tumor). Anionic phospholipid concentrations are also found to affect initiation of DNA replication. [12]

Signal apoptosis or cell death-Lipid biosynthesis and concentration regulation are dynamic yet tightly controlled cellular processes. Some lipids are formed in the membrane itself while others in cellular organelles. One pathway for apoptosis or programmed cell death via enzymes called caspases is a chemical signal characterized by an increase in concentration of cardiolipin (a lipid in the mitochondrial membrane, which is produced from recycled cell membrane lipids). The concentration of lipids and the integrity of the plasma membrane thus influence the concentration of several other cellular lipids and secondary messengers, sometimes triggering fatal signals like apoptosis.[13]

Cell–cell communication - The cell membrane is the cell's means of communicating with its external environment. A number of receptor proteins on the cell membrane and glycosylated (carbohydrate attached) lipids on the outer leaflet of the membrane efficiently sense foreign particles or other molecules. Cells communicate through chemical signals (i.e. molecules). Secretions from the membrane of one cell are recognized by the membrane receptors on the

surrounding cells thus transferring signals like growth factors etc. from one cell to another.

Regulate traffic of messenger molecules and ions in and out of cells - The semi permeable nature of the membrane is probably its most important property on account of which it allows only certain molecules to pass through it while preventing the others. For example, the hydrophobic core of the membrane is a protective barrier preventing the free movement of hydrophilic molecules or ions through it. However several embedded proteins form systems, called ion pumps and gated ion channels which allow the movement of ions across the membrane. This is important in maintaining the optimum concentration of ions like Na^+, K^+ in the cells which are in turn responsible for binding to and activation of several functionally important proteins.

In signal transduction - Signal transduction pathway comprises of initiation, transfer and translation of a trigger into a cellular response. Often the trigger is an increase in particular ionic concentrations, binding of a molecule to one of the surface receptor proteins, or presence of foreign cells, like bacteria. Extensive studies on individual membrane components and their roles in signal transduction show their importance in these pathways.[14],[15]. A common signal transduction at the membrane is the one involving G-Proteins where a G-protein linked receptor picks up a signal at the exoplasmic end, which activates the G-protein at the cytosolic end of the membrane. The G-protein is generally associated with an enzyme which it activates. This enzyme upon activation generates the cellular response via a single or series of steps. The enzyme activation as well as its interaction with other proteins in the cell, takes place in the presence of anionic lipids like phosphoinositides which interact with these proteins and hold them close to the membrane.

1.5 Lipids Rafts : Structurally distinct, functionally important

The lateral organization of membrane components into domains was noted by Singer and Nicholson in 1972. In their fluid mosaic model [5], they proposed that a small fraction of lipids may interact with the membrane proteins leading to their restricted diffusion. In 1982, experimental evidence suggesting the existence of these domains was provided by Knarovsky [16].

A renewed interest and active research in this area began a little over ten years ago with the development of a formal hypothesis for these microdomains within the membrane [17] which are now commonly referred to as lipid rafts or membrane rafts. The picture of the cell membrane structure that emerged with the discovery of these domains was far more complex than the earlier simpler model. Previously, lipids and proteins in the membranes were considered to constitute a liquid disordered phase. According to the new picture, membranes also consist of another phase - a liquid ordered phase - the microdomains, which exhibit temporal dynamicity in size and morphology and are compositionally different from the surrounding liquid disordered phase. A consensus regarding the definition of membrane rafts was reached during the Keystone Symposium 2006 on Lipid Rafts and Cell Function, which states that - Membrane rafts are small (10200 nm), heterogeneous, highly dynamic, sterol- and sphingolipid- enriched domains that compartmentalize cellular processes. Small rafts can sometimes be stabilized to form larger platforms through protein-protein and protein-lipid interactions. [18] Rafts have been associated with many functions carried out by the cell membrane. In Ref. [19] rafts were classified based on their functions into two different categories : (i) Trafficking and sorting - Microdomains under this category typically participate in or serve as sites for signaling, localization of other proteins or in endocytosis and exocytosis pathways. (ii) Disease related - There are several bacteria and viruses that target certain microdomains to spread infection, E. coli, Salmonella, Influenza virus, Measles virus to name a few. Some metabolic(insulin resistance) and ageing disorders also are a result of improper compartmentalization of molecules in the microdomains. A third category - Special composition consisting of a microdomain without cholesterol was identified [20]. However no specific functions pertaining to these microdomains are observed as yet. Due to their functional importance, small molecules that facilitate the formation of lipid rafts are actively being pursued as possible targets to treat diseases.

Though there is now sufficient evidence to acknowledge the presence of lipid rafts and their functional significance, their lifetime and the factors responsible for their formation, are not well established. While some experiments show the existence of stable rafts under physiological conditions [21], there are other experiments that support the formation of rafts under special conditions like signaling events involving interaction of proteins, increase in ion concentration,

increase in concentration of certain lipids in the membrane or interaction of components in smaller rafts to form larger detectable rafts. One of the reasons for this disagreement is the lack of appropriate probes and techniques for the detection and extraction of lipid rafts from cellular membranes. An understanding of the driving forces and mechanisms involved in the formation and functioning of these microdomains is thus essential to push this area of research forward.

1.5.1 Electrostatically induced lipid rafts

A high concentration of cholesterol and sphingomyelin have been identified as an inherent property of lipid rafts. However, some lipids like PIP2 have a polyunsaturated acyl chain which make the separation of PIP2s into cholesterol rich regions unfavorable. The bent in the acyl chains introduces breaks in the interaction of the hydrophobic tails of the lipids with sterols and shingomyelin. Owing to their high charge (typically -4e), the repulsion between PIP2s would make the clustering difficult to achieve. However, PIP2 clusters have been found in the cytosolic layer of the cell membrane, in regions that serve as active sites for signaling and membrane-protein interactions [22]. One of the means by which PIP2 clusters can be created and maintained is by the electrostatic interactions of PIP2s with positively charge proteins and ions. It is observed that natively unfolded proteins like MARCKS and Ca^2+ ions induce and stabilize the rafts to prepare the membrane for signaling events. The mechanism involved is however unclear. Experiments show that a simple polybasic peptide or positively charged cations (primarily Ca^2+) can create and maintain clusters of PIP2 (Phosphatidylinositol-4, 5-bisphospate) within the membrane [23, 24, 25, 26]. Such clustering is a result of electrostatic interactions and hydrogen bonds [27, 28, 29, 30, 31]. Recently, experiments on supported lipid monolayers by Levental and colleagues have shown that clustering is observed at normal PIP2 ($\approx$ 0.1 mol %) and high calcium levels (1mM) [32]. Wang et al [21] observed the clustering of PIP2 molecules into 40nm domains at physiological concentrations of calcium and high PIP2 concentration ($\approx$ 10 mol %). In a more recent study using spectroscopic techniques, Sarmento et al [33] showed that PIP2 forms smaller domains ($\approx$ 15 PIP2 molecules) at physiological con-

centration of both calcium and PIP2. The ambiguity in the results could be attributed to the limitations of the experimental techniques used and lack of a standard definition and theoretical backing to understand the mechanism that causes the clustering of lipids. The motivation for this study arises from the need to gain insight into the non-specific electrostatic interactions between membranes and ions that are expected to drive the formation of clusters in this case.

1.6 Modeling Cell Membranes

[1] Studying ion distribution in the vicinity of membranes, signal transfer in the cell membrane and protein lipid interaction in the light of electrostatics has been the focus of many experimental studies using phospholipid monolayers [34, 35]. Advancements in technologies like x-ray crystallography and microscopy have aided in understanding processes taking place at the membranes. However progress in developing models for these membranes which can explain underlying mechanisms for the corresponding experimental observations, has been relatively slow. One of the several challenges in analyzing these membranes has been to come up with a reasonable description of systems consisting of discretely charged membranes in contact with electrolytes [36]. Previous models treat these membranes as uniformly charged, ignoring their discreteness, which is inherent in the lipid layers of cell membranes. One of the aims of this study is thus to develop a coarse-grained model that faithfully accounts for the electrostatic correlations at large distances and long time scales, yet sufficiently general to incorporate effects of specific chemical interactions. This minimalist model provides a suitable starting point to study the case of complex phospholipids and the influence of electrostatic effects in their structure.

Electrostatic interactions are crucial in determining how molecules diffuse and interact in aqueous media. Yet, due to the low water dielectric constant, electrostatic effects become either of the same magnitude or just marginally stronger than many of other competing interactions, which are often highly dependent on the specific chemical structure of the molecule. It is pre-

[1] Excerpts have been taken from the paper : S. Vangaveti, A. Travesset, *Ionic distribution next to surfaces of discrete interfacial charges*,(published)

cisely this subtle combination of diverse interactions and the long range nature of electrostatic interactions that makes the description of macromolecules in aqueous media so challenging.

All Atomic vs Coarse Grained Model The considerations for building a good coarse-grained model can be summarized in this famous quote by Albert Einstein – "Everything should be made as simple as possible, but not simpler."

In developing models for membranes, as is the case with any other model, the problem at hand determines the characteristics and details required to come up with the most explanatory yet most simple model. For example to study the binding site of a protein and a corresponding phospholipid, atomic details are essential to completely characterize the interaction. On the other hand, to study the membrane flexibility and curvature, a hydrophilic head group particle with a hydrophobic chain of interacting beads may be sufficient. With the model developed through this study we plan to explore processes like ion-membrane interactions during signaling, formation of micro domains in lipid membranes etc. These target processes are a result of collective interactions of a large number of structurally diverse lipids carrying charges ranging from 0e to -4e.

An all atomic simulation can certainly be useful in all cases, to model macromolecules with atomic precision where all interactions are, in principle, taken into account, the hefty computational demands for simulating those systems, make an exhaustive analysis challenging. Moreover, even with achievable results from all atom simulations, there is still an obvious need for simpler models that conceptualize our understanding in terms of a small number of degrees of freedom that can be directly related to experimentally accessible parameters. So using a coarse grained description of a lipid is a logical choice to solve such problems. Coarse graining is in fact a common practice in simulations used in the study of bilayer lipid membrane properties, with the level of coarse graining varying from one model to other [37, 38, 39]. Some models treat lipids as rigid amphiphilic molecules with the hydrophobic end represented by a rod [40], while some others like the Martini model add more structure to both the head group and the alkyl chains by representing four heavy particles as one, thus reducing the number of sites of interaction [38]. Given the charge on phospholipids, electrostatics plays an important role in determining membrane properties. These models however, use a truncated electrostatic

potential, thus undermining the long range nature of electrostatic interactions.

Uniform or Discrete The unavoidable starting point of any discussion on electrostatics on aqueous media is the standard Poisson-Boltzmann theory (PB) [41, 42], which despite its relative simplicity, successfully describes a rich phenomenology [41, 42, 43, 35]. Within PB theory ions are considered as point-like, the solvent is considered implicitly, the macromolecule is modeled as a continuum of surface charge and the interactions are modeled within mean field. While many of the deficiencies of PB theory have been reviewed elsewhere [44, 45, 46, 47, 48], the particular approximation of replacing discrete charges of macromolecules by a continuum distribution has been relatively overlooked, despite that the experimental literature in amphiphilic systems provides clear examples where ionic distributions show significant differences in systems with the same surface charge [49, 50, 51]. In fact, the idea that charge discreteness has a minor effect on the long distance and large time scales has been supported by a number of theoretical calculations. Already in the 70s, Nelson and McQuarrie [52] approximately solved the PB equation for discrete charges, but subsequent experimental work did not validate those predictions[36]. More recently, different models have revisited the problem [53, 54, 55, 56] using different approximations and somehow confirmed that charge discreteness does not provide significant quantitative or qualitative differences from a continuum distribution. Numerical simulations of Madurga et al. [57] compared different arrangements of discrete charges with continuum distributions and found virtually identical results except for the case where the interfacial charges penetrate into the bulk. Subsequent MD simulations by Calero and Faraudo [58] further analyzed this case and did find that discrete charges do have a dramatic effect in ionic distributions; The potential of mean force between interfacial charges and mobile counterions, for example, is well described by a simple Coulomb potential, thus confirming early predictions in Ref. [59] based on the idea of Bjerrum pairing, see also Ref. [60]. Yet, a precise characterization of the effects of discrete charges as well as the ensuing correlation effects in its distribution as well as on the large distances and long time scales of a macromolecule is still an open issue.

Before dwelling further into the effect of discrete charges, it is worth reviewing some results that have been obtained for ionic distributions next to a continuum distribution. Calculations

within the Modified Poisson Boltzmann (MPB) theory [61, 62] or the more accurate Anisotropic Hypernetted Chain Approximation (AHNC) of Kjellander and Marcellja [63, 64, 65] provide virtually exact results, particularly at medium to high ionic strength. Still, theories with more transparent physical interpretations, albeit less accurate, have been developed. Shklovskii and collaborators [44] describe the immediate layer of counterions next to the charged interface as a strongly two dimensional correlated liquid whose properties are well characterized [66] (the "Wigner Crystal"). MC simulations for multivalent (trivalent and tetravalent) ions have provided some validation to these theories[67, 68]. Somewhat related, yet developed within a more formalistic framework is the strong coupling (SC) expansion of Netz and collaborators [69, 45], which predicts an exponential decay of the ionic distribution close enough to the charged interface.

Modeling a distribution of electric charges in terms of a continuum distribution immediately eliminates effects resulting from the intrinsic discreteness of electric charges, i.e. correlation effects. A familiar example is provided by table salt (NaCl) whose crystalline structure at room temperature is entirely stabilized by electrostatic correlations, encoded in the Madelung constant. In the case of cell membranes, charges appear on individual lipids (introducing discreteness) but the charge on different classes of lipids is also different. Lipids like phosphatidyl serine have an effective charge of $-1e$ while those like phosphoinotides may have charges as high as $-4e$. Considering these properties of membranes a discrete model should provide a more realistic description of cell membrane properties as opposed to a uniform one. The description of the phenomenology in real experiments however, involves interactions whose origin lies in the ability of ions to form weak covalent bonds with interfacial groups [70], water restructuring[71], charge regulation [72] and many other effects that are often poorly understood in experiments. It is for this reason that a common approach to describe real experiments has been to supplement PB with a region immediate to the charged interface, the Stern layer [41], which empirically describes all these effects by introducing new parameters such as an effective dielectric constants, binding constants, Stern layer size, etc. Despite that these parameters do not have a rigorous theoretical basis and need to be determined from experiments and are strongly specific to each particular system, thus considerably limiting the predictive power of

the theory, they have proven quite useful in modeling experimental results, such as for example SDS isotherms [73], carboxylic acids monolayers [74] or phospholipid systems[50] among many others. These examples highlight the fact that even if an exact mathematical solution to the problem of ionic distributions next to a charged interface would be at hand, detailed predictive theories for real experiments still require significantly more insight.

1.7 Primary Objectives of this Study

The purpose of this study is to formulate a general coarse grained model of the lipid monolayers to study and analyse the behavior of lipid membranes in various environments and their interactions with proteins and other lipids. This would help in understanding how the lipid head groups and ions interact to form biologically relevant structures or phases. Such interactions as described earlier are believed to play a significant role in clustering charged anionic lipids to form functional rafts.

CHAPTER 2. ELECTROSTATIC CORRELATIONS AT STERN LAYER: PHYSICS OR CHEMISTRY?

A paper published in the Journal of Chemical Physics

Alex Travesset and Sweta Vangaveti

2.1 Abstract

We introduce a minimal free energy describing the interaction of charged groups and counterions including both classical electrostatic and specific interactions. The predictions of the model are compared against the standard model for describing ions next to charged interfaces, consisting of Poisson-Boltzmann theory with additional constants describing ion binding, which are specific to the counterion and the interfacial charge ("chemical binding"). It is shown that the "chemical" model can be appropriately described by an underlying "physical" model over several decades in concentration, but the extracted binding constants are not uniquely defined, as they differ depending on the particular observable quantity being studied. It is also shown that electrostatic correlations for divalent (or higher valence ions) enhance the surface charge by increasing deprotonation, an effect not properly accounted within chemical models. The charged phospholipid phosphatidylserine is analyzed as a concrete example, with good agreement with experimental results. We conclude with a detailed discussion on the limitations of "chemical" or "physical" models for describing the rich phenomenology of charged interfaces in aqueous media and its relevance to different systems, with a particular emphasis on phospholipids.

2.2 Introduction

The standard model for describing charged interfaces in aqueous media discriminates between a Stern layer, where ions bind to interfacial groups, and a diffuse layer, where ions are distributed over a characteristic distance before attaining bulk values. While the diffuse layer is universally described by Poisson-Boltzmann theory [41] (or by more sophisticated theories for higher electrolyte concentrations [75, 76, 77]), the description of the Stern layer, on the other hand, resorts to more phenomenological models. A common approach has been to describe ion binding and release as a chemical reaction with some characteristic binding constants [72, 78, 41], which are attributed to specific chemical interactions and are assumed to be beyond the scope of classical statistical mechanics. Most commonly, the binding constants are extracted by directly fitting the experimental data. This approach has been extremely successful in describing many experiments, such as for example, the electrostatic properties of phospholipid systems [50]. Yet, electrostatic interactions are the quintessential example of long-range interactions and binding constants appropriately describe short-range interactions only, thus raising an obvious question about the actual meaning of such binding constants. In addition, at a more practical level, in molecules with many different charged groups it is not generally possible to perform a sufficient number of independent experiments to unambiguously determine all the necessary binding constants.

Over the past years, different approaches treating Stern and diffuse layers entirely within the context of classical statistical mechanics have been proposed [44, 79, 45, 47]. In this way, as noted by Lyklema [46, 80], the community investigating aqueous electrolytes has branched out into two, almost completely independent communities, one that uses the standard "chemical" model and its variations, and another embracing the "physical" approach. Despite some notable successes from "physical" models (see for example Ref. [81, 82, 83]), the bulk of experimental data remains most commonly described by resorting to "chemical" models.

There are definite examples of chemical interactions at the Stern layer, the most relevant is probably proton release and binding, the mechanism by which acids or bases become charged in aqueous solution. A complete description of the proton is beyond the scope of classical

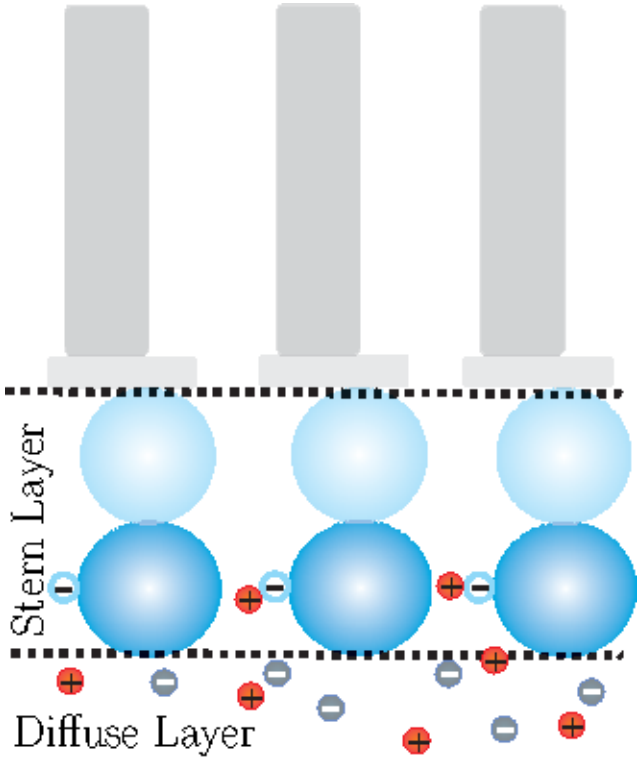

Figure 2.1 Schematic representation of a charged system, with a distinction between Stern and Diffuse layer.

statistical mechanics, so any theory that accounts for proton release and binding must include a parameter (such as the pK_a), which can only be computed from a full quantum chemistry calculation. Yet, when it comes to ions with the electronic structure of a noble gas (such as Na^+, Cs^+, Ca^{2+}, etc..) it should be expected that in most cases, a classical electrostatics description would suffice, and that the chemical binding constants extracted from experiments provide an effective description that can be superseded by an appropriate classical statistical mechanical calculation.

The main motivation for this paper grew from the need to provide a "physical" model that describes the electrostatic properties of amphiphilic models, particularly phospholipids such as Phosphatidic acid (PA) and Phosphatidil-Inositol-Bisphosphate (PIP_2) among others, which participate in almost all signalling pathways across the cell membrane by exquisitely exploiting its electrostatic properties [28, 84, 15]. Because these phospholipids include many different charged groups, the description of their electrostatic properties based on the standard "chemical" approach is far more complex than the one needed for zwitterionic phospholipids such as Phosphatidylcholine (PC) or Phosphatidylethanolamine (PE) or singly charged ones such as Phosphatidylserine (PS). The focus of this paper will be on presenting the general framework of the model, leaving the detailed predictions and modifications needed to describe signalling phospholipids for a subsequent publication.

Despite the somewhat focussed motivation for this paper, the model and results presented find a general applicability to a broad range of systems, extending beyond phospholipids or amphiphilic systems. The paper aims to bridge the gap between "physical" and "chemical" descriptions. This is a recent trend on the research in this area; In Ref. [59] it was shown that the concept of Bjerrum pairing, suitably generalized for charged interfaces, provides a convenient way to estimate binding constants from a purely physical model in reasonable agreement with experiments. Ref. [85] presents sophisticated Monte Carlo simulations that account for pH variations thus allowing the description of experimental results without resorting to additional parameters. Other groups have systematically accounted for precise mobility measurements by using MonteCarlo or integral equation methods without additional assumptions [86] and a considerable effort has been devoted to combine "chemical" and "physical" effects in the field

of polyelectrolytes [87, 88, 89, 90].

The critical element in this paper is the role of interfacial charges. This has been a recurrent topic in the statistical mechanics of interfaces. Already in the seventies, Nelson and McQuarrie solved the PB equation for discrete charges [52], but experiments [36] failed to validate their findings. More recent treatments [54, 53, 56, 55] have revisited the problem, finding that discrete charges adds to relatively minor corrections to an approximation where the interface is treated as a smooth background. The crucial aspect between the interaction of interfacial charges and ions is that describes a strong correlation [59] (see also [60]), which cannot be described as a perturbation from the uniform case. Recent numerical simulations by Madurga et al. [57] have clearly shown that distributions of ions in the diffuse layer are greatly affected by the discrete nature of interfacial charges if those are sufficiently exposed to the aqueous solution.

2.3 Model

2.3.1 The model

The system consists of a monolayer (with molecular area A_c) of amphiphilic molecules (AL)s forming a charged interface. ALs are acidic or basic and its charge is regulated by its pK_a value. The monolayer is in contact with an aqueous solution of fixed pH containing counterions and co-ions, of general valences. The model we consider builds on three assumptions (see Fig. 2.1):

1. *Electrostatic correlations are relevant only within the Stern layer.*

2. *Counterions and co-ions within the diffuse layer are weakly correlated and are therefore described by Poisson-Boltzmann theory.*

3. *Non-idealities associated with mixing entropies of different species are ignored.*

The justification for assumptions 1 and 2 will be elaborated and justified further below. The last assumption, which is common in most theoretical treatments, will not be discussed any further; It is expected to induce small quantitative errors that can be corrected by additional parameters into the model.

The free energy (F_S) of the system is made of four contributions

$$F_S = F_{Diff} + F_{Prot} + F_{Mix} + F_{Corr} \ , \tag{2.1}$$

where the first term is the free energy associated with building the diffuse layer of counterions, the second term is the free energy associated with proton binding and release, the third term is the entropy of mixing the different species within the monolayer and the last term accounts for the free energy associated with electrostatic correlations. In this paper, only the case of a single pK_a will be considered. The AL head group can be either neutral or charged, according to

$$\mathrm{AL}^- + \mathrm{H}^+ \quad \longleftrightarrow \quad (\mathrm{AL})\mathrm{H} \tag{2.2}$$

$$\mathrm{AL}^- + \mathrm{c}^q \quad \longleftrightarrow \quad (\mathrm{AL})\mathrm{c}^q \ , \tag{2.3}$$

The first reaction involves proton release and binding and it is a chemical reaction, with an equilibrium constant that is the natural exponential of the pK_a value (in molar units). The second process is a physical process that accounts for ion binding and involves many body effects not entirely describable by a binding constant, as elaborated further below.

The fraction of deprotonated ALs is defined as

$$f_{AL} = ([\mathrm{AL}^-\mathrm{c}^q] + [\mathrm{AL}^-])/([\mathrm{AL}^-\mathrm{c}^q] + [\mathrm{AL}^-] + [(\mathrm{AL})\mathrm{H}]) \tag{2.4}$$

while the fraction of head-groups with bound counterions is

$$f_b^{(q)} = [\mathrm{AL}^-\mathrm{c}^q]/([\mathrm{AL}^-\mathrm{c}^q] + [\mathrm{AL}^-] + [(\mathrm{AL})\mathrm{H}]) \ . \tag{2.5}$$

where [..] denotes concentration (in molar units). Unless there is ambiguity, the super-index q will be dropped from f_b. By definition $f_b < f_{AL}$, as only deprotonated AL are assumed to bind counterions.

It is convenient to introduce the parameter b^0

$$b^0 = \lambda_D/\lambda_G^0 \ , \text{ where } \ \lambda_G^0 = \frac{A_c}{2\pi q l_B} \ , \tag{2.6}$$

with λ_D and l_B being the Debye and Bjerrum lengths and q the counterion valence.

The free energy associated with the diffuse layer F_{diff} is given by PB theory (assumption 2). The surface charge includes deprotonated ALs and counterions bound to the head-group

$$\frac{F_{Diff}}{N_{AL}k_BT} = |f_{AL} - qf_b|\mathcal{F}_{PB}(b^0(f_{AL} - qf_b)) \ , \tag{2.7}$$

where N_{AL} is the total number of ALs at the interface, and $\mathcal{F}_{PB}$ is the Poisson-Boltzmann free energy. For example, $\mathcal{F}_{PB}(x) = 2(\log(x + \sqrt{x^2+1}) + (1 - \sqrt{1+x^2})/x)$ for both monovalent counterions and co-ions. For other valences it is not possible to express $\mathcal{F}_{\mathcal{PB}}$ in closed analytical form, but it is not difficult to compute numerically (see Appendix 2.A). We recall that if $f_{AL} < qf_b$, the originally negative interface becomes positively charged, an effect that is known as charge inversion or charge reversal [46, 80].

The free energy expression (F_{Prot}) describing proton release and binding is given by

$$\frac{F_{Prot}}{N_{AL}k_BT} = f_{AL}(\mathrm{pK}_a - \mathrm{pH})\log(10) \ , \tag{2.8}$$

and is derived in detail in appendix 2.C.

The free energy (F_{Mix}) associated with mixing the different interfacial species is

$$\begin{aligned} \frac{F_{Mix}}{N_{AL}k_BT} &= f_b\log(f_b) + (f_{AL} - f_b)\log(f_{AL} - f_b) \\ &+ (1 - f_{AL})\log(1 - f_{AL}) \ . \end{aligned} \tag{2.9}$$

The only term left is the one describing electrostatic correlations (F_{Corr}) within the Stern layer. The basic strategy is to account for static correlations as if the system were frozen on a given configuration, and account for thermal fluctuations as perturbations to this configuration. The free energy is

$$\frac{F_{Corr}}{N_{AL}k_BT} = \mathcal{F}_{Corr}(f_{AL}, f_b) - f_b\log(v_0[c]) + \mathcal{F}_{bound}(f_b) \ , \tag{2.10}$$

here, $\mathcal{F}_{Corr}$ encodes the electrostatic correlations of the static system and is computed as a Madelung energy by placing both AL charges and bound ions on either a triangular or a square lattice. Differences in free energies between square or triangular lattices are much smaller than other approximations made, so either case provides equally acceptable results. The term $\mathcal{F}_{Corr}$ accounts for the many body effects that arise from the long-range nature of electrostatic

interactions, and it reduces to the leading term of the free energy of a one component plasma [66] if the interface is approximated as a uniform charge. Further details are discussed in the appendix 2.D. Despite that the calculation places the charges in a two-dimensional crystalline state, the expression is assumed to describe the liquid state also. Justification is provided in the context of the one component plasma [66].

The second term is the favorable entropy of releasing counterions into the bulk solution and the last term $\mathcal{F}_v$ is the thermal free energy associated with counterions bound to the head group. The difference between the last two terms is basically the entropy loss of counterions upon binding. We recall that v_0 defines an arbitrary reference volume, so only the sum of the last two terms defines a term free from arbitrary quantities. The final expression, whose detailed derivation is given on appendix 2.D, is

$$\frac{F_{Corr}}{N_{AL}k_BT} = -f_{AL}^{3/2}\gamma(f_b)\frac{l_B}{a_L} - f_b\log(2\pi r_0^3[c]\sqrt{\frac{11l_B|q|}{2\pi r_0}}) \ , \tag{2.11}$$

The quantity r_0 is the equilibrium separation between counterion and AL charges, a_L is the average distance between nearest neighbor ALs and $\gamma(f_b)$ is a function that encodes electrostatic correlations and whose explicit expression for the relevant cases discussed in this paper is given in Eq. 2.25 and Table 2.1.

Generalization to systems with both mono and divalent salts is straight-forward, except for the γ-function in $\mathcal{F}_{Corr}$, which requires a minor adjustment, discussed in the appendix, see Eq. 2.26.

2.3.2 Free energy minimization

The quantities f_{AL} as well as the different $f_b^{(q)}$s are the main observables to be computed. They are obtained by minimizing the free energy Eq. 2.1. Both f_{AL} and $f_b^{(q)}$ are not only measurable quantities but completely determine other measurable quantities, such as, for example, the ζ-potential. For future reference, we quote the equation determining the minimum of the

free energy (particularized for a single counterion specie of valence q):

$$\begin{aligned} f_{AL} &= \frac{1+K_m[c^q]\exp(-\frac{qe\psi(0)}{k_BT})\exp(\frac{\partial\mathcal{F}_{Corr}}{\partial f_b^{(q)}})}{1+10^{\mathrm{pK}_a-\mathrm{pH}}\exp(-\frac{e\psi(0)}{k_BT})\exp(-\frac{\partial\mathcal{F}_{Corr}}{\partial f_{AL}})+K_m[c^q]\exp(-\frac{qe\psi(0)}{k_BT})\exp(\frac{\partial\mathcal{F}_{Corr}}{\partial f_b^{(q)}})} \\ f_b^{(q)} &= \frac{K_m[c^q]\exp(-\frac{qe\psi(0)}{k_BT})\exp(\frac{\partial\mathcal{F}_{Corr}}{\partial f_b^{(q)}})}{1+10^{\mathrm{pK}_a-\mathrm{pH}}\exp(-\frac{e\psi(0)}{k_BT})\exp(-\frac{\partial\mathcal{F}_{Corr}}{\partial f_{AL}})+K_m[c^q]\exp(-\frac{qe\psi(0)}{k_BT})\exp(\frac{\partial\mathcal{F}_{Corr}}{\partial f_b^{(q)}})} \end{aligned} \quad (2.12)$$

where $\psi(0)$ is the contact potential and $K_m \equiv 2\pi\sqrt{\frac{2\pi r_0}{11 l_B}} r_0^3$. Despite appearances, This equation is quite involved as $\mathcal{F}_{corr}$ depends both on f_{AL} and $f_b^{(q)}$, and the contact value potential $\phi(0)$ must be obtained self-consistently from the PB equation for a surface charge density $\sigma = -e\frac{f_{AL}-qf_b^{(q)}}{A_c}$. In this paper, the minimum solution was obtained by directly minimizing the free energy by using the MATLAB optimization package.

2.3.3 The "chemical" or LPB model

The standard model (or "chemical" model) will be revisited within the context of the previous formalism. The correlation term Eq. 2.11 can be rewritten as

$$\begin{aligned} \frac{F_{Corr}}{N_{AL}k_BT} &= -f_b\log(K_m\exp(\frac{f_{AL}^{3/2}l_B}{f_b a_L}\gamma(f_b))[c]) \\ &\equiv -f_b\log(K_B^{eff}(f_b,f_{AL})[c])\ . \end{aligned} \quad (2.13)$$

The quantity $K_B^{eff}(f_b, f_{AL})$ is not a binding constant as it depends on the variables f_b, f_{AL} as well as surface density. However, if it is replaced by some mean value $K_B^{(q)}$ that interpolates between the range of f_b, f_{AL} appropriate for each system, then the equations that minimize the free energy simplify to

$$\begin{aligned} f_{AL} &= \frac{1+K_B^{(q)}[c^q]\exp(-\frac{qe\psi(0)}{k_BT})}{1+10^{\mathrm{pK}_a-\mathrm{pH}}\exp(-\frac{e\psi(0)}{k_BT})+K_B^{(q)}[c^q]\exp(-\frac{qe\psi(0)}{k_BT})} \\ f_b^{(q)} &= \frac{K_B^{(q)}[c^q]\exp(-\frac{qe\psi(0)}{k_BT})}{1+10^{\mathrm{pK}_a-\mathrm{pH}}\exp(-\frac{e\psi(0)}{k_BT})+K_B^{(q)}[c^q]\exp(-\frac{qe\psi(0)}{k_BT})}. \end{aligned} \quad (2.14)$$

These equations define the "chemical model", which consists of a Langmuir absorption isotherm (with binding constant $K_B^{(j)}$) coupled to the Poisson-Boltzmann equation and will be referred

to as the LPB model herein. In this way, the LPB model, which has been the standard model to analyze experimental results, for example in phospholipid systems [91, 92, 74, 93, 94], appears as an approximate effective description for the underlying physical model.

2.4 Results

A preliminary comparison with simulation results on simple models is provided in the Appendix Sect. 2.E and its implications are further discussed in the conclusions. The results section will be entirely focused on comparison with experiments.

2.4.1 A note on coarse-graining phospholipid systems

Glycerol based phospholipids contain two hydrophobic acyl chains and a phosphate group attached to its glycerol backbone. The phosphate group is charged and has and additional group attached to it. If the additional group is serine, the phospholipid is PS. It should be noted that there are two acid (carboxyl and phosphate) and one basic (the amino) groups in PS, see Fig. 2.2. There are therefore 3 pK_as for PS. The carboxylic and amino groups have been measured to be 3.6 and 9.8 respectively [92], while the one in the phosphate group is probably low (1 or less). Thus, at physiological conditions, the overall -1 charge of PS results from two negative and one positive charges. In this paper, the overall PS will be coarse-grained as a -1 charge with pK_a=3.6, as shown in Fig. 2.2. This approximation has been adopted in all descriptions of experimental data and its limitations are further discussed in the conclusions.

2.4.2 PS as an example

Unless specified otherwise, it will be assumed that the area per molecule is $A_c \approx 70\text{Å}^2$ and the equilibrium counterion PS-head group distance $r_0 = 2.8\text{Å}$ (see Eq. 2.11 and Table 2.1). This distance is the minimum separation between an oxygen atom ($\sim$1.4Å) and a counterion such as K^+. These distances correspond to crystallographic radius, as both MD simulations [95, 96, 60] and experimental results[97] show that counterions dehydrate upon binding.

Fig. 2.3 shows f_{AL} and f_b for PS in contact with a monovalent salt solution at neutral pH. PS becomes fully deprotonated at about 10^{-3}M, and at this point, about 40% of the PS head groups

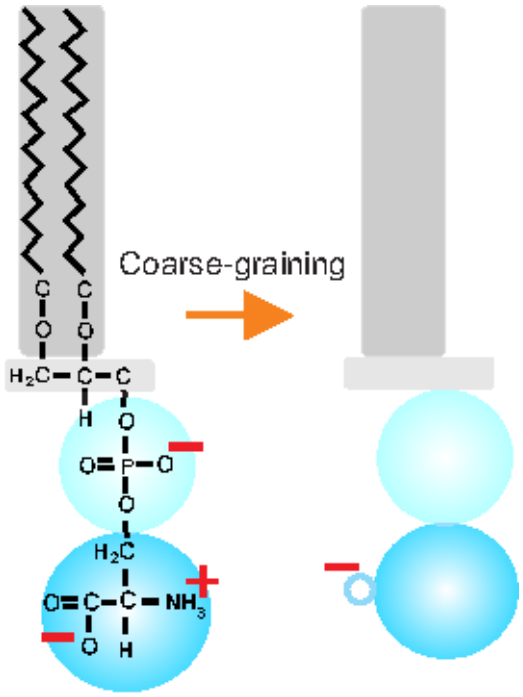

Figure 2.2 Schematic representation of the coarse graining of PS.

bind counterions. An attempt to fit the theoretical results within LPB (see SubSect 2.3.3) shows that the binding constant extracted from Fig. 2.3 depends on the particular quantity that is analyzed. If the degree of deprotonation is the quantity of interest, the value $K_B^{(1)} = 0.75\mathrm{M}^{-1}$ is obtained. If, on the other hand, the amount of ionic binding is what is measured, the value is sensibly smaller $K_B^{(1)} = 0.1\mathrm{M}^{-1}$, while a ζ-potential would measure a combination of the two quantities and hence, an intermediate value for the binding constant. Experimentally determined values are within the range ($K_B^{(1)} = 0.1 - 1.0$) [91, 92, 36, 93], and we interpret this dispersion as reflecting the approximate validity of LPB. More concretely, this dispersion reflects the inherent inaccuracy of describing the Stern layer with short-range forces only.

We can estimate the range of expected values for the binding constants that would be extracted from an experiment by analyzing the minimum free energy equations Eq. 2.12. For fully deprotonated PS, with f_b ranging between 0.1 and 1 (as a significant amount of binding is required) at the molecular area $A_c = 70\text{Å}^2$ it is

$$K_B^{(1)} \approx K_m \exp((a_1 + 2f_b a_2)) \sim (0.08 - 0.5)\mathrm{M}^{-1} \ , \tag{2.15}$$

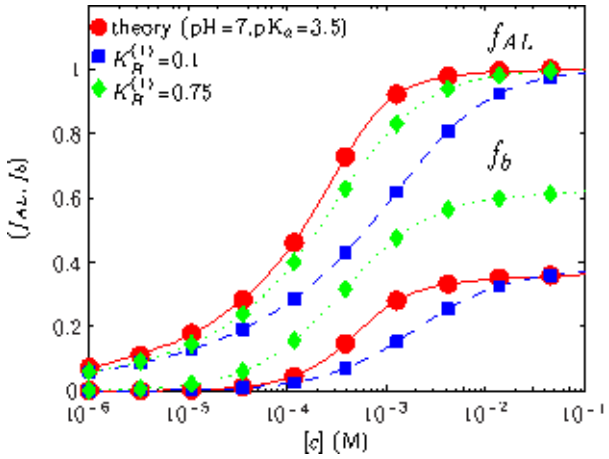

Figure 2.3 Plot of f_{AL} and f_b as a function of concentration at neutral pH. The result of the theory is compared with the predictions of LPB with two different binding constants.

where a_1, a_2 are defined in Eq. 2.25 and explicit values are given in Table 2.1. Reported binding constants for ions such as K^+ are within this range, while slightly higher values have been quoted for Na^+. Obvious to say that the previous formula has systematic errors arising from the approximations involved in the free energy, but it is difficult to provide a rigorous estimate of these errors.

Divalent counterions at neutral pH fully deprotonate PS ($f_{AL} = 1$), even at trace concentrations $< 10^{-6}$M, with a Stern layer that basically neutralizes all the PS charges ($f_b \sim 0.5$), as clear from Fig. 2.4. In these situations, where f_b varies over such a narrow range, the present model is completely equivalent to LPB with the binding constant obtained from Eq. 2.13

$$K_B^{(2)} = K_m \exp(\frac{l_B}{a_L}(a_1 + a_2)) \approx 7\mathrm{M}^{-1} \ , \tag{2.16}$$

in excellent agreement with experimental results $K_B \sim 10\mathrm{M}^{-1}$[91] as well as with other, less sophisticated theoretical estimates [59]. In Fig. 2.4 the comparison between the free energy of this model and LPB ($K_B^{(1)}$=10) clearly shows the equivalence between both models. Above 0.1M the interface is slightly positively charged, thus exhibiting the phenomenon of charge inversion [46, 60].

In order to provide a better illustration on the effect of divalent ions on PS and the inequivalence of the present model with LPB, results at pH=5.2 are shown in Fig. 2.5. Here

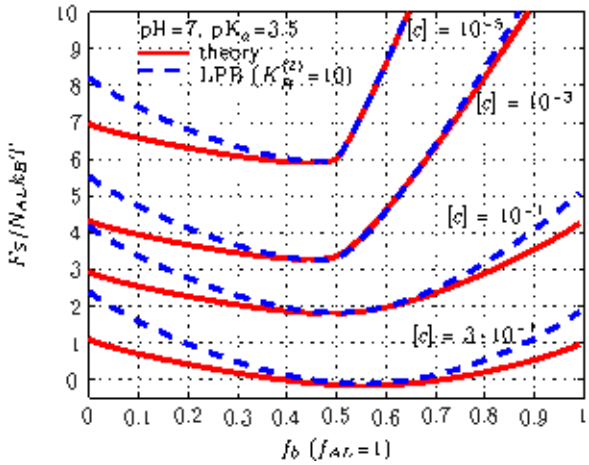

Figure 2.4 Free energy as a function of f_b for $f_{AL} = 1$ at neutral pH. Also plotted are the results of the LPB model with $K_B = 10$. for $[c] = 0.3$M $f_c > 1/2$ thus showing charge inversion. The free energies have been shifted by a constant for proper comparison.

again, the theoretical curve is well described by LPB with $K_B^{(2)} = 10$, but only for concentrations $[c] > 10^{-3}$, while at low concentrations LPB predicts a partially protonated PS. Results for lower pH values show more dramatic differences. This figure also illustrates how the free energy gain from electrostatic correlations forces higher deprotonation than predicted by LPB. It is also noticeably that although the onset of charge inversion is the same, its magnitude is enhanced (as compared with LPB) at large concentrations, as correlations grow for increasing f_b.

Fig. 2.6 analyzes a system with both mono and divalent salts. The monovalent salt concentration was taken as $[c^{(1)}]$=0.1M, which is the limit of applicability for PB. As divalent salt concentration is increased, divalent ions replace the monovalent ones at the Stern layer. It is remarkable that the effect of divalent salt is already significant for $[c^{(2)}] > 10^{-5}$M, four orders of magnitude lower than the monovalent salt concentration in the system. This particular system (PS with divalent ions at fixed [NaCl]=0.1M) was extensively studied in Ref. [91]. Experiments reported excellent agreement of ζ-potential measurements with LPB ($K_B^{(1)} = 0.6$, $K_B^{(2)} = 10$). These binding constants are in agreement with the ones predicted by this theory for solutions with only monovalent or divalent salts. A more detailed analysis, shown in Fig. 2.6 shows that

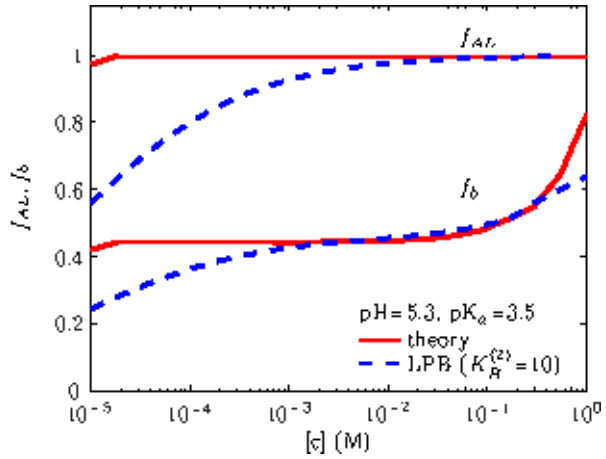

Figure 2.5 Plot of f_{AL} and f_b as a function of concentration at pH=5.2. The result of the theory is compared with LPB with $K_B = 10$. The enhanced deprotonation is attributed to long-range electrostatic effects, as discussed in the text.

the quantities $f_b^{(1)}$ and $f_b^{(2)}$ are quite sensitive to the value of $K_B^{(1)}$ and in fact $K_B^{(1)} \sim 1$ fits well $f_b^{(1)}$ but shows some slight discrepancy for $f_b^{(2)}$ while $K_B^{(1)} \sim 0.3$ fits $f_b^{(2)}$, but with some discrepancy on $f_b^{(1)}$. If the ζ-potential, which is a combination of $f_b^{(1)}$ and $f_b^{(2)}$, would be fitted instead, another value for $K_B^{(1)}$, intermediate between the two, would be obtained. Although those are not dramatic variations, do reflect, once again, the limitations of LPB, as previously discussed for monovalent ions.

2.5 Conclusions

2.5.1 Summary of results

This paper has presented a minimal model that describes both the Stern and diffuse layer by classical electrostatics, except for protons (hydronium ions), which require the introduction of a chemical binding constant (the pK$_a$). The model leads to a set of equations that can be solved self-consistently by numerical minimization. Despite its relative simplicity, the model successfully describes experimental results on PS without resorting to fitting parameters.

The model compares well with available simulation results as shown in Appendix 2.E, thus extending a previous model based on Bjerrum pairing [59]. In particular, the potential of mean

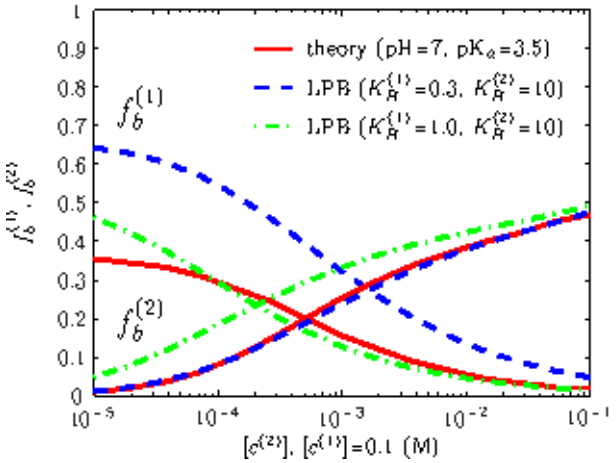

Figure 2.6 Plot of f_{AL} and f_b as a function of divalent salt concentration for fixed monovalent concentration $[c^{(1)}] = 0.1$M at neutral pH. The result of the theory is compared with the predictions from LPB with two different values for the binding constants.

force clearly reveals the fundamental role played by discrete interfacial charges as opposed to a smooth charge distribution. It also points the limitations of the model at large electrolyte concentration of multivalent ions (less than 0.1M for divalent ions), as in this case, correlations significantly spread beyond the Stern layer, a situation that is not accounted by the present model.

Our results provide a clear explanation on the success of chemical models to describe experimental data, allows to highlight its limitations and points to effects that cannot accurately be accounted by those. Measurable quantities computed from the model can be described with reasonable accuracy by the standard chemical model (or LPB, see SubSect. 2.3.3) over several decades in salt concentration. Yet, the actual values of the binding constants extracted by fitting the model by LPB show an inherent dispersion, depending on the particular observable studied. Rather interestingly, this dispersion is within the range of experimentally reported values for binding constants, but it does reflect the limitations of describing the long-range electrostatic force by binding constants that can only account for short-range interactions.

The effect of long-range electrostatics at the Stern layer become more dramatic for ions of higher valency. The enhanced (as compared with monovalent ions) electrostatic correlation free energy makes it more favorable to increase the interfacial charge via deprotonation and replace

the Stern layer with divalent (or higher valency) counterions, as shown in Fig. 2.5. This effect is expected to become more dramatic for AL with many charged groups and is not accurately described by the LPB model as shown in Fig. 2.5. The same effect has been theoretically discussed in Ref. [60], and there is experimental evidence on monolayers of PA and PIP_2 at the air-water interface [97, 98, 51, 99].

Despite its limitations, unless high precision data is obtained on a simple system where parameters such as molecular area and charge can be precisely controlled over a wide range of values, chemical models generally provide a reasonable effective description of experimental results.

2.5.2 Chemical vs physical effects

Except for the proton, which requires the specification of the pK_a, the remaining ions have been assumed to interact with the charged interface via classical electrostatics. Due to its inherent stability, ions with the electronic structure of a noble gas, such as the alkali (Na^+,K^+,etc..), alkali earth ions (Ca^{2+},Ba^{2+}, etc..) or Halogens (Cl^-,Br^-,I^-,etc..) are the obvious candidates to be described by classical electrostatics, while other soluble ions such as transition metals (Cu^{2+},Pb^{2+}, Cd^{2+}, Ni^{2+}, Fe^{2+}, etc..) are likely to exhibit some degree of covalent bonding with most interfacial groups.

Some support for this hypothesis can be given by the analysis of stability constants [100], which account for the binding constants of ions to certain ligands. Sticking to the example of carboxylic groups, a look at the entries for simple carboxylic acids (formic, acetic and propanoic), shows binding constants within the range (with some dispersion) $K_B^{(1)} \sim 0.5, K_B^{(2)} \sim 10\mathrm{M}^{-1}$, the typical values obtained from our model, and thus supporting the idea of a classical electrostatic interaction between those ions and carboxylic groups. Entries for the transition metal ions, however, are between 5 to 10 times larger, thus providing strong evidence for some degree of covalency or chemical specificity. Even for ions such as Ca^{2+} the situation is not as simple; the entry for Carbonic acid with Ca^{2+} shows four entries, the first two correspond to binding to $CaCO_3^{2-}$ and $CaCO_3H^-$ and have values $K_{B,2}^2 = 1400$ and $K_B^2 = 10.0$, while the two additional entries are solubility products (calcite and aragonite crystals) with $CaCO_3^{2-}$,

thus showing that besides the classical electrostatic interactions corresponding to the first two entries (see Ref. [59] and [101] for the first, which corresponds to Bjerrum pairing), Ca^{2+} ions show some degree of covalent interaction, depending on the ligand. Similar conclusions are reached by analyzing phosphate, amino or any other groups.

Another source for specific ionic effects are related to explicit solvent effects. Ions have hydration sheaths, and those are distorted or eliminated upon binding. Generally, it should not be a dominant effect as most commonly, cations bind to interfacial oxygens, so upon binding, they trade one oxygen (from the water molecule at its hydration sheath) to another, with basically no change in enthalpy, and if anything, a gain in entropy for the water molecules that leave the hydration sheath. Yet, even for those cases where these free energies need to be included, the dehydration involves short-range interactions and are, therefore, describable by binding constants, which can be computed, for example, from more detailed atomistic simulations.

A general model applicable to all situations requires the inclusion of specific interactions related to the ions and the charged or uncharged groups at the interface. The critical quantity that needs to be known is the ionic-specific free energy ΔG_{Spec}, defined as the free energy gain once the universal electrostatic interaction has been subtracted. Once this quantity is known, an unambiguous binding constant can be defined and a term like Eq. 2.14 is added in addition to the free energy Eq. 2.1. The next issue is how to determine ΔG_{Spec}. A rough estimate is probably obtained by subtracting from the binding free energy the reference free energy of an interfacial-counterion pair, which can be calculated within the present theory. For example, taking 10 M^{-1} as the reference binding constant for a purely electrostatic interaction, and given that $K_B^{(2)} = 40$ M^{-1} for binding of Ni^{2+} to PS^-, this gives $\Delta G_{Spec}^{PS} = -3.40 k_B T$ for PS^{-1}-Ni^{2+}. Of course this number is specific for that particular system. First principle calculations, without resorting to experimental data, would certainly require sophisticated quantum chemistry calculations.

2.5.3 Implications for phospholipid systems

Concrete application to a simple coarse-grained model of PS shows good agreement with experimental results[91], despite the questionable approximation of modelling PS as consisting

of a single negative charge, as discussed in Subsect. 2.4.1. The large values of ion binding constants in zwitterionic phospholipids such as PC [91] ($\sim 3\mathrm{M}^{-1}$) show that the positively charged amino group is sufficiently far apart to preempt the negatively charged oxygen within the phosphate group to bind counterions, which could be relevant for PS also. These considerations demand a more detailed modelling of the phospholipid head group, where all charges are included. In fact, Ref. [91] reports that the binding constant for Ca^{2+} with PS is enhanced by a factor of almost 3 at low monovalent salt concentration, a result that is not reproduced by our model (data not shown). This is a large enhancement, not observed in other molecules for decreasing ionic strength[100], but a more detailed analysis is needed. These considerations become even more relevant for investigating complex phospholipids such as PA[97] or PIP_2 [94]. It is not difficult to incorporate the nuances required to describe those phospholipids, and they will be fully addressed in a subsequent publication. Those effects are key for a proper understanding of electrostatic induced phase separation in lipid mixtures, as discussed, for example, in Ref. [102].

2.5.4 Outlook

As for the question posed in the title of this paper on whether electrostatic correlations near charged interfaces are described by physics (universal) or chemistry (specific), the answer seems clear: any model that aims to be complete and realistic must incorporate both.

Acknowledgements

AT acknowledges endless discussions with J. Faraudo and C. Calero and D. Vaknin for his many insightful remarks and inspiring experimental results. This work is supported by NSF CAREER award DMR-0748475.

2.A General Expression for PB with both Monovalent and Divalent Salts

Here we just quote the main formulas for the free energy of a planar charged interface in contact with a solution containing both monovalent and divalent salt with respective bulk

concentrations $c^{(1)}$ and $c^{(2)}$ within PB. The expression is

$$\frac{\mathcal{F}}{Nk_BT} \equiv \mathcal{F}_{PB} = |\frac{e\psi(0)}{k_BT}| - \frac{1}{2b}\mathcal{Y}(\frac{e\psi(0)}{k_BT}, \frac{c^{(2)}}{3c^{(2)}+c^{(1)}}) \tag{2.17}$$

where N_B is the number of charges (of valence -1) at the interface and b has been defined in Eq. 2.6 (and used here with $q = 1$). The Debye length is $\lambda_D = 1/\sqrt{8\pi l_B(3c^{(2)}+c^{(1)})}$ and the function $\mathcal{Y}(x,a)$ is defined as

$$\begin{aligned}\mathcal{Y}(x,a) &\equiv \frac{1-3a}{2\sqrt{2}a}\log\left(\frac{1-a+2a\exp(-x)+2\sqrt{a(1-a)\exp(-x)+a^2\exp(-2x)}}{(1+\sqrt{a})^2}\right) \\ &+ \frac{a\exp(-2x)+(1+a)\exp(-x)+2(1-a)}{\sqrt{(1-a)\exp(-x)+a\exp(-2x)}} - 3\end{aligned} \tag{2.18}$$

The relation between the surface charge σ and the contact potential $\psi(0)$ is obtained from the PB equation, and can only be solved analytically for the case of monovalent salts. For the other cases it is solved numerically and the result is inserted into Eq. 2.17, thus providing the free energy.

2.B Derivation and Details of the Different Terms Forming the Free Energy

2.C Derivation of F_{Prot}

The free energy of a charged interface consisting of N_B charges is given within PB by

$$\begin{aligned}\frac{F}{k_BT} &= 2N_B(\log(b+\sqrt{b^2+1}) + (1-\sqrt{1+b^2})/b) \\ &+ \sum_a N_a(\log(N_a v_0/V) - 1) \equiv \frac{F_E}{k_BT}\end{aligned} \tag{2.19}$$

where b is the ratio of the Debye and the Guoy-Chapman length. The last term, which is the same for other counterion and co-ion valences, is the bulk entropy of the ionic species. Because the interface gets charged by releasing protons, there are $N^1_{prot} = N_B$ protons in bulk whose origin are the interfacial groups, so the last term in Eq. 2.19 is dependent on N^1_{prot}. It will be assumed that the number of protons in bulk N^0_{prot} largely exceeds the ones released by charging the interface ($N^1_{prot}/N^0_{prot} << 1$).

The free energy is computed from a reference state where all the interfacial groups are deprotonated $N_B = N_{AL}$ (or $N_{prot} = N_{AL}$), thus the second term in Eq. 2.19 becomes

$$\frac{F_E}{k_B T} = \frac{F_{ref}}{k_B T} + N^1_{prot} \log(N^0_{prot} v_0 / V) \ , \tag{2.20}$$

where F_{ref} is independent of N^1_{prot}. If the reference volume v_0 is taken as $v_0 = 1\mathrm{M}$ the previous term becomes $\log(N^0_{prot} v_0/V) \equiv -\mathrm{pH}\log(10)$.

Generally, protons have a favorable free energy (ε_A) to remain bound to the AL head group. This is taken into account as

$$\frac{F_A}{k_B T} = -\varepsilon_A (N_{AL} - N_B) \ . \tag{2.21}$$

The energy ε_A is related to the binding constant K_a between AL groups and protons according to $\mathrm{K}_a = \frac{1}{v_0}\exp(-\varepsilon_A/k_B T)$. If $v_0 = 1M$, then $\mathrm{pK}_a = \log_{10}(K_a)$ and $\varepsilon_A = k_B T \log(10)\mathrm{pK}_a$. Consistently using the reference volume $v_0 = 1M$, the two terms Eq. 2.20 and Eq. 2.21 become

$$\frac{F_{Prot}}{N_{AL} k_B T} = f_{AL}(\mathrm{pK}_a - \mathrm{pH})\log(10) \ , \tag{2.22}$$

which is the result quoted in Eq. 2.8.

2.D Derivation of F_{Corr} (1 pK_a case)

This term contains three contributions. The first term is the static electrostatic energy, where both interfacial charges and counterions are at fixed positions, and is the equivalent of the Madelung energy for ionic crystals. The remaining two terms have a thermal origin and will be considered further below. The static electrostatic energy is computed by placing the AL charges on a planar lattice. It is assumed that counterions are contained on the same plane defined by the lattice, and that the free energy is expressed as a function of the lattice constant a_L, which is related to the molecular area A_c as $a_L = \sqrt{\frac{2A_c}{\sqrt{3}}}$ (triangular) or $a_L = \sqrt{A_c}$ (square). The free energy is computed from

$$\mathcal{F}_{Corr} = \frac{1}{2}{\sum_{i,j}}' q_i q_j \frac{e^2}{\varepsilon_w r_{ij}} \ , \tag{2.23}$$

where the prime indicates that the term with $i = j$ is not included in the summation. Because this summation runs over the entire lattice, it requires the use of Ewald summation techniques

for systems with two-dimensional periodicity [103]. The result is

$$\frac{\mathcal{F}_{Corr}}{N_{AL}k_BT} = -f_{AL}^{3/2}\gamma(f_b)\frac{l_B}{a_L} \ , \tag{2.24}$$

where $\gamma(f_b)$ is a function of the fraction of counterions bound to the head-group f_b. For $f_b = 0$, the results are the Madelung energies of a triangular ($\gamma = 2.107$) or a square ($\gamma = 1.95$) lattice. The sum Eq. 2.23 is evaluated at two values of f_b ($f_b = 1/2$ and $f_b = 1$) (see Fig. 2.7) and the full $\gamma(f_b)$ function is constructed as a polynomial that interpolates among these two values

$$\gamma(f_b) = a_0 + a_1 f_b + a_2 f_b^2 \ . \tag{2.25}$$

Evaluation of the Ewald sum for intermediate values of f_b did not show any significant improvement by considering a higher order polynomial or by optimizing its coefficients by a best fit. It should be pointed out that the function $\gamma(f_b)$ involves an approximation, as the coefficients a_i are computed at $f_{AL} = 1$, so the expression for the correlation energy is expected to become somewhat inaccurate for $f_{AL} << 1$.

The function $\gamma(f_b)$ is dependent on the relative position of the counterions with respect to the AL charges. Numerical minimization shows that the minimum electrostatic energy in Eq. 2.24 occurs when the counterions are as close as possible to the AL charged groups. The γ-function was therefore computed for given molecular area and typical AL-counterion distance of r_0, as shown in Fig. 2.7. Reasonable variation on the positions of the counterions typically change Madelung energies by less than 10%. The a_i coefficients for the different cases relevant to this paper are shown in Table 2.1. If both monovalent and divalent ions are involved, the γ-function is dependent on the two variables $f_b^{(1)}$ and $f_b^{(2)}$:

$$\begin{aligned} \gamma(f_b^{(1)}, f_b^{(2)}) &= a_0 + a_1^{(1)} f_b^{(1)} + a_1^{(2)} f_b^{(2)} + \\ &+ a_2^{(1)}(f_b^{(1)})^2 + a_2^{(2)}(f_b^{(2)})^2 + a_2^{(1,2)} f_b^{(1)} f_b^{(2)}, \end{aligned} \tag{2.26}$$

where only the $a_2^{(1,2)}$ coefficient is unknown as the others have already been determined in Table 2.1. This coefficient was computed by evaluating the Ewald sum for $f_b^{(1)} = 1/4$ and $f_b^{(2)} = 1/4$ and obtaining the unknown coefficient from Eq. 2.26 and the actual results in Table 2.1. The result for a triangular lattice with $A_c = 70\text{Å}^2$ and $r_0 = 2.8\text{Å}$ is $a_2^{(1,2)} = 4.93$.

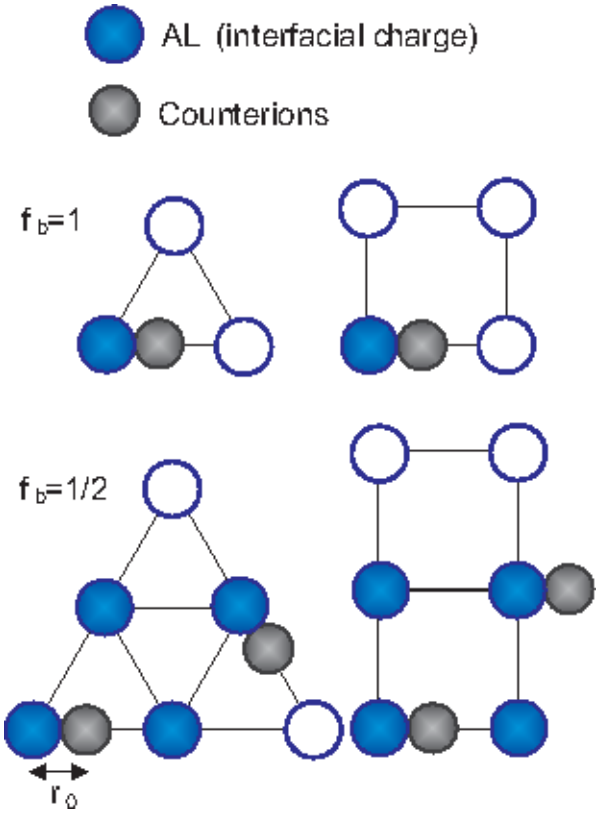

Figure 2.7 Configurations used to compute the static correlation energy $f_b = 1$ and $f_b = 1/2$. The configuration $f_b = 1/2$ can be used to compute $f_b^{(1)}$ and $f_b^{(2)}$ by placing a divalent and a monovalent charge on every site. Empty circles do not belong to the unit cell and are obtained from lattice translations.

Table 2.1 Coefficients for the electrostatic correlation energy (See Eq. 2.25), computed as described in the text for different counterion valences (q). The top value is computed for a triangular lattice while the bottom one is for the square.

	$A_c = 70\text{Å}^2$			$A_c = 40\text{Å}^2$		
q_{AL}=-1	Mono	Div	Tri	Mono	Div	Tri
a_0	2.107	2.107	2.107	2.107	2.107	2.107
	1.950	1.950	1.950	1.950	1.950	1.950
a_1	0.116	1.635	4.760	0	0.475	2.975
	0.130	1.298	4.924	0	0.589	3.540
a_2	1.268	5.346	12.03	0.834	5.406	12.166
	1.196	5.096	10.60	0.864	4.882	10.600

Similarly as for protons, counterion binding and release involves changes in bulk entropy. Adapting the same derivation (see Appendix 2.C) leads to the second term in F_{Corr}

$$\frac{F}{N_{AL}k_BT} = -f_b \log(v_0[c]) \ , \tag{2.27}$$

where v_0 is an arbitrary volume.

Bound counterions are not immobile, as assumed in the calculation of the first term Eq. 2.24, but do fluctuate from their equilibrium positions, and this is the origin of the third contribution to F_{Corr} in Eq. 2.11. The fluctuation free energy of counterions bound to the head-group requires a repulsive short-range potential between counterions and AL charges, which is assumed to be of the form $V(r) = 4\epsilon(\frac{\sigma}{r})^{12}$. It is also assumed that the dominant electric field relevant for counterion fluctuations is the one from its nearest AL charge. In this way, the attractive electrostatic force and the repulsive short-range lead to an equilibrium distance r_0, with quadratic fluctuations at leading order.

$$\delta\mathcal{F}_{Corr}(r) = \frac{11|q|e^2}{2r_0^3\varepsilon_w}(r-r_0)^2 \equiv \frac{\kappa}{2}(r-r_0)^2 \ , \tag{2.28}$$

so the fluctuation free energy per particle becomes

$$2\pi \int dr r^2 \exp(-\frac{\kappa(r-r_0)^2}{2k_BT}) = \sqrt{\frac{2\pi}{11}}\frac{2\pi r_0^3}{\sqrt{ql_B/r_0}} \ , \tag{2.29}$$

where $\frac{\kappa r_0^2}{k_BT} = \frac{11qe^2}{K_BTr_0\varepsilon_w} = 11q\frac{l_B}{r_0} >> 1$ has been used to simplify the above expression. It is assumed that the AL charge is anchored to the head group and therefore the available solid angle is 2π [59], as opposed to 4π (if the AL charge was in solution). The free energy is

$$\mathcal{F}_{bound} = f_b \log(\frac{v_0}{2\pi r_0^3}\sqrt{\frac{l_B|q_c|}{r_0}}\sqrt{\frac{11}{2\pi}}) \ . \tag{2.30}$$

The physical interpretation is that counterions fluctuate over a distance $\sim r_0\sqrt{r_0/l_B|q_C|}$ along the direction of the AL-counterion axis.

The three terms Eq. 2.25, Eq. 2.27 and Eq. 2.30 provide the explicit expressions for the electrostatic correlation free energy Eq. 2.11.

Table 2.2 Comparison between the results of simulations (Ref.[58]) and the theoretical results for *sigma* at three different 2:1 salt concentrations. The results correspond to a square lattice with $q_A L$=-1 interfacial charges with r_0=3Åand bare σ=-0.1nm^{-2} (A_c=1000Å^2)

[c]	σ (MD)	σ(theor.)	Error
(M)	nm^{-2}	nm^{-2}	%
0.023	-0.0079	-0.0074	6
0.033	-0.0078	-0.0070	10
0.058	-0.0074	-0.0062	16

2.E Comparison with Numerical Simulations

Recent numerical simulations by Calero and Faraudo [58] have explored in detail the role of interfacial charges by performing numerical simulations of an electrolyte primitive model of 2:1 salt near discrete interfacial negative charges on a plane and arranged in a square lattice. Although the paper is mainly focused on high electrolyte concentrations, where the role of electrostatic correlations becomes significant beyond the Stern layer, it is possible to provide some comparison with the present theory. A more systematic comparison will be provided in the future.

We will first consider the density of charge, $\sigma = -e\frac{1-2f_b^{(q)}}{A_c}$ (note that $f_{AL} = 1$ and only divalent ions are considered). The comparison MD simulation versus theory for σ, shown in Table 2.2 show good agreement for the lowest concentrations and diverge slightly at the largest concentra- tion. Most likely, this divergence is due to the neglect of screening effects at the Stern layer, which would decrease the correlations and with it, the number of counterions bound to head groups. These effects can easily be incorporated into the sum defining the gamma coefficients Eq. 2.24. Although relevant for comparing with simulation results, the effect of screening at the Stern layer may not need be included in some experiments. In order to extent the results to even higher concentrations 0.1M, activity coefficients that depart from unity need to be considered, a result not included by the present theory, as PB theory is assumed. We point out that it is possible to account for activity coefficients by including Bjerrum pairing in bulk. [104, 105]

Another important quantity is the potential of mean force. This quantity elucidates the

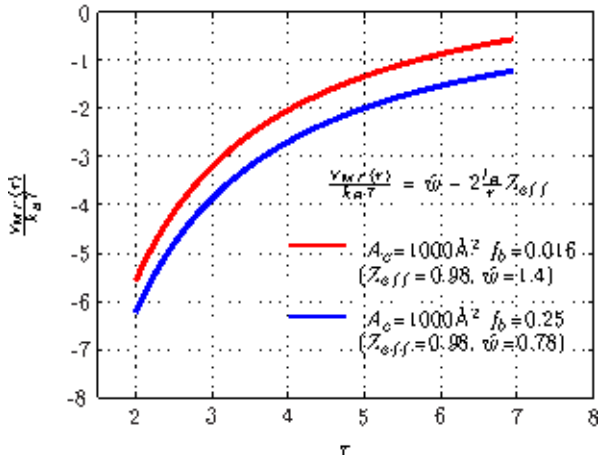

Figure 2.8 Plot of the potential of mean force for the same system as in the previous figure. The fits to the potential shown are indistinguishable from the model.

role of discrete charges and provides a clear insight on the consequences of the present theory. Results for the potential of mean force V_{MF} are shown in Fig. 2.8 for the same simulations described previously, where it is shown that the potential of mean force has a simple analytical form of the type

$$\frac{V_{MF}(r)}{k_BT} = \hat{w} - 2\frac{l_B}{r}Z_{eff} \tag{2.31}$$

where Z_{eff} is close but smaller than 1. The second term of the potential (with $Z_{eff} = 1$) is the prediction from Bjerrum theory [59], while $\hat{w}$ encodes additional correlations among counterions as well counterions and interfacial charges. Those predictions are in excellent agreement with the numerical simulations by Calero and Faraudo [58] and clearly show the distinct role played by interfacial charges: In a smooth distribution, the potential of mean force could never display a $1/r$ decay, as its origin is the direct (Bjerrum) interaction between the counterion and the interfacial charge closest to it.

2.F Connection with Bjerrum Pairing Theory

Bjerrum pairing theory [59] is the LPB theory

$$\frac{F_{Corr}}{N_{AL}k_BT} = -f_b \log(K_B v_0[c]) \ , \tag{2.32}$$

with the explicit expression for K_B borrowed from Bjerrum pairing theory [101, 104]

$$K_B = 2\pi \int_{r_0}^{|q_c l_B|/2} dr r^2 \exp(q\frac{l_B}{r}) \ . \tag{2.33}$$

This expression is closely related to the effective K_B^{eff} defined in Eq. 2.13. This is more clearly seen in the limit $ql_B/r_0 >> 1$, where the Bjerrum constant above becomes

$$K_B \approx 2\pi \frac{r_0^4}{ql_B} \exp(ql_B/r_0)(1 + 4r_0/(ql_B) + \cdots) \tag{2.34}$$

The term in the exponential is the electrostatic energy when particles are frozen in their positions (Eq. 2.24), while the pre-factor contains the free energy of the fluctuations Eq. 2.30. Compared with more rigorous expressions such as Eq. 2.16 the simple expression above does not depend on f_{AL},f_b, molecular area A_c etc.., but it nevertheless provides a reasonable semi-quantitative estimate for binding constants [59].

Bjerrum pairing assumes a hard core potential and the formulas used in this paper are for softer $1/r^{12}$-potentials, which explains the different analytical prefactors. Finally, the expansion Eq. 2.34 is significantly inaccurate for $q_C l_B/r_0 \lesssim 20$ as in that case, fluctuations from r_0 are not small.

CHAPTER 3. GENERAL SOLUTION TO THE ELECTRIC DOUBLE-LAYER WITH DISCRETE INTERFACIAL CHARGES

A paper published in the Journal of Chemical Physics

Sweta Vangaveti and Alex Travesset

3.1 Abstract

We provide extensive molecular dynamics simulations of counterion and coion distributions near an impenetrable plane with fixed discrete charges. The numerical results are described by an explicit solution that distinguishes the plasma ($\sqrt{A_c}/\sigma > 3$) and the binding regime ($\sqrt{A_c}/\sigma < 3$) where σ is the ion diameter and $A_c = |e/\nu|$ (ν is the surface charge density). In the plasma regime, the solution consists of a product of two functions that can be computed from simpler models and reveals that the effects of the discreteness of the charge extends over large distances from the plane. The solution in the Binding regime consists of a Stern Layer of width σ and a diffuse layer, but contrary to standard approaches, the strong correlations between ions within the Stern Layer and the diffuse layer require a description in terms of a "displaced" diffuse layer. The solution is found to describe electrolytes of any valence at all concentrations investigated (up to 0.4M) and includes the case of additional specific interactions such as Van Der Waals attraction and other generalizations. We discuss some open questions.

3.2 Introduction

Describing charged molecules in aqueous solutions presents considerable challenges as the charge, both its magnitude and distribution, is highly dependent on the environment, and, in addition, the high dielectric constant of water renders electrostatic interactions only marginally

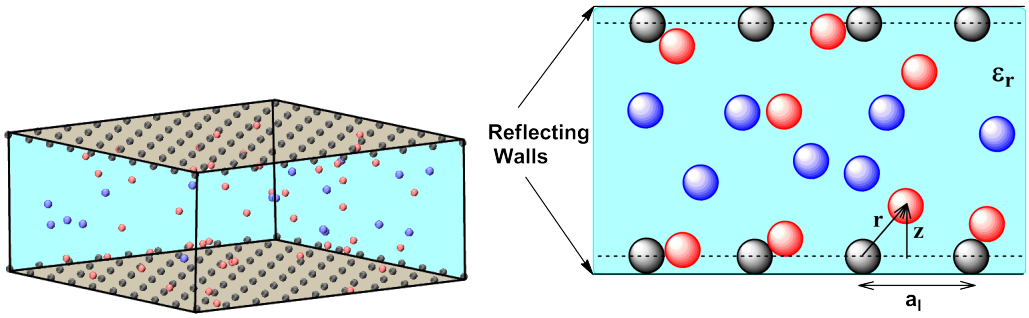

(a) The PDDL model (b) Cross sectional view

Figure 3.1 The Planar Discrete Double Layer model. The charges at the interface are in gray, counterions in red and coions in blue.

stronger than thermal effects and other competing interactions. Furthermore, because of its long-range nature, coarse-graining electrostatic interactions presents significant difficulties, as for example, replacing discrete electric charges by a continuum distribution immediately eliminates effects resulting from the intrinsic discreteness of electric charges, i.e. correlation effects. A familiar example is provided by table salt (NaCl) whose crystalline structure at room temperature is entirely stabilized by correlations.

A reasonable approach to coarse-graining electrostatics is provided by the Single Particle Equivalent Charge (SPEC) approximation, where a group of charges is replaced by a single particle whose charge is given by the equivalent charge (the sum of all the individual charges) of the group. The SPEC approximation naturally leads to consider models such as the Planar Discrete Double Layer (PDDL) model, shown in Fig. 3.1, which consists of immobile charges on a plane in contact with an electrolyte solution.

In this paper, we provide a general solution to the PDDL model. Our study is motivated by the need to provide a rigorous framework to describe electrolytes in contact with charged amphiphilic systems, such as monolayers and bilayers, that goes beyond the classical description of the problem in terms of a Stern layer, which encodes all interfacial effects, followed by a diffuse layer. Despite this practical motivation, the paper will entirely be focused on the statistical mechanical description of the PDDL model, leaving its implications for future studies.

The unavoidable starting point of any discussion on electrostatics in aqueous media is the

standard Poisson-Boltzmann theory (PB) [41, 42], which despite its relative simplicity, successfully describes many experimental systems [41, 42, 43, 35]. Even within PB, the solution to the PDDL model presents enormous difficulties; A first approximate numerical solution was provided already in the seventies by Nelson and McQuarrie[52] and more recently, the problem has been revisited [54, 55] including also approximations that go beyond PB[53, 56], leading to the conclusion that the differences between the PDDL and the standard double layer, where the charge is uniformly distributed on the plane, amounts to minor quantitative details. Madurga et al. [57] considered simulations of the PDDL where the plane of the interfacial charges is at different positions with respect to the reflecting wall, see Fig. 3.1, and observed significant differences in the ionic distribution only when the interfacial charges are sufficiently exposed to the electrolyte solution. Subsequent MD simulations of the PDDL by Calero and Faraudo[58] with divalent counterions did show that charge discreteness has a dramatic effect on the structure of ionic distributions; They found that the potential of mean force (more appropriately, the *radial* potential of mean force) between interfacial charges and mobile counterions was well described by a simple Coulomb potential, thus confirming early predictions in Ref. [59] based on the generalization of Bjerrum pairing, see also Ref. [60]. Related studies[106, 107] have studied discreteness effects for two plates without salt at small separations, and found significant differences between discrete and uniform distributions.

Before dwelling further into the effect of discrete charges, there are some results of the standard double layer that are worth reviewing. Calculations within the Modified Poisson Boltzmann (MPB) theory [61, 62] or the more accurate Hypernetted Chain Approximation (HNC) [108] and its anisotropic version (AHNC) by Kjellander and Marcellja [63, 64, 65] provide, in many cases, almost exact results, particularly at medium to high ionic strength. Still, given the mathematical complexities of these theories, models with more transparent physical interpretations, albeit far less accurate, have been developed. Shklovskii and collaborators [44] describe the immediate layer of counterions next to the charged interface as a strongly two dimensional correlated liquid, whose properties are well characterized [66] (the "Wigner Crystal"). Monte Carlo simulations for multivalent (trivalent and tetravalent) ions have provided some validation to these theories[67, 68]. Somewhat related, yet developed within a more

formalistic framework is the strong coupling (SC) expansion of Netz and collaborators [45].

The organization of the paper is as follows, we will first present the details of the model and some necessary definitions in Sect. 3.3. The results of our numerical simulations are provided in Sect. 3.4. We summarize the numerical results into an general solution in Sect. 3.5. General implications and future challenges with the solution are discussed in Sect. 3.6.

3.3 Model and Observables

The PDDL consists of an impenetrable wall with fixed charges of valence q_0 arranged in a square lattice with lattice constant a_L, as shown in Fig. 3.1. i.e. the wall has a surface charge $\nu_0 = q_0/A_c$, where the molecular area is $A_c = a_L^2$. The wall is in contact with a solution containing counterions and co-ions of respective valence q_1 and q_2. Sufficiently far from the wall, in bulk, the concentration of these ions is n_α^b ($\alpha = 1, 2$ for counterions and coions respectively) and satisfies the neutrality condition $\sum_{\alpha=1}^{2} q_\alpha n_\alpha^b = 0$. All charges have a finite radius, introduced as a short-range potential V_{SR}, so that the total interaction between any two ions is given by

$$V_{TOT}(r) = k_B T \frac{q_\alpha q_\beta l_B}{r} + V_{SR}(r) \ , \tag{3.1}$$

where $l_B \equiv \frac{e^2}{\varepsilon_r k_B T} \approx 7.1$Å is the Bjerrum length, and $\varepsilon_r = 78$ is the dielectric constant of water, which is treated implicitly. For simplicity, we will assume that the short-range interaction potential is the same for all ionic species. Critical in our study is the number density distribution

$$n_\alpha(\vec{r}) = \sum_{i=1}^{N_\alpha} \langle \delta^3(\vec{r} - \vec{r}_i^{\,\alpha}) \rangle \ , \tag{3.2}$$

where $\alpha = 1, 2$ depending on whether counterions or coions are considered and N_α is the total number of ions of type α. The vector $\vec{r}$ is defined such that it has the origin at one of the interfacial charges, (see Fig.3.1). The function $n_\alpha(\vec{r})$ has the same periodicity as the underlying lattice. We also consider the two point correlation function

$$n_{\alpha,\beta}(\vec{r}, \vec{r}') = \sum_{i=1}^{N_\alpha} \sum_{j=1}^{N_\beta} \langle \delta^3(\vec{r} - \vec{r}_i^{\,\alpha}) \delta^3(\vec{r}' - \vec{r}_j^{\,\beta}) \rangle \ , \tag{3.3}$$

where again, both $\vec{r}$ and $\vec{r}'$ have their origin at an interfacial charge. The potential of mean force of counterions or co-ions with respect to the interfacial charge is defined as

$$\frac{w_\alpha(\vec{r})}{k_BT} = -\ln(g_\alpha(\vec{r}))\ , \tag{3.4}$$

where the pair distribution function is $g_\alpha(\vec{r}) \equiv n_\alpha(\vec{r})/n_\alpha^b$ and n_α^b is the value of the ion concentration in bulk, sufficiently far from the interface. It is also of interest to consider the potential of mean force of mobile ions, defined as

$$\frac{w_{\alpha,\beta}(\vec{r},\vec{r}')}{k_BT} = -\ln(g_{\alpha\beta}(\vec{r},\vec{r}')) \tag{3.5}$$

where $g_{\alpha\beta}(\vec{r},\vec{r}') \equiv n_{\alpha,\beta}(\vec{r},\vec{r}')/n_\alpha(\vec{r})n_\beta(\vec{r}')$.

Anticipating results, it is worth considering the case where the number density Eq. 3.2 is rotationally invariant, that is, only a function of r and z (see Fig. 3.1) and can be written as a product of two functions, each one depending on r and z respectively

$$n_\alpha(r,z) = \hat{n}_\alpha(z)\exp\left[-\frac{\hat{w}_\alpha(r)}{k_BT}\right] \tag{3.6}$$

In this particular situation, the number density function as a function of the radial distance r is given by

$$n_\alpha^R(r) \equiv \int_0^r \frac{dz}{r} n_\alpha(r,z) = \frac{\exp[-\frac{\hat{w}_\alpha(r)}{k_BT}]}{r}\int_0^r dz\hat{n}(z)_\alpha \tag{3.7}$$

A radial potential of mean force can be defined from $w_\alpha^R(r) = -\ln n_\alpha^R(r)/n_\alpha^b$, which from Eq. 3.7 is

$$w_\alpha^R(r) = \hat{w}_\alpha(r) - k_BT\ln(\frac{1}{r}\int_0^r dz\frac{\hat{n}_\alpha(z)}{n_\alpha^b})\ , \tag{3.8}$$

Only when $\hat{n}_\alpha(z) = n_\alpha^b$, that is, when $n_\alpha(r,z)$ becomes independent of z, it is that $w_\alpha^R(r) = \hat{w}_\alpha(r)$, otherwise these two functions differ, as clear from the second term in Eq. 3.8. The number density as a function of distance from the interface $n_\alpha^D(z)$ can be related from simple geometrical arguments to $n_\alpha(r,z)$, or equivalently, to $\hat{n}_\alpha(z)$ and $\hat{w}(r)$ from the formula

$$\begin{aligned} n_\alpha^D(z) &= \hat{n}_\alpha(z)\left(2\pi\int_z^{\sqrt{a_L^2/4+z^2}} drr\exp(-\hat{w}_\alpha(r)/k_BT)\right. \\ &+ \left.(1-\frac{\pi}{4})a_L^2\right)\ , \end{aligned} \tag{3.9}$$

where it is assumed that $\hat{w}_\alpha(r) \approx 0$ for $r > a_L/2$. It should be noted that $n_\alpha^D(z)$ can be calculated directly from the simulation as the number density of ions at distance z, so Eq. 3.9 can be used as a self-consistency test on the validity of the calculated $\hat{n}_\alpha(z)$ and $\hat{w}(r)$. For completeness a summary of all the different functions defined and a brief description is given in Table 3.1.

Table 3.1 Summary of functions used in this paper (α=cc (counterions) or co (coions))

Function	Description
$n_\alpha(\vec{r})$	Number density of ions of type α (Eq. 3.2)
$w_\alpha(\vec{r})$	Potential of mean force of α ions with respect to the interfacial charges (Eq. 3.5)
$n_\alpha^R(r)$	Radial number density of α ions next to a particular interfacial charge at the origin (Eq. 3.7)
$w_\alpha^R(r)$	Radial potential of mean force of α ions next to a particular interfacial charge at the origin (Eq. 3.7)
$n_\alpha^D(z)$	number density at coordinate z of α ions, averaged over the other two coordinates. (Eq. 3.9)
$\hat{n}_\alpha(z)$	z-dependent function if $n_\alpha(\vec{r})$ can be written as a product of two functions (Eq. 3.6).
$\hat{w}_\alpha(r)$	r-dependent function if $n_\alpha(\vec{r})$ can be written as a product of two functions (Eq. 3.6)

3.3.1 Simulation methods

We consider a system consisting of $N_0 \equiv N_I$ interfacial charges, $N_1 \equiv N_{cc}$ counterions and $N_2 \equiv N_{co}$ co-ions. The short range potential V_{SR} in Eq. 6.1 is of the Lennard-Jones type

$$V(r) = 4\epsilon_{LJ}\left[\left(\frac{\sigma}{r}\right)^{12} - \left(\frac{\sigma}{r}\right)^{6}\right] + v_0 \tag{3.10}$$

where the cut-off is taken as $r_c = \lambda\sigma$. Three different values of (λ, v_0), namely $(1,0)$,$(2^{1/6}, \epsilon_{LJ})$ and $(3,0)$ were used. The first case is the one used in [58], it is repulsive but it has a discontinuity in the force at the cut-off value. The second case is the familiar repulsive WCA potential,

which is both continuous in energy and force at the cut-off value, and the last case includes a Vander Waals attraction, which models specific interactions of ionic species. Unless specified otherwise, $\epsilon_{LJ} = 1$ kcal/mol and $\sigma = 3$ Å. Results obtained using the $(1, 0)$ case and the WCA potential were indistinguishable, so unless otherwise specified, results with the $(1, 0)$ case will be the ones reported. Both the interfacial and co-ion charges were taken as monovalent and negative ($q_I = -1$, $q_{co} = -1$), but different valences for counterions $q_{cc} = 1, 2, 3$ were considered. The system was investigated by MD using the LAMMPS package (version 5 Sep 2010)[109]. The simulations were carried out in the canonical ensemble with a Noose-Hoover thermostat with a temperature of $T = 300$K. The equations of motion were solved with the Verlet algorithm. The system consists of a slab containing the electrolyte limited by two impenetrable planes perpendicular to the z-axis, where the interfacial charges are placed, (see Fig.3.1). The system is periodic in the x,y directions but not in the z direction. The electrostatic interactions were computed using 2D Ewald summation with slab geometry. We considered simulations with molecular areas $A_c = 40, 70, 100, 361, 501.8$Å^2 as well as different concentrations (0.02M to 0.4M). Another set of simulations where the systems are two dimensional and ions interact via Yukawa potential were also performed. The complete list of all simulations as well as the technical details necessary to reproduce them can be found in the supplementary material in Sect. 4.1. The systems were equilibrated by monitoring typical observables such as the energy, density and the diffusion coefficient. A typical equilibration run took of the order of $3{\cdot}10^5$ time steps and production runs involved $4{\cdot}10^5$ time steps, although larger sets of data were collected in particular cases.

3.3.2 Units of length and temperature

The natural dimension of length is given by the diameter of the charges, σ. Although it would probably be more appropriate to express all lengths in units of σ, we opted for expressing lengths in Å and concentrations in M. Because $\sigma = 3$Å, it is straight-forward to convert from one system of units to another, except for the fact that there is another natural length in the problem, the Bjerrum length $l_B = \frac{e^2}{\varepsilon k_B T} = 7.1$Å. In this study, the Bjerrum length is never

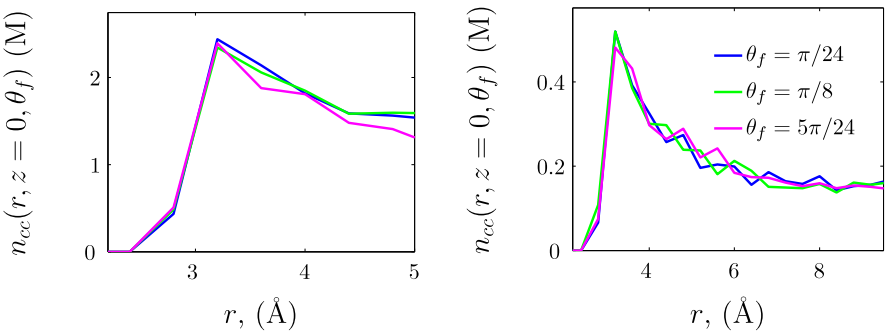

(a) $A_c = 100\text{Å}^2$ (b) $A_c = 361\text{Å}^2$

Figure 3.2 Number density distribution n_{cc} as a function of r for different values of the azimuth coordinate θ ranging from 0 to $\pi/4$. Results in the figure are for monovalent counterions at concentration 0.05M ($A_c = 100\text{Å}^2$) and 0.08M ($A_c = 361\text{Å}^2$).

changed, i.e. the temperature is constant and hence, the solution presented corresponds to the case $l_B/\sigma = 2.36$. The other two characteristic lengths, the Debye-length λ_D and the Gouy-Chapman length λ_{GC}, which depend on ionic strength and molecular area respectively, were extensively varied, as discussed further below.

Obviously, the case where l_B can take any arbitrary value would provide an additional parameter to investigate. For example, the limit $l_B/\sigma \to \infty$ can be investigated from [110] and $l_B/\sigma \to 0$ reduces to PB theory, but other more intricate situations are likely to occur. These possibilities will not be investigated further in this paper.

3.4 Results

3.4.1 Monovalent ions

We first present a detailed characterization of the number density distribution function (Eq. 3.2) and its associated potential of mean force (Eq. 3.4). In general, $n_\alpha(\vec{r})$ is a function of three coordinates (r, θ, z), but as it follows from Fig. 3.2 the number density distribution is rotationally invariant, i.e. independent of the azimuth coordinate θ, and it is a function of (r, z) only (see Fig. 3.1 for a definition of the coordinates).

We next investigate the dependence of $w_\alpha(r, z)$ as a function of r and z. Fig. 3.3(a) shows

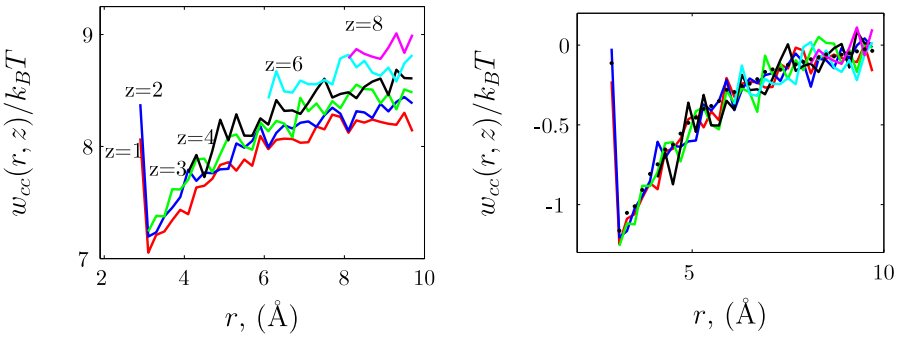

(a) $w(r,z)_{cc}$ (b) $w(r,z)_{cc}$(shifted)

Figure 3.3 The function $w(r,z)_{cc}$ for fixed values of z (in Å). The molecular area is A_c=361 Å^2. The figure on the right is the potential shifted by a constant $\mathcal{F}_\alpha(z)$, as defined in Eq. 3.11. Results are for monovalent counterions at concentration 0.08M

$w_\alpha(r,z)$ plotted as a function of r for a given z. In Fig. 3.3(b), the same potential is plotted, now shifted by a constant $\mathcal{F}_\alpha(z)$, which depends on z only, thus establishing that the potential of mean force can be written as

$$w_{cc}(r,z) = \hat{w}_\alpha(r) - k_BT\ln(\frac{\hat{n}_\alpha(z)}{n^b_\alpha}) \equiv \hat{w}_\alpha(r) + \mathcal{F}_\alpha(z)\ . \tag{3.11}$$

This implies that the number density distribution is a product of two functions, one depending on r and another on z, a case already considered in Eq. 3.6. The function $\hat{w}_\alpha(r)$ is extracted from a fit to the master curve from Fig. 3.3(b) and $\hat{n}_\alpha(z)$ from the actual value of the shift $\mathcal{F}_\alpha(z) \equiv -k_BT\ln(\frac{\hat{n}(z)_\alpha}{n^b_\alpha})$. Eq. 3.11 is a general result, which holds for all concentrations and for molecular areas where rotational invariance applies.

3.4.2 Dilute solutions, divalent ions

Similarly as for the monovalent case, the number density for divalent counterions is independent of the azimuth θ, is a function of (r,z) only, as shown in Fig. 3.4, and can be expressed as a product of the two functions defined by Eq. 3.6, as shown in Fig. 3.5.

The function $\hat{n}_{cc}(z)$ for different molecular areas is plotted in Fig. 3.6. The difference between $\hat{n}_{cc}(z)$ and $n^D_{cc}(z)$ is entirely due to the effect of the charge discreteness, and it is quite significant, specially for larger molecular areas. The accuracy of representing the density

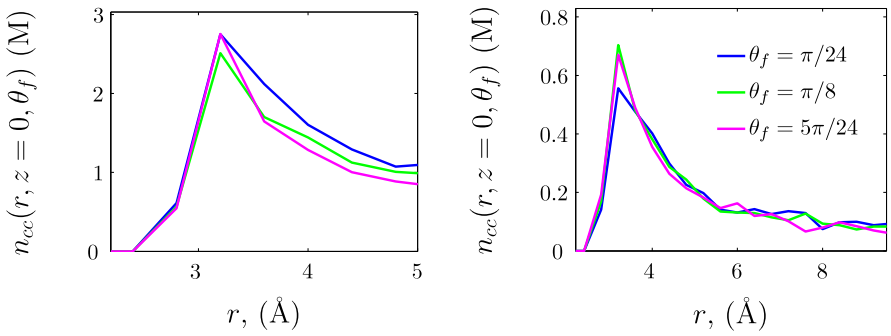

(a) $A_c = 100\text{Å}^2$ (b) $A_c = 361\text{Å}^2$

Figure 3.4 Number density distribution n_{cc} Eq. 3.7 as a function of r for different values of the azimuth coordinate θ ranging from 0 to $\pi/4$. Results in the figure are for divalent counterions at concentration 0.02M.

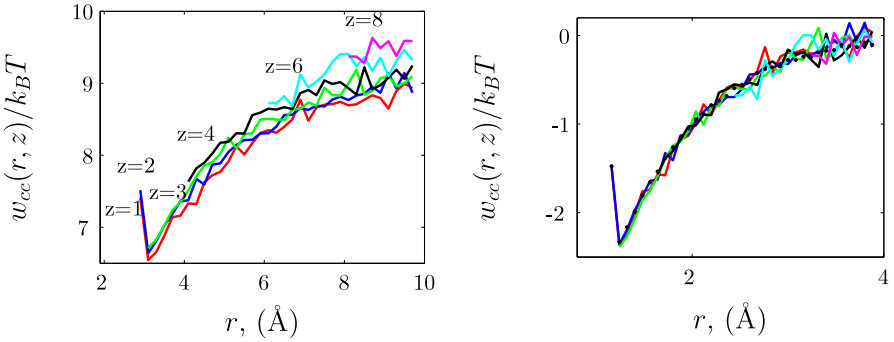

(a) $w(r, z)_{cc}$ (b) $w(r, z)_{cc}$(shifted)

Figure 3.5 The function $w(r, z)_{cc}$ at fixed values of z (in Å). The molecular area is A_c=361 Å^2. The figure on the right is the potential shifted by a constant $\mathcal{F}_\alpha(z)$, as defined in Eq. 3.11. Results are for divalent counterions at concentration 0.04M

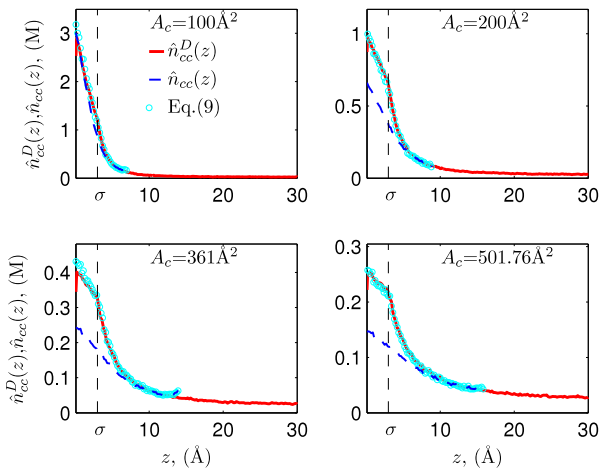

Figure 3.6 The function $\hat{n}_{cc}(z)$ (blue dashed line) for different molecular areas. Also shown is the actual number density $n^D_{cc}(z)$ (red solid line) obtained from simulation, as well as $n^D_{cc}(z)$ independently obtained from Eq. 3.9 (cyan markers). Counterions are divalent and the bulk ion concentration is 0.02M.

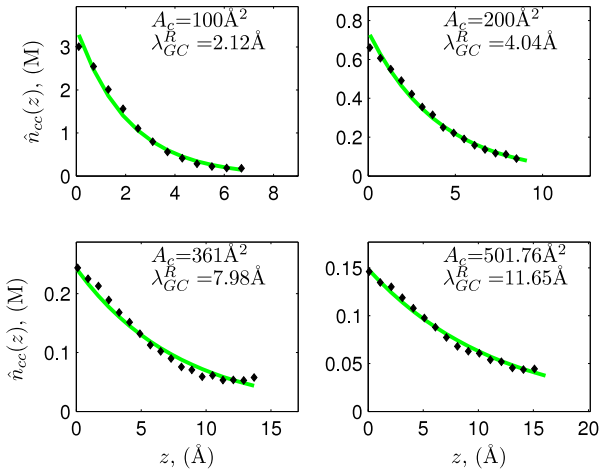

Figure 3.7 The function $\hat{n}_{cc}(z)$ (black diamond markers) for different molecular areas together with the corresponding exponential fit (green solid line). Counterions are divalent and the bulk ion concentration is 0.02M.

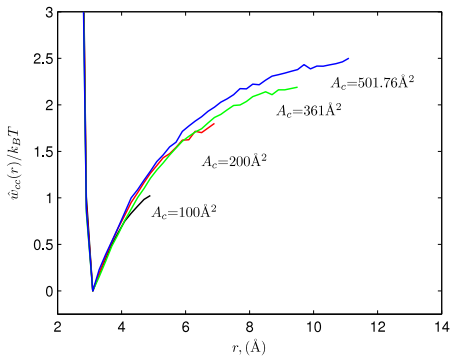

Figure 3.8 Function $\hat{w}_{cc}(r)$ for different molecular areas and divalent counterions at concentration 0.02M. Each plot is shifted by a constant so that the value at the minimum is the same for all molecular areas.

distribution as the product of two functions (Eq. 3.6) is cross-checked by comparing $n^D_{cc}(z)$ as computed from simulations, with the one computed from Eq. 3.9, which makes use of both $\hat{n}_{cc}(z)$ and $\hat{w}_{cc}(r)$. As shown in Fig. 3.6 the results are, within the accuracy of simulations, completely indistinguishable. As apparent, while $n^D_{cc}(z)$ shows an obvious kink at $z = \sigma$, $\hat{n}_{cc}(z)$ is a smooth function, approximately described (for $z \leq a_L/2$) by a simple exponential

$$\hat{n}_{cc}(z) \propto \exp(-\frac{z}{\lambda^R_{GC}}) \ , \tag{3.12}$$

where λ^R_{GC} is a renormalized Gouy-Chapman length. As shown in Fig. 3.7, the exponential fit is reasonable, but the figure hints at a more nuanced function. The name of λ^R_{GC} as a renormalized Gouy-Chapman length in Eq. 3.12 is motivated by the fact that the density distribution of an isolated mobile charge near a constant electric field decays exponentially, with a decay length given precisely by the actual Gouy-Chapman length. In fact, the values of λ^R_{GC} depend linearly on molecular area, see Fig. 3.7, as it is the case with λ_{GC}, but λ^R_{GC} is very sensitive to the bulk ion concentration, as shown in Fig.3.10.

3.4.3 Beyond dilute concentrations, divalent ions

The analysis of dilute concentrations was extended to systems at higher divalent bulk ion concentrations in the range 0.1-0.4M, where the Debye length becomes of the same order as σ. Compared with the dilute case, the kink at $z = \sigma$ in $n^D_{cc}(z)$ becomes more pronounced

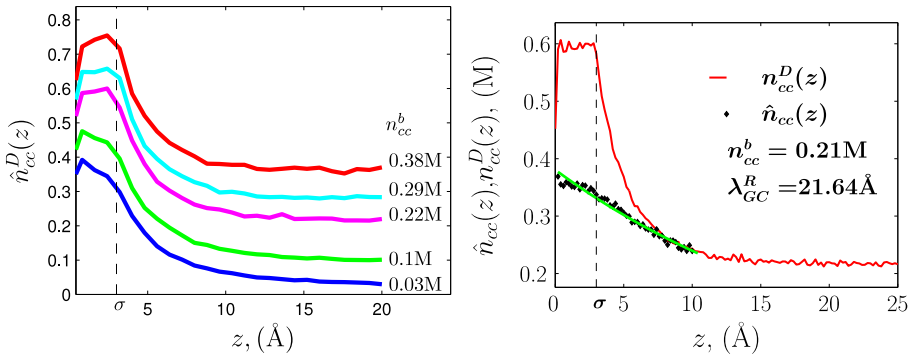

(a) $n_{cc}(z)$ for different concentrations (b) $n_{cc}(z)$, $\hat{n}_{cc}(z)$

Figure 3.9 (a) Number density distribution $n^D_{cc}(z)$ for different bulk concentration values. (b) $n^D_{cc}(z)$,$\hat{n}_{cc}(z)$ and the corresponding exponential fit (Eq. 3.12) for $n^b_{cc} = 0.21$M. The results are for divalent ions at molecular area $A_c = 361$Å^2

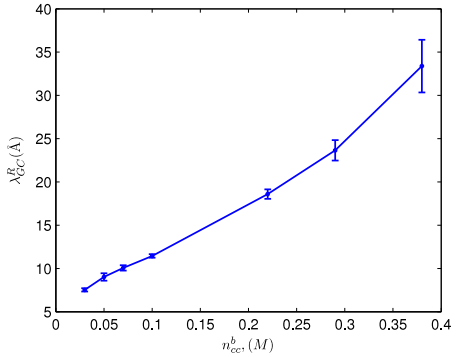

Figure 3.10 The renormalized Gouy-Chapman length λ^R_{GC} vs bulk ion concentration for divalent ions, molecular area $A_c = 361$Å^2.

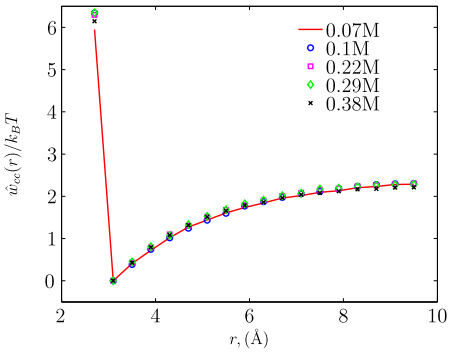

Figure 3.11 The function $w^R_{cc}(r)$ for different divalent counterion concentrations at fixed molecular area A_c=361Å^2.

(Fig.3.9(a)), resulting in a plateau for $z < \sigma$. An exponential decay is also found, but only for $z > \sigma$.

Rather remarkably, the function $\hat{w}_\alpha(r)$ is, within the accuracy of the simulation, independent of concentration, as shown in Fig.3.11. This provides clear evidence that $\hat{w}_\alpha(r)$ reflects a universal property of the interface.

3.4.4 Deviations from perfect lattice with divalent counterions

The interfacial charges in the simulations discussed so far are arranged as an ideal square lattice. However, situations where charges significantly deviate from a periodic structure are quite relevant, for example, in describing a liquid. A random distribution can be achieved by allowing each charge to be moved from its ideal position on a square lattice $\vec{r}_p \equiv (x, y, 0)$ to a new position $\vec{r}'_p$ defined as

$$\vec{r}'_p \equiv (x \pm \delta x, y \pm \delta y, 0), \text{ where } 0 \leq \delta x \leq d, 0 \leq \delta y \leq d \tag{3.13}$$

where $\delta x, \delta y$ are chosen as random numbers uniformly distributed within the allowed interval. According to the Lindemann criteria, $d = 0.1a_L$ is the boundary between a solid and a liquid. Simulations reported in this section correspond to $d \equiv (0.1a_L, 0.2a_L, 0.3a_L)$.

The $\hat{w}_{cc}(r)$ function shows only slight deviations from the one corresponding to a perfect lattice for the largest value of d only. The function $\hat{n}_{cc}(z)$ is affected by the positional disorder introduced by Eq. 3.13, particularly for the largest value of d, where deviations from the simple exponential Eq. 3.12 are apparent, see Fig. 3.12(b).

3.4.5 Divalent ions with Van der Waals attraction

The case where charges have an additional Van Der Waals attraction is considered by using a cut-off value as defined by $(\lambda, v_0) \equiv (3, 0)$, in the short range potential V_{SR} (Eq 5.3). The case of divalent ions with additional van der Waals attraction is again represented in terms of a product of two functions, as defined by Eq. 3.6. Comparison between cases where Van der Waals interactions are turned off and on are shown in Fig. 3.13(a). Both $\hat{w}_{cc}(r)$ functions follow very similar trends. The function $\hat{n}_{cc}(z)$ however is not described by a simple exponential.

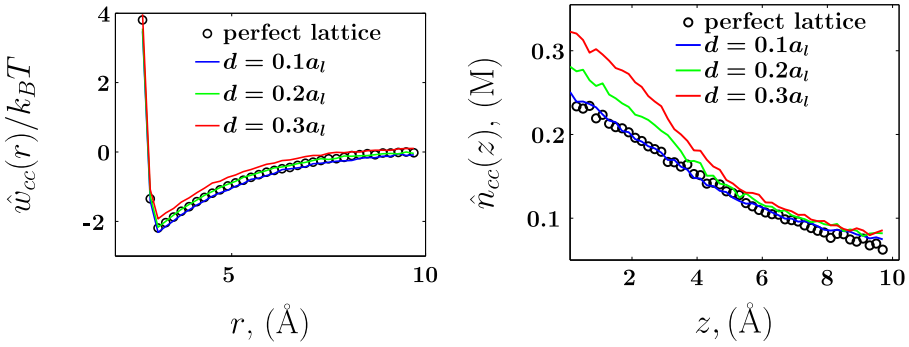

(a) $\hat{w}_{cc}(r)$ (b) $\hat{n}_{cc}(z)$

Figure 3.12 Disordered lattices, see Eq. 3.13, with divalent counterions (a) $\hat{w}_{cc}(r)$ function for different d values (b) $\hat{n}_{cc}(z)$ for different d values. Results for divalent counterions at A_c=361Å^2,conc=0.02M.

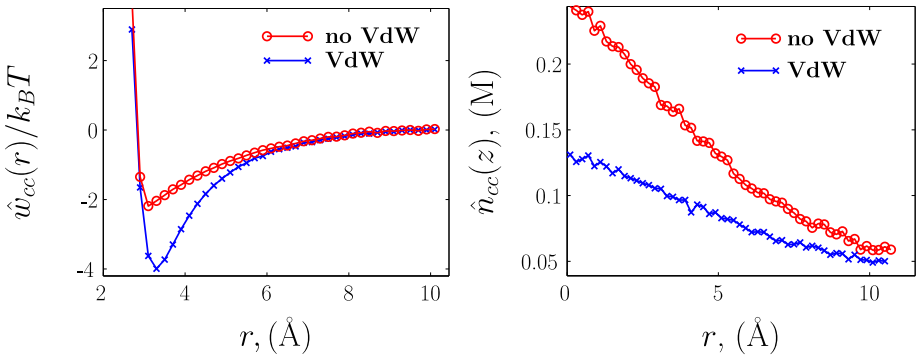

(a) $\hat{w}_{cc}(r)$ (b) $\hat{n}_{cc}(z)$

Figure 3.13 Systems with VdW attractions. (a) $\hat{w}_{cc}(r)$ for a system with ($\lambda = 3$) and without ($\lambda = 1$) VdW attraction. (b) $n_{cc}(z)$ for a system with and without VdW attractions. Results for divalent counterions at A_c=361Å^2 and conc=0.02M.

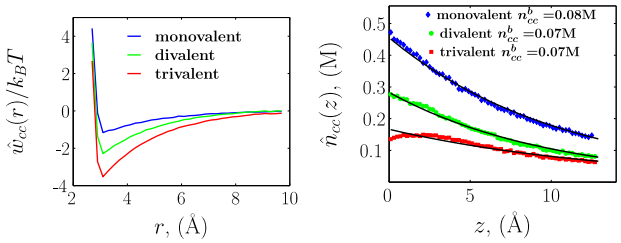

(a) $\hat{w}_{cc}(r)$ (b) $\hat{n}_{cc}(z)$

Figure 3.14 (a) Comparison of the different $\hat{w}_{cc}(r)$ and (b) $\hat{n}_{cc}(z)$ for different counterion valence at molecular area A_c=361Å^2 (and about the same bulk concentration, 0.07-0.08M). The markers represent the calculated $\hat{n}_{cc}(z)$ values and solid lines represent the exponential fits. The corresponding λ^R_{GC} values are 10.22Å(monovalent),10.08Å (divalent),13.88Å (trivalent).

.

3.4.6 Trivalent counterions

In systems with trivalent counterions, the functions $\hat{n}_{cc}(z)$ and $\hat{w}_{cc}(r)$ are shown in Fig. 3.14 compared with their equivalent for monovalent and divalent ions at roughly the same concentration. The function $\hat{n}_{cc}(z)$ for trivalent ions show significant deviation from the simple exponential Eq. 3.12 for $z < \sigma$. The function $\hat{w}_{cc}(r)$ shows a more pronounced dip with increasing valence, thus implying an enhancement of electrostatic correlations, see Fig. 3.14(a).

In all simulations performed (see Supplementary Material in Sect.4.1) trivalent counterion systems exhibit charge inversion, some more pronounced than others. Effects related to charge inversion will not be discussed further in this paper.

3.5 General Solution to the PDDL

The complete solution to the PDDL can be divided into three regimes, defined by $a_L > 3\sigma$, the *large molecular area or plasma regime*, $\sigma < a_L < 3\sigma$, the *small molecular area or binding regime* and $a_L < \sigma$, the *uniform regime*. The plasma regime shows a density distribution described by the product of the two functions in Eq. 3.6, and is indicative of counterions forming a two dimensional strongly correlated liquid at the interface, while the *binding* regime

is indicative of counterions localized in certain binding sites. Although descriptions in terms of a two dimensional strongly correlated liquid have been introduced before[44], the plasma describing the PDDL differ from the one component plasma, as clear below. The binding regime has also been considered in Ref. [111] within some approximations that will be analyzed further. The *uniform* regime describes the trivial case where interfacial charges are so close that its discreteness becomes irrelevant.

3.5.1 Solution in the plasma regime (Large Molecular Area)

The number density distribution is expressed as a product of two functions (Eq. 3.6) for $z < a_L/3$, thus leading to a solution valid for all investigated molecular areas, concentrations, counterion valence, arrangement of interfacial charges or specific ion interactions defined by

$$n_{cc}(r,z) = \begin{cases} \hat{n}_{cc}(z) \exp\left[-\frac{\hat{w}_{cc}(r)}{k_B T}\right] & \text{for } z < z_{match} \\ \text{Diffuse Layer (DL)} & \text{for } z \geq z_{match} \end{cases} \tag{3.14}$$

The function $\hat{n}_{cc}(z)$ is approximately described by a simple exponential (Eq. 3.12), but for divalent ions at large concentrations, trivalent ions and disordered systems a slightly more complex form is found. At this point, we could not find a transparent interpretation of $\hat{n}_{cc}(z)$ based on a simple physical description. We will return to this point in the conclusions. The function $\hat{w}_{cc}(r)$ represents the lateral correlations of ions within the immediate layer near the charged interface, and it can be given a clear interpretation, leading to a rigorous determination from simple models, as described in Subsect 3.5.1.1. The description of the diffuse layer within PB theory is the simpler choice, but in some cases becomes inadequate and more refined models, such as the HNC[108, 63] are needed. The point where both descriptions match z_{match} is estimated from $z_{match} \sim a_L/3$, as this is where the electric field of a discrete system becomes equivalent to a uniform distribution[59]. For monovalent ions, however, z_{match} can be chosen closer to the interface (than $a_L/3$), as discussed in Subsect. 3.5.1.2.

3.5.1.1 Physical Interpretation of $\hat{w}_\alpha(r)$

The function $\hat{w}_\alpha(r)$ is obtained from numerical simulations as the master curve from shifted $w_{cc}(r,z)$, see for example Fig. 3.3 or Fig. 3.5. In Fig. 3.8, the function has been plotted for

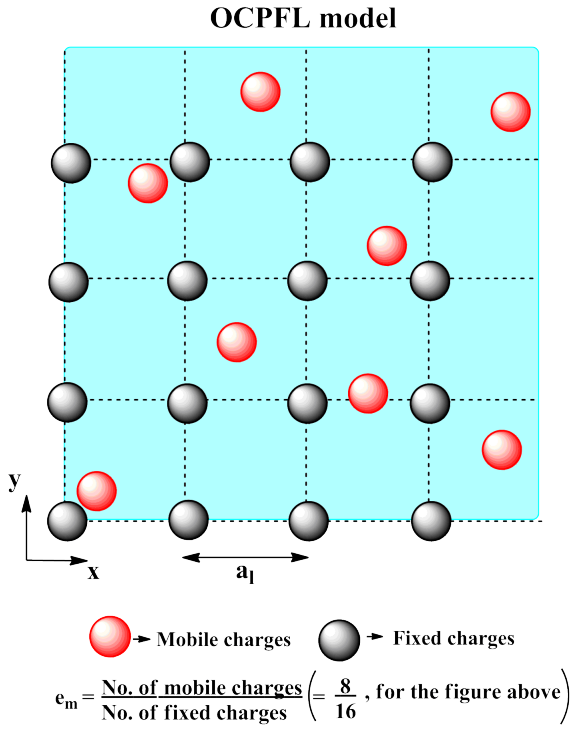

Figure 3.15 A representation of the two dimensional one component plasma in a fixed square lattice, OCPFL model, characterized by e_m given by ratio of mobile charges (red spheres) to fixed charges (gray spheres).

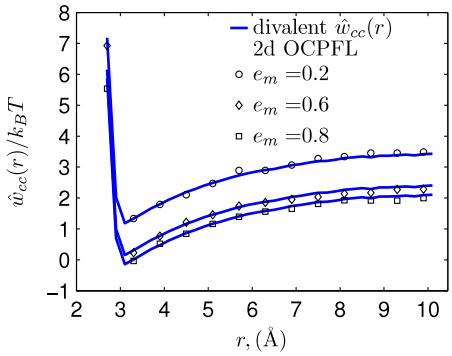

Figure 3.16 Comparison of the potential of mean force of the 2d OCPFL (markers $\diamond, \square, o, .$) against $\hat{w}_{cc}(r)$(blue solid line). The results are for divalent ions at molecular area $A_c = 361\text{Å}^2$. (e_m is the ratio of mobile/fixed charges, see Fig. 3.15).

different molecular areas showing universality at short distances. Also, from Fig. 3.11, $\hat{w}_\alpha(r)$ is independent of concentration.

The interpretation of $\hat{w}_\alpha(r)$ as encoding lateral correlations can be made completely transparent by considering the potential of mean force of a two dimensional one component plasma in a fixed lattice (OCPFL) of molecular area A_c. This model, shown in Fig. 3.15, consists of mobile ions of valence q interacting with charges at fixed positions. The mobile ions are restricted to the plane defined by the interfacial charges and interact with a three-dimensional Coulomb potential and a short-range potential described by V_{SR}, see Eq. 5.3. The OCPFL model includes a parameter e_m (see Fig. 3.15), which is the ratio of mobile to fixed charges (charge neutrality is imposed by adding a uniform background, as it is done in the standard one component plasma[66]). The potential of mean force for the OCPFL is, with great accuracy, independent of e_m, which in turn, implies that correlations among mobile counterions are subleading to the ones among fixed and mobile ions.

The agreement between the function $\hat{w}_\alpha(r)$ and the potential of mean force computed from the OCPFL (see Fig. 3.15) is exact within the accuracy of the numerical results for all cases studied: Divalent counterions (Fig. 3.16), monovalent ions (Fig. 3.17(a)), deviations from perfect lattice (Fig. 3.17(b)), inclusion of VdW attraction (Fig. 3.18(a)) and trivalent ions (Fig. 3.18(b))).

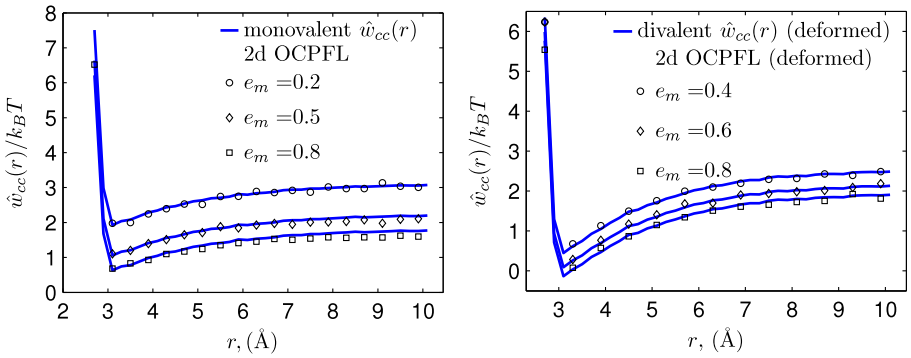

(a) OCPFL,monovalent (b) OCPFL,divalent deformed

Figure 3.17 Comparison of the potential of mean force of the 2d OCPFL (markers $\diamond, \square, o$) against $\hat{w}_{cc}(r)$(blue solid line) for (a) monovalent (b) divalent ions with deformed lattice, at molecular area $A_c = 361\text{Å}^2$.(e_m is the ratio of mobile/fixed charges, see Fig. 3.15).

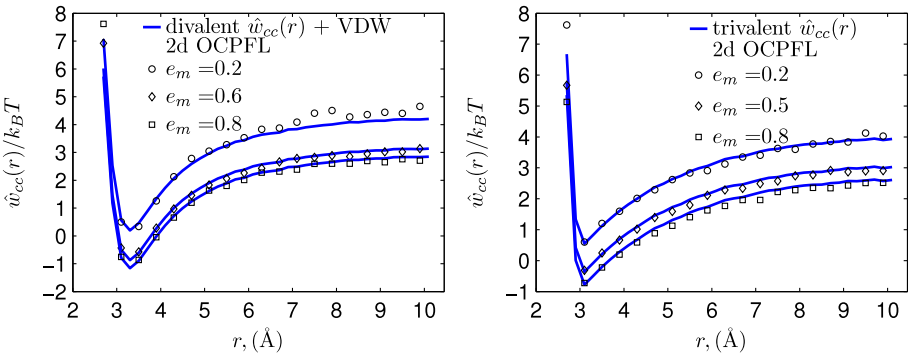

(a) OCPFL,divalent VdW attraction (b) OCPFL,trivalent

Figure 3.18 Comparison of the potential of mean force of the 2d OCPFL (markers $\diamond, \square, o$) against $\hat{w}_{cc}(r)$(blue solid line) for (a) divalent with VdW attraction (b) trivalent ions, at molecular area $A_c = 361\text{Å}^2$.(e_m is the ratio of mobile/fixed charges, see Fig. 3.15).

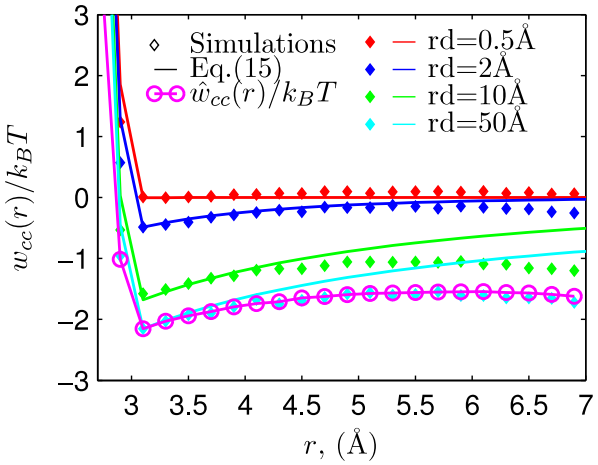

Figure 3.19 Potential of mean force for a OCPFL model, see Fig. 3.15, where particles interact via a Yukawa potential. The filled ⋄ markers are simulation results, solid lines are the approximation given by Eq. 3.15. The $\hat{w}(r)$ function is shown in magenta (o markers).Case of monovalent counterions at molecular area $Ac = 100\text{Å}^2$.

In order to establish to what extent the function $\hat{w}_\alpha(r)$ encodes long range effects, an OCPFL model where instead of a standard Coulomb potential, the ions interact through a Yukawa potential with decay length r_d, was considered. Here, the decay length is voided of any physical content and it is just a convenient parameter interpolating between a short-range potential (for $r_d << a_L$) and a long-range potential for ($r_d \to \infty$). If the potential of mean force for the OCPFL is dominated by local interactions, it can be approximated as

$$w_{Yu}(r) \approx k_BT \frac{q_\alpha q_\beta l_B}{r} \exp(-r/r_d) + V_{SR}(r) \ , \tag{3.15}$$

As shown in Fig. 3.19, for short-range potentials (large decay lengths $r_d/a_L \geq$), this approximation describes very accurately the simulation data, but it starts to fail as the decay length becomes larger (of the order $r_d/a_L \sim 2$). As $r_d/a_L >> 1$, simulation data becomes indistinguishable from $\hat{w}_{cc}(r)$. In this way, it is established that the function $\hat{w}_\alpha(r)$ is dominated by long-range, many body correlation effects.

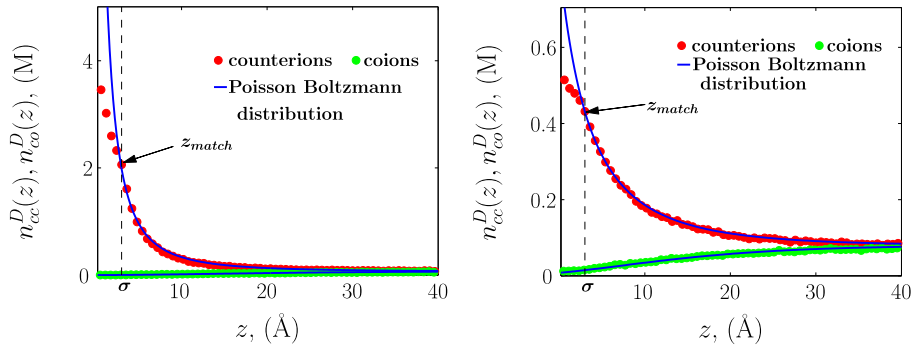

(a) A_c=100Å^2, PB (b) A_c=361Å^2, PB

Figure 3.20 The counterion distribution $n_{cc}(z)$ (red markers) and the Poisson Boltzmann distribution (blue) for the monovalent counterion systems. As described in section 3.5.1.2, $z_{match} \approx \sigma$.

3.5.1.2 The diffuse layer

The ion distribution within the diffuse layer is described by an equivalent ion distribution next to a uniformly charged plane with a surface charge defined by Gauss law, i.e.

$$\begin{aligned} \nu_{equiv} &= \frac{q_I}{A_c} + q_{cc}\int_{z=0}^{z=z_{match}} dz n_{cc}^D(z) + \\ &+ q_{co}\int_{z=0}^{z=z_{match}} dz n_{co}^D(z) \ , \end{aligned} \tag{3.16}$$

in addition, the continuity in the number density as computed for $z > z_{match}$ and $z < z_{match}$ must also be met. The matching point z_{match} is given by $a_L/3$, as this point defines the minimum distance where the electric field of the discrete interfacial charges is indistinguishable from a uniform distribution, as discussed in Ref. [59]. We now investigate this in more detail.

Results for monovalent ions are shown in Fig. 3.20, and the diffuse layer is accurately described by PB theory. In fact, for all cases analyzed, it was found that, with almost negligible error, $z_{match} \approx \sigma$, that is, the diffuse layer is only one counterion diameter away from the plane $z = 0$, see Fig. 3.1, which is possible because $\hat{w}_{cc}(r)$ for $r > \sigma$ is almost a constant function, i.e. electrostatic correlations are weak, as it follows from Eq. 3.6.

The case of divalent ions shows a diffuse layer that begins at $z_{match} \approx a_L/3$, as shown in Fig. 3.21. Contrary to the case with monovalent ions, z_{match} is larger than σ, and the counterion distribution for $z < z_{match}$ described by Eq. 3.6, reflects a genuine effect due to the discreteness

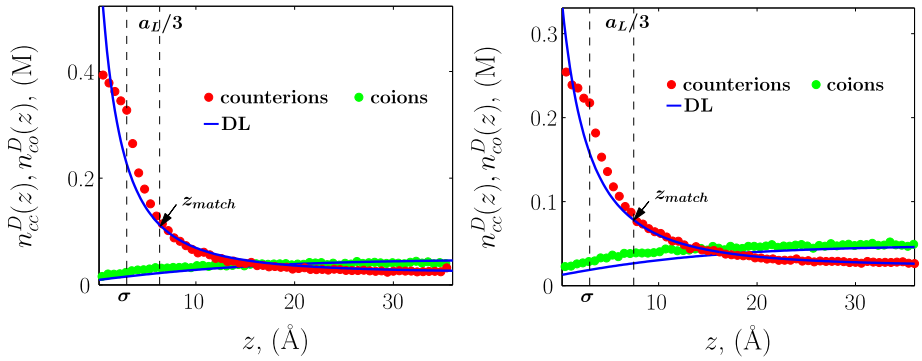

(a) A_c=361Å^2, PB (b) A_c=501Å^2, PB

Figure 3.21 The counterion distribution $n_{cc}(z)$ (red markers) and the Diffuse Layer (DL) distribution (blue), which is described by PB as discussed in the main text, for divalent counterion systems, with $z_{match} \approx a_L/3$. (For a magnified plot showing the difference between the PB predictions and results from simulation for the region $\sigma < z < a_L/3$, see supplementary material in Sect. 4.2)

of the interfacial charges, as it is not reproduced by any uniform distribution. Although clear from Fig. 3.21, an additional plot provided in the supplementary material Sect.4.2 makes this point more obvious.

Because for $z \geq z_{match}$ exact uniform distributions are precisely described by PB theory (see supplementary material for details in Sect.4.3), the diffuse layer within the plasma regime can be described by PB theory, except at the smaller molecular areas $100 < A_c \lesssim 200$Å^2, where PB theory becomes somewhat inaccurate. Similar inaccuracies occur in the binding regime, so we refer there for further details on this case.

3.5.2 The binding regime

The binding regime is defined by $a_L < 3\sigma$ and it is characterized by $z_{match} \approx \sigma$. As shown in Fig. 3.22(a), the number density of counterions shows a dependence on azimuthal angle θ, and counterions are found with higher probability along the shortest path separating the two interfacial charges, see Fig. 3.22(b), indicative of a binding site.

The description of the DL presents some difficulties; The obvious choice would consist of a uniform distribution defined at $z_{match} = \sigma$ with a surface charge defined by Eq. 3.16, yet,

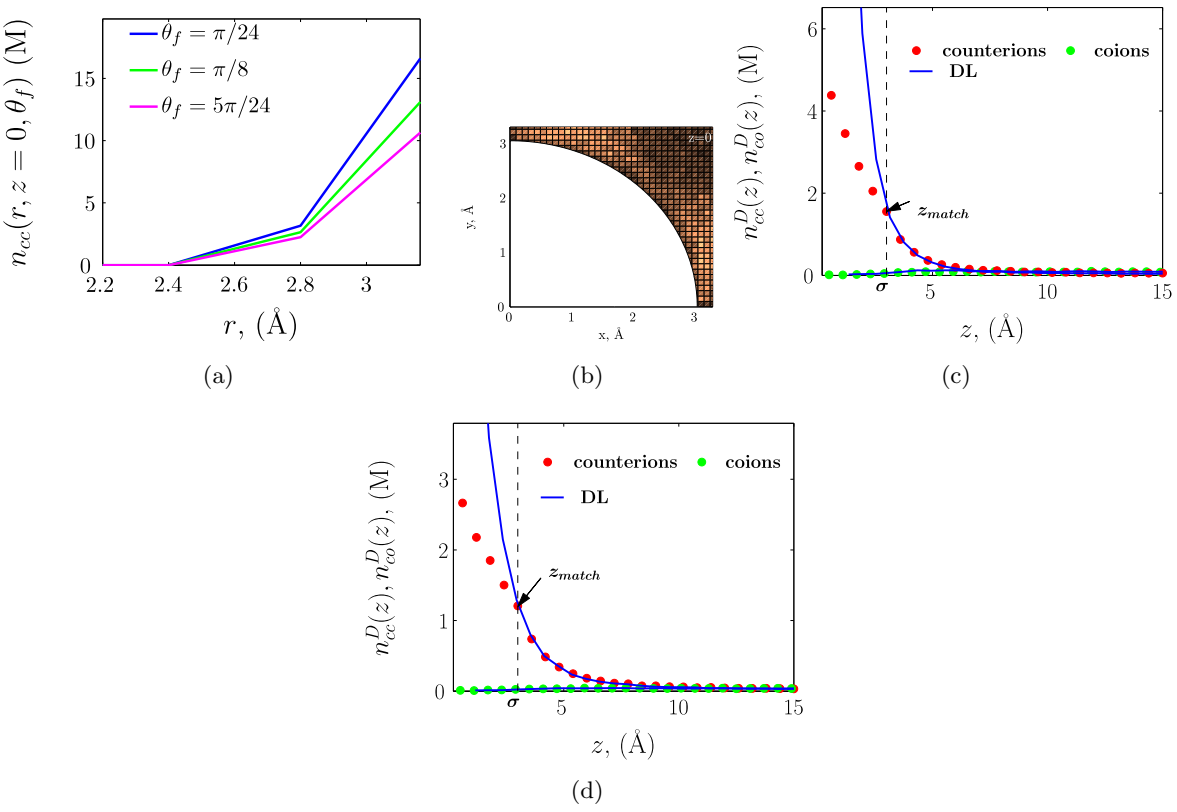

Figure 3.22 (a) Number density distribution n_{cc} as a function of r for different values of the azimuth coordinate θ ranging from 0 to $\pi/4$. Case of divalent counterions at concentration 0.08M ($A_c = 40\text{Å}^2$) (b) Counterion density $n_{cc}(x, y, z = 0)$ around an interfacial charge for the same case as in (a), as a function of cartesian coordinates x,y (counterion density increases from dark to light shades of brown). (c) A_c=70Å^2 and (d) A_c=100Å^2, counterion distribution $n^D_{cc}(z)$ (red markers) and the counterion distribution for the case of a uniformly charged interface (blue) for the divalent counterion systems. As described in section 3.5.2, $z_{match} \approx \sigma$.

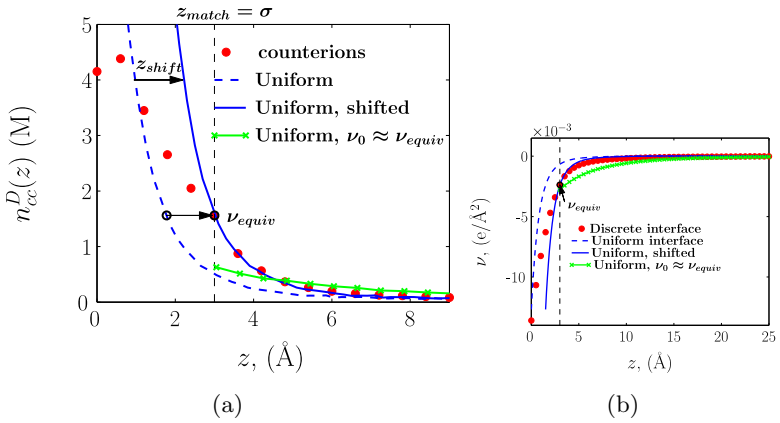

Figure 3.23 Results for A_c=70Å^2 (concentration 0.047M) (a) Counterion distribution $n_{cc}^D(z)$ (red markers) and the counterion distribution for the case of a uniformly charged interface (blue dashed line) for the divalent counterion systems. Result for the uniform surface charge simulation with ν_0=ν_{equiv} is also shown (green) (b) Corresponding ν values as a function of z.

as shown in Fig. 3.23(a) such approximation leads to dramatic errors; This is indicative of strong correlations among counterions at $z < \sigma$ and $z > \sigma$, as the source of error arises from smoothing the counterions at $z < \sigma$ by a continuum distribution, i.e. neglect of discreteness within the Stern layer. A satisfactory description of the DL however, is possible by considering the counterion distribution from a uniform surface charge of $\nu_0 = -e/A_c$, and then shifting the $z = 0$ plane by an amount z_{shift} such that the surface charge at $z = z_{match}(= \sigma)$ satisfies Eq. 3.16 (see Fig. 3.23). As shown in Fig. 3.22(c) and Fig. 3.22(d), such approximation provides an exact (within numerical errors) description of the diffuse layer for $z \geq z_{match}(= \sigma)$.

3.6 Conclusions

3.6.1 Summary

We have provided an general solution to the problem of determining the counterion/coion distributions near a plane consisting of discrete charges (PDDL model, see Fig. 3.1). The solution is summarized in Fig. 3.24 and is parameterized by the ratio a_L/σ, where σ is the charge diameter and a_L the average separation of the charges at the interface. There are basically three regimes; the Plasma regime $a_L > 3\sigma$ consists of a distribution defined as a

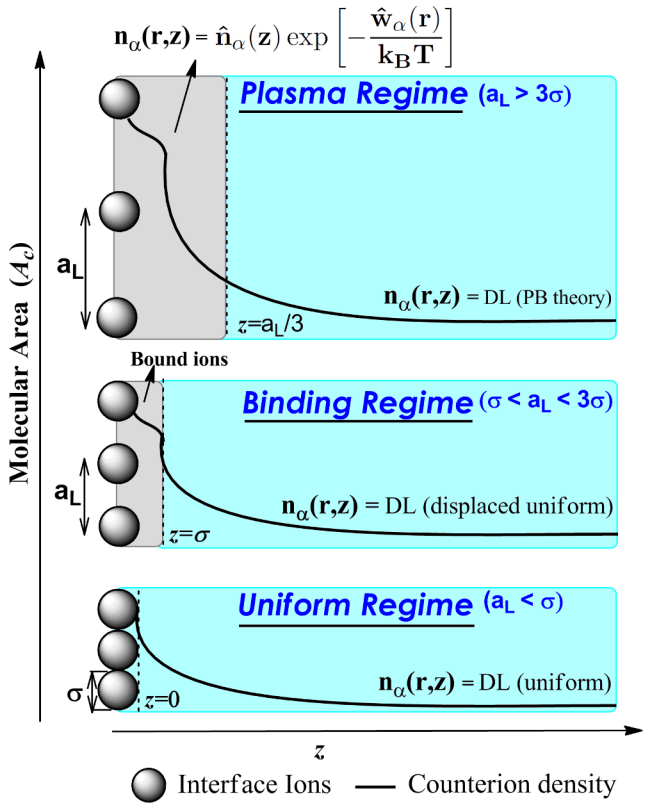

Figure 3.24 Summary of the results. DL is the Diffuse Layer (description provided in main text).

product of two functions (see Eq. 3.6) – $\hat{w}_\alpha(r)$ corresponds to a 2d model (see Fig. 3.15) and $\hat{n}(z)$ to a decay function (see Fig. 3.7), followed by, a diffuse layer basically consistent with the PB theory. The Binding regime $\sigma < a_L < 3\sigma$, consists of a Stern layer whose thickness is given by the diameter of the counterion and a diffuse layer strongly correlated to the Stern layer. The uniform regime for $a_L < \sigma$ is described by a standard diffuse layer.

The proposed solution is completely general, as it describes counterion multivalency (Fig. 3.6), inclusion of Van Der Waals attractions (Fig. 3.18), interfacial disordered positions (Fig. 3.17) within the plane at any electrolyte concentrations (Fig. 3.11) below 0.4M. At higher concentrations, oscillations in the density distribution are expected[63, 62], but this case has not been investigated in this paper.

The results presented show that the common approach of dividing a generic interface into a Stern Layer, where counterions are strongly interacting, and a diffuse layer, which at least for dilute concentrations can be described within PB theory, is only valid for monovalent counterions and becomes grossly inaccurate for divalent counterions at any surface charge and electrolyte concentration: At low surface charge (high molecular area) because the effects of charge discreteness extend up to a distance of $a_L/3$, while at high surface charge (small molecular area), counterions within the diffuse layer are strongly correlated with the ones within the Stern layer, thus negating any approximation where the Stern layer is approximated as a uniform surface charge. The differences between the osmotic pressure of a plane with discrete and uniform charges discussed in [106, 107] is in agreement with these findings.

3.6.2 Outlook

The solution described by Eq. 3.24 reproduces the MD simulations with remarkable precision (1% or less). Still, it remains a challenge to develop subsequent analytical and/or numerical approaches that address the following two questions:

1. Rigorous characterization of the $\hat{n}_\alpha(z)$ function (in the plasma regime).

2. Analytical expressions interpolating the partial solutions at matching points.

Although a simple exponential with a renormalized Gouy-Chapman length describes $\hat{n}_\alpha(z)$ for most of the simulations, this is an empirical expression, in contrast with the transparent interpretation provided for the $\hat{w}_\alpha(r)$ function, which allows to compute it from simpler models (the OCPFL model). It remains as a future challenge to provide a more rigorous characterization for $\hat{n}_\alpha(z)$. In this paper, we assumed that the complete solution is an interpolation of partial solutions, which match (together with derivatives) at a single point. Clearly, the interpolation will require a determination of smoother interpolating functions. Overall, our results hint to an underlying well defined expansion whose nature has yet to be clarified.

Acknowledgments We are indebted to Monica H. Lamm for discussions as well as for providing us with computer facilities. We also acknowledge discussions and interest from C. Calero, J. Faraudo and D. Vaknin. This work is supported by NSF through the grant CAREER DMR-0748475.

3.A Description of the PDDL in Terms of Bjerrum Pairing

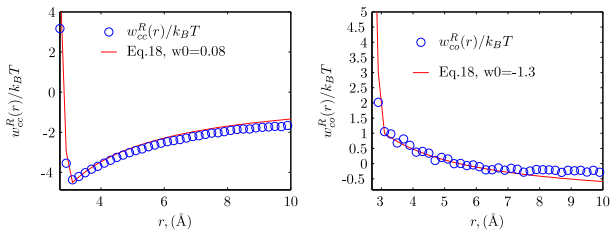

Figure 3.25 The radial potential of mean force $w^R_\alpha(r)$ for counterions (left) and coions (right). The blue markers represent simulation results and the red solid line is calculated using Eq. 3.18. Results are for divalent ions at $A_c = 361\text{Å}^2$ at concentration 0.026M.

Strongly correlated systems can be alternatively described in terms of binding constants, calculated from Bjerrum theory, which encode the short-range correlations, complemented with a description of the long-range effects that can be done within PB theory. Such approach has been extremely successful to describe the case of ionic criticality, see Ref. [104] for example. Extensions of this ideas for the PDDL have also been presented[59].

Recently, Calero and Faraudo [58] have shown that the radial potential of mean force $w_{cc}^R(r)$ and $w_{co}^R(r)$ is well described by the simple Bjerrum theory

$$\frac{w_{cc}^R(r)}{k_BT} = q_{cc}q_0\frac{l_B}{r} + w_0 \ , \tag{3.17}$$

for $r \lesssim a_L/3$, where w_0 is a constant, independent of r but sensitive to electrolyte concentration. This is illustrated in Fig. 3.25, which uses a slightly more accurate version of the previous equation

$$\frac{w_{cc}^R(r)}{k_BT} = V_{SR}(r) + q_{cc}q_0\frac{l_B}{r} + w_0 \ , \tag{3.18}$$

where V_{SR} is the short range potential, as defined in Eq. 6.1. This expression implies, within numerical errors, that the radial potential of mean force is a short-ranged function, as it is only dependent on the interaction of the counterion to its nearest interfacial charge. On the other hand, $w_{cc}^R(r)$ is related to $\hat{w}_{cc}(r)$, which as extensively discussed, cannot be expressed as a local function, see Fig. 3.16 and the subsequent discussion, through Eq. 3.8. Furthermore, the distribution beyond the interfacial charges is not well described by PB theory in any situation. Still, the description within a Bjerrum approach offers significant advantages and, based on the good agreement of simulations with Eq. 3.18, it may provide a reasonable approximation to the free energy in relevant situations. A detailed investigation of these issues will be left for subsequent work.

CHAPTER 4. SUPPLEMENTARY MATERIAL : GENERAL SOLUTION TO THE ELECTRIC DOUBLE LAYER WITH DISCRETE INTERFACIAL CHARGES

4.1 Discrete Interfacial Charge Systems

The parameters used in the simulations are listed in Table 6.1. The interaction potential is implemented using the pair style $lj/cut/coul/long$.

Table 4.1 MD parameters simulation

hline	Parameter	Value
Lennard Jones	epsilon(ϵ_{LJ})	1 kcal/mol
	sigma(σ_{LJ})	3.0 Å
	rcut($rcut_{LJ}$)	3.0 Å
Coulomb (Ewald summation)	cut-off	100 Å
	precision	$1e^{-4}$
Reflecting walls in z direction	zlo	-0.1 Å
	zhi (varying)	Lz+0.1Å
Ensemble	Integrator	nvt
	Temperature	300 K
	Relaxation Constant	100fs
Equilibration Run	# of steps @ time-step	3×10^5@$5.0fs$
Production Run	# of steps @ time-step	4×10^5@$5.0fs$

Simulations with Yukawa potential were carried out using the parameters listed in Table 6.1 except that the interaction potential is implemented using the pair style $lj/cut/coul/debye$. The coulombic term, in this case, has an additional exponential damping factor exp(-r/rd), where the values of rd can be varied to control the strength of the electrostatic interactions.

The interfacial charge q_I and the coion charge q_{co} were set to -1e. The counterion ion charge q_{cc} was set to 1,2 or 3 for simulations of 1:1,2:1,3:1 electrolytes respectively. Periodic

Table 4.2 Simulations for Monovalent Counterions (1:1 electrolyte)

A_c (Å^2)	N_{cc}	N_{ic}	N_{co}	zhiÅ	c_BM	λ_{GC}^R
100	1400	1250	150	100	0.07	2.87
361	2000	1250	750	100	0.08	10.22
501.76	2500	1250	1250	90	0.09	16.15

Table 4.3 Simulations for Divalent Counterions (2:1 electrolyte)

A_c (Å^2)	N_{cc}	N_{ic}	N_{co}	zhiÅ	c_BM	λ_{GC}^R
70	3000	2500	3500	50	0.099	1.55
100	700	1250	150	100	0.022	2.12
100	800	1250	350	100	0.049	2.20
100	1000	1250	750	100	0.103	2.36
200	750	1250	250	80	0.026	4.04
361	800	1250	350	71	0.026	7.53
361	1000	1250	750	71	0.045	9.02
361	1250	1250	1250	71	0.07	10.07
361	1500	1250	1750	71	0.096	11.45
361	2650	1250	4050	71	0.21	18.59
361	4000	1250	6750	90	0.28	23.65
361	5000	1250	8750	90	0.38	33.38
501.76	1000	1250	750	150	0.015	10.63
501.76	1000	1250	750	90	0.026	11.65
501.76	1500	1250	1750	90	0.056	14.36

boundary conditions were applied to the x and y directions. The movement of the ions along the z direction is restricted by two reflecting walls one placed at zlo, and the other at zhi. These walls ensure that the ions have access only to one side of the interface as is the case in many real systems whose properties this model aims to predict.

These simulations were carried out for different molecular areas A_c, where Ac=a_L^2, as well as for different number of counterions and coions in order to model different electrolyte concentrations. Tables 4.2, 4.3, 4.4 list simulation details for the different cases.

Table 4.4 Simulations forTrivalent Counterions (3:1 electrolyte)

A_c (Å^2)	N_{cc}	N_{ic}	N_{co}	zhiÅ	c_BM	λ_{GC}^R
70	2400	2500	2300	50	0.106	1.47
100	500	1250	250	100	0.018	1.85
100	600	1250	550	100	0.043	2.00
100	800	1250	1150	100	0.092	2.28
361	800	1250	1150	100	0.026	10.19
361	800	1250	1150	71	0.036	11.06
361	1000	1250	1750	71	0.056	12.75
361	1000	1250	1750	60	0.065	13.88
501.76	700	1250	850	90	0.016	13.81
501.76	800	1250	1150	90	0.021	15.13
501.76	1000	1250	1750	90	0.034	17.71

4.2 Comparison of Uniformly Charged Interface Simulations with PB Theory

The uniform surface charge simulations were carried out for the systems listed in the table 4.3. The uniform surface charge was generated by placing the interfacial charges in a plane $z = -3a_L$ and $z = zhi + 3a_L$ while restricting the mobile ions to the region $0 \leq z \leq zhi$.

In case of divalent systems with $a_L > 3\sigma$, (here σ is the diameter of the ions), the results from the uniform simulation and the predictions from the PB theory ((Fig. 4.1(c), 4.1(d)), are indistinguishable for $z > a_L/3$. The diffuse layer (DL) for these systems is the region $z > a_L/3$, and so the PB description can be used to describe the DL in this case.

For systems with small values of a_L, ($a_L < 3\sigma$), the PB theory cannot be used to describe the counterion distribution for the uniformly charged interface simulations. The results from the simulation differ from the PB predictions for all z (Fig. 4.1(a), 4.1(b)).

4.3 Effect of Discreteness of the Interface for the Divalent Counterion Systems Extends Beyond Stern Layer

The counterion density distribution in the plasma regime ($a_L > 3\sigma$), for the divalent counterion systems shows an intermediate region between the Stern layer ($z \leq \sigma$) and the diffuse

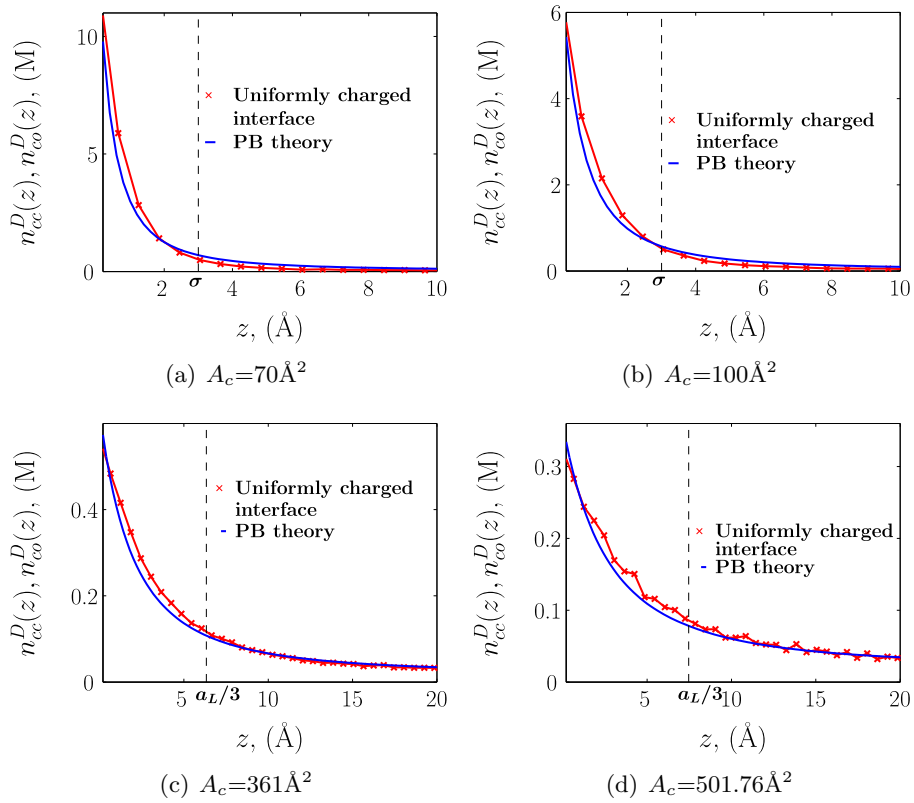

(a) A_c=70Å^2 (b) A_c=100Å^2

(c) A_c=361Å^2 (d) A_c=501.76Å^2

Figure 4.1 (color online). The counterion distribution $n_{cc}(z)$ for uniform charge simulations (red markers) and the corresponding Poisson Boltzmann distribution (blue) for the divalent counterion systems. (only counterion distributions are shown)

layer (DL) which in this case begins at $z = a_L/3$. As shown in Fig. 4.2, neither the Poisson Boltzmann (PB) theory nor the the results from uniform simulation can reproduce this region satisfactorily. The three (PB, uniform and discrete interfacial charge systems) are indistinguishable in the region $z > a_L/3$. However for $z < a_L/3$ the difference between the predictions from PB or the uniform simulations and the results from discrete simulation is significant.

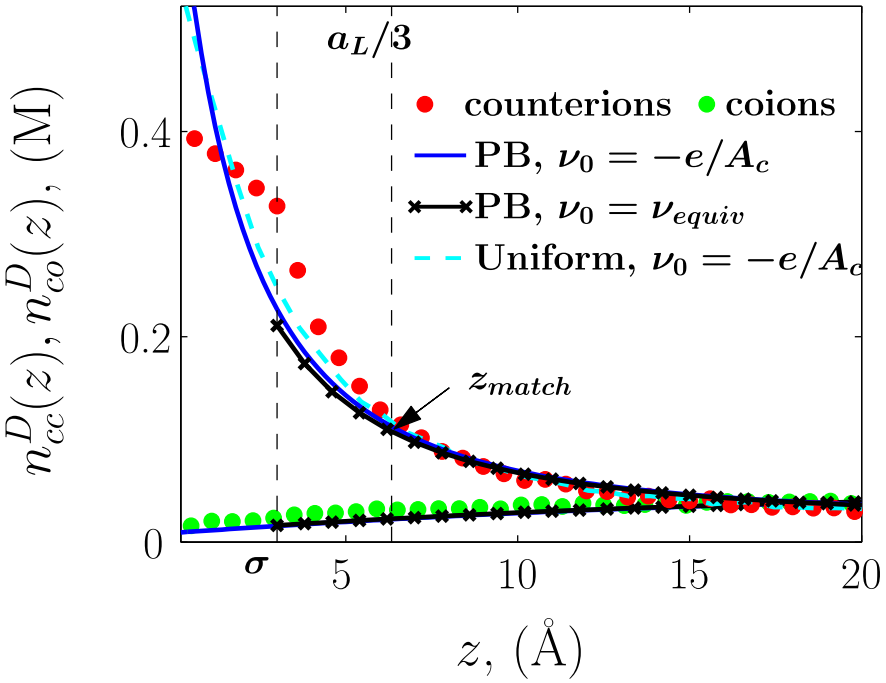

Figure 4.2 (color online). The counterion distribution $n_{cc}(z)$ for discrete charge simulations (red markers), the corresponding uniform charge simulation (cyan dashed lines), and Poisson Boltzmann distribution (blue) for divalent counterion system at A_c=361Å^2.

CHAPTER 5. SEPARATION OF THE STERN AND DIFFUSE LAYER IN COARSE-GRAINED MODELS ; THE CASE OF PHOSPHATIDYL SERINE, PHOSPHATIDIC ACID AND PIP2 MONOLAYERS

A paper submitted to the Journal of Chemical Physics

Sweta Vangaveti and Alex Travesset

5.1 Abstract

We present a rigorous description on how to separate the Stern and diffuse layer in general systems into two regions that can be analyzed separately. The Stern layer can be described in terms of Bjerrum pairing and the diffuse layer in terms of Poisson-Boltzmann theory (monovalent) or Strong coupling theory plus a slowly decaying tail (divalent). We consider three anionic phospholipids: Phosphatidyl Serine (PS), Phosphatidic acid (PA) and Phosphatidylinositol(4,5)bisphosphate (PIP2), which we describe within a minimal coarse-grained model as a function of ionic concentration. The case of mixed lipid systems is also considered, which shows a high level of binding cooperativity as a function of PIP2 localization. Implications for existing experimental systems of lipid heterogeneities are also discussed.

5.2 Introduction

For long, cell membranes, were considered to be passive barriers that merely protect the cellular contents they enclose. In recent years, several studies have revealed their active role in many processes such as signal transduction, cell to cell communication just to name a few [11]. As concrete examples, the production and depletion of phosphatidic acid is associated with functions like apoptosis in plants [112] or managing the cell's response to biotic and abiotic

stresses [113]. Phosphatidyl serine initiates blood coagulation and regulates cell death [114]. Phosphoinositides serve as second messengers in signal transduction pathways [115], activate several ion channels [116] and also serve as signaling lipids.

Critical for membrane function is the lateral heterogeneity of lipids within cell membranes. Lipid clustering is observed to depend on cholesterol concentration [117]. An observation more relevant to this paper is that lipid organization can result from electrostatic interactions. MARCKS or even a simple polybasic peptide can create and maintain clusters of PIP2 (Phosphatidylinositol-4, 5-bisphospate) within the membrane [23, 24, 25, 26], which can be explained by a combination of electrostatic and hydrogen bonds [27, 28, 29, 30, 31]. Recently, experiments on supported lipid monolayers by Levental and colleagues have shown that clustering is observed at normal PIP2 (≈ 0.1 mol %) and high calcium levels (1mM) [32]. Wang et al [21] observed the clustering of PIP2 molecules into 40nm domains at physiological concentrations of calcium and high PIP2 concentration (≈ 10 mol %). In a more recent study using spectroscopic techniques, Sarmento et al [33] showed that PIP2 forms smaller domains (≈ 15 PIP2 molecules) at physiological concentration of both calcium and PIP2.

The aim of this paper is to characterize non-specific electrostatic effects as inducing lipid clustering. The traditional approach when studying the interaction of a charged surface with an electrolyte is to use the Poisson Boltzmann (PB) theory [41]. However, in lipid membranes, the inherent discreteness of the charged surface cannot be ignored. Molecular dynamic simulations show a substantial effect on the ion distribution arising from the discreteness of the interface [58, 118]. The interactions of the ions with the interfacial charges in these simulations is approximately described by a Bjerrum pairing model as proposed in [59], see also[60]. The level of discreteness is also important. In Ref. [119], a single particle model of PIP2 (with a charge -4e) has been used to show the clustering of PIP2 within different pH environments as a function of PIP2 mol fractions. However, the extended structure of a PIP2 molecule introduces additional screening effects which a single particle model may not appropriately capture. The high surface charge density for a single particle model for example, distorts to a great extent the

ion distribution within the Stern and diffuse layer (refer supplementary material in Sect.6.2).

A previous study with a simpler model [111] has shown that the absorption of monovalent and divalent ions to a membrane can be attributed purely to the electrostatic interactions between the ions and the membrane. The simple model treated lipids as a single particle with an equivalent charge (SPEC)[118]. In this paper, we go beyond this description and introduce a minimal model of the lipids where the single particle in the SPEC model is replaced by the simplest structure of different lipid headgroups. The interaction of the membrane with an electrolyte is extensively studied for three lipids - Phosphatidylserine (PS), Phosphatidic acid (PA) and Phosphatidylinositol-4, 5-bisphospate (PIP2).

5.3 Model Description

The three anionic lipids that are the focus of this study are glycerophospholipids or phosphoglycerides. These lipids contain a glycerol phosphate backbone, that connects a hydrophilic head group to a hydrophobic tail. A reduced structure of the lipids is used in this study as shown in Fig. 5.1. The hydrophobic tail that makes up the bulk of a lipid structure does not interact with the aqueous environment, surrounding the cell, and hence is omitted. Hydrogen atoms are not included as separate atoms in any of the structures.

The specifics of each of the three phospholipids (PS, PA, PIP2) are discussed below:

(i) Phosphatidyl Serine (PS) consists of a serine group as its head-group . There are three charge centers in this headgroup arising from the phosphate group in the glycerol phosphate backbone (pKa $\approx$ 1), the amino group on serine (pKa = 9.8) and the carboxyl group on serine(pKa = 3.6). [92]. This gives the PS group a net charge of -1e. (Fig. 5.1(a))

(ii) Phosphatidic acid (PA), consists of a phosphate group as the head-group. The charge on a PA group varies between -1e and -2e depending on the number of oxygens in the phosphoryl group that are deprotonated. The extent of deprotonation is controlled primarily by the pH. [120] (Fig. 5.1(b)).

(iii) Phosphatidylinositol-4,5-bisphosphate or PtdIns(4,5)P2 (PIP2) belongs to the family of phosphatidylinositol. It has phosphorylations on the 4th and the 5th position on the inositol

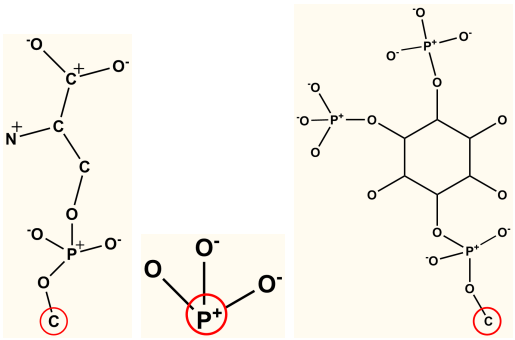

(a) PS (b) PA (c) PIP2

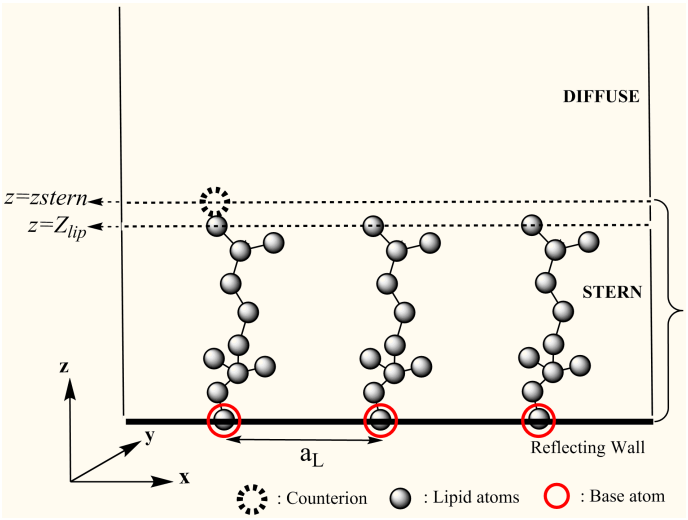

(d) Cross sectional view

Figure 5.1 (Color online) **(a)-(c)** Headgroup structure of phospholipids used in this paper - Phosphatidylserine (PS), Phosphatidic acid (PA), Phosphatidylinositol-(4,5)-bisphosphate (PIP2) **(d)** Cross sectional view of the simulation box. Atom marked with a red circle in each case represents the baseatom.

ring. The charge on PIP2 varies between -3e and -5e depending on its environment and its interaction with proteins [121] (Fig. 5.1(c)).

In this study, a charge of -1e, -1e and -4e is assigned to PS, PA and PIP2 respectively.

A monolayer of lipids is constructed using a specified number of lipid headgroups that are arranged such that each lipid occupies an area Ac, in the x-y plane. The baseatom of each headgroup is marked in Fig. 5.1. This atom lies in the z=0 plane. Typical size of the systems consists of 10x10 = 100 lipids in the monolayer. Results of simulations with larger (25x25) systems were usually indistinguishable from the (10x10) systems. Results of smaller systems showed some deviations arising from their finite size. The electrolyte in contact with the monolayer has N_{cc} counterions (charge q_{cc}) and N_{co} coions (charge q_{co}). In bulk, the concentration of these ions is n^b_α ($\alpha = cc, co$ for counterions and coions respectively) and satisfies the neutrality condition $\sum_{\alpha=1}^{2} q_\alpha n^b_\alpha = 0$.

5.4 Notations and Terminology

This section includes definitions of frequently used terms in the context of the paper.

n_α(x,y,z): The primary observable in the simulations is the number density of the ions n_α(x,y,z) given by

$$n_\alpha(x, y, z) = \Sigma_i^{N_\alpha} \langle \delta(x - x_i)\delta(y - y_i)\delta(z - z_i) \rangle \tag{5.1}$$

where $\alpha = cc, co$ for counterions and coions respectively and N_α is the total number of ions of type α. The ion concentration along one of the coordinates is obtained by averaging over the other two. In this paper, ion concentration refers to the number density of the ions along z, $n_\alpha(z)$, averaged over x and y coordinates (unless stated otherwise).

Stern layer refers to the region of the simulated system which is in close proximity to the lipid monolayers. Given that Z_{lip} is the z-coordinate of the atom farthest from the baseatom at z=0, the stern layer refers to the region $z = 0$ to Z_{stern} where $Z_{stern} = (Z_{lip} + r_c)$. $r_c = 2^{1/6}\sigma$,

where σ is the diameter of the counterions (as shown in Fig. 5.1(d)). The values of Z_{stern} for the three lipids are tabulated in table 5.1.

$\nu_{\mathbf{avg}}$: The charge on the Stern layer surface is a result of the contributions of the interfacial charges and the counterions and coions present within the Stern layer. The average surface charge at the Stern layer (ν_{avg}) for a simulation can be calculated as

$$\nu_{avg} = \frac{q_{ic}}{\mathrm{Ac}} + \frac{\sum_\alpha q_\alpha \int_{z=0}^{Z_{Stern}} \int_{t=0}^{t_{sim}} n_\alpha(z,t)\mathrm{dz\ dt}}{t_{sim}} \tag{5.2}$$

where q_{ic} is the charge from the interface groups and α=cc,co; $n_\alpha(z,t)$ represents the density of counterions and coions at a particular z averaged over the other two coordinates at time t, t_{sim} is the total time of the simulation.

Stern surface : A plane parallel to the xy plane at $z = Z_{stern}$. It marks the end of the Stern layer and the beginning of the diffuse layer.

Four different types of simulations were considered (see Fig. 5.2) , which are described as follows:

Type IA simulations: These simulations are set up according to the description in section 5.3 & 5.5. The phospholipids are arranged in the monolayer in a gel phase. The lipid headgroups are packed using PACKMOL [122] to generate monolayers of each kind of lipid with the condition that the baseatom in each case is restricted to the z=0 plane. The rest of the lipid structure extends in the same side of the z=0 plane.

Type IB simulations: These simulations are the same as Type IA simulations, except that the phospholipids are arranged in the monolayer in a crystalline phase. The lipid head groups are arranged such that each lipid occupies the lattice site of a square lattice (area=Ac). The separation between adjacent baseatoms of the lipid structure is given by $a_L(=\sqrt{Ac})$, the lattice

Table 5.1 Region defined as the Stern layer for different lipids

Lipid	Z_{lip}(Å)	Z_{stern}(Å)
PA	0.5	0 to 3.8
PS	7.2	0 to 10.5
PIP2	8.2	0 to 11.5

constant.

Type II simulations: These simulations simulate the Stern layer only, while the diffuse layer is substituted by a uniform electric field. To carry out these simulations, first the average number of counterions and coions that reside in the Stern layer at any instant, is calculated for a corresponding Type IB simulation run. The number of coions is small and hence ignored. The calculated number of counterions are placed randomly within the Stern layer. The counterions are mobile, but restricted to the Stern layer. A uniform background charge is added to maintain charge neutrality.

Type III simulations: This type consists of simulations of the diffuse layer only keeping the Stern configuration fixed. A representative snapshot from the Type IB simulation having a Stern layer surface charge of $\nu = \nu_{avg}$ (Eq. 5.2) is chosen. A simulation is set up such that the Stern layer of the chosen snapshot is frozen i.e. all atoms and ions within the Stern layer are fixed. The number of mobile ions in the diffuse layer is adjusted to maintain the same bulk ion concentration as that of the corresponding complete simulation (type IB). A reflecting wall is placed at the Stern surface to prevent the mobile ions from entering the Stern layer.

Type IV simulations: This is a variation of type III simulations. The diffuse layer is simulated keeping the Stern layer frozen. The Stern layer configuration in this case is constructed by placing a specified number of counterions at the identified binding sites of randomly chosen lipids in the monolayer. The number of counterions is such that the net surface charge at the Stern surface is equal to ν_{avg} from the corresponding type IB simulation.

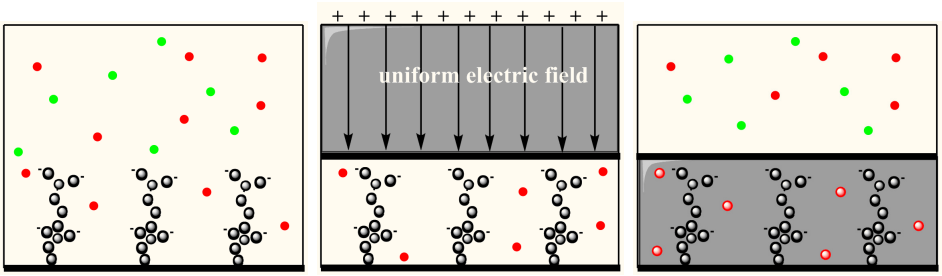

(a) typeI simulations

(b) typeII simulations (Diffuse layer replaced by a uniform electric field)

(c) typeIII simulations (Frozen Stern layer)

(d) typeIV simulations (Counterions placed at binding sites in the frozen Stern layer)

Figure 5.2 (Color online) Types of simulations. Grey areas indicate regions in the system where particles are immobile (frozen regions). The counterions (red), coions (green) and the atoms of the lipid group (grey) are shown in each case. Lipid group atoms are immobile in all cases.

5.5 Simulation Methods

We consider a system consisting of N_I lipids, N_{cc} counterions and N_{co} co-ions. The finite size of the ions is modeled as a short range interaction between the ions, which is of the Lennard-Jones type

$$V(r) = 4\epsilon_{LJ}\left[\left(\frac{\sigma}{r}\right)^{12} - \left(\frac{\sigma}{r}\right)^{6}\right] \tag{5.3}$$

where the cut-off is $r_c = 2^{1/6}\sigma$. The value of sigma used for all pairs of atoms in the lipid headgroups is an average value of all the bond lengths between atoms in the lipid headgroup $\sigma = r_{lip} = 1.5$Å. For all other interacting ion pairs it is σ=3Å. The co-ions are monovalent ($q_{co} = -1$). Different counterion valencies, $q_{cc} = 1, 2, 3$ were considered, out of which $q_{cc} = 2$ was extensively studied. The charge on the interfacial groups varies depending on the lipid, $q_{ic} = -1$ or -4. Water is modeled implicitly as a constant dielectric medium (dielectric constant, $\epsilon_r = 78$).

The systems were investigated by molecular dynamic simulations using the LAMMPS package (version 3 Feb 2013)[109]. The simulations were carried out in the canonical ensemble with a Noose-Hoover thermostat with a temperature of $T = 300$K. The equations of motion were solved with the Verlet algorithm. The system consists of a slab containing the electrolyte limited by two impenetrable planes perpendicular to the z-axis, modeled as reflecting walls on either end of the simulation box. These walls prevent ions from moving behind the phospholipid. The walls coincide with the planes containing the base atom of the lipid headgroup on both sides of the simulation box. This mimics the hydrophobic environment of a real phospholipid membrane.

The system is periodic in the x and y directions but not in the z direction. The electrostatic interactions were computed the PPPM method. We considered simulations with molecular areas Ac=70, 100, 361Å^2 as well as different concentrations. A complete list of simulations as well as the technical details necessary to reproduce them can be found in the supplementary material in Sect.6.1. The systems were equilibrated by monitoring typical observables such as the energy, density and the diffusion coefficient. A typical equilibration run took of the order of $2{\cdot}10^5$ time steps and production runs involved $5{\cdot}10^5$ time steps, although larger data sets

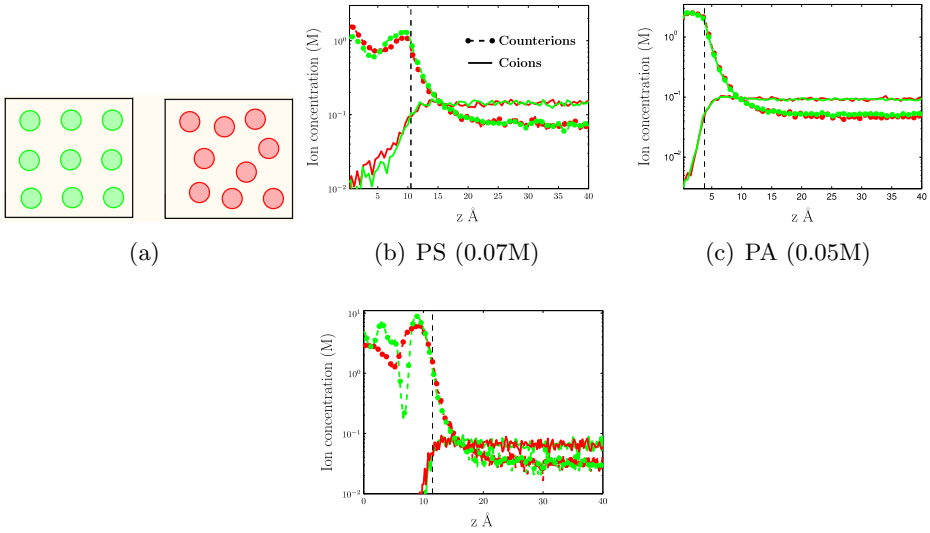

(a) (b) PS (0.07M) (c) PA (0.05M)

(d) PIP2 (0.03M)

Figure 5.3 (Color online) **(a)** Crystalline vs gel phase **(b)-(d)** Plot of n_{cc}(z) and n_{co}(z), ion distributions for perfect lattice (green) and distorted lattice (red). These results were checked for Ac= $70, 100, 361 \text{Å}^2$. Results for Ac=70Å^2 and 2:1 electrolyte are shown. The concentration of the electrolyte and Stern layer boundary (black dashed line) indicated in each case.

were collected in particular cases.

5.6 Results

5.6.1 Arrangement of lipids within the monolayer : crystalline vs gel phase

The effect of lipid arrangement within the monolayer on the ion distribution was studied by comparing type IA and type IB simulations (Fig. 5.3(a)). The ion distribution for both cases is compared in Fig. 5.3((b)-(d)). The results for the two sets of simulations in each case show some differences in the Stern region but become indistinguishable within the diffuse layer. Differences in the Stern layer are expected because the ion distributions are influenced by the arrangement of lipids. However, the energy and the number of mobile ions in the Stern layer for both cases was approximately the same (differences $\approx$ 0.1kJ/mol in total energy). Since

either arrangement does not influence the ion profile in the diffuse layer or the number of ions in the Stern layer, for the ease of analysis, the crystalline phase is chosen over the gel phase, for the remainder of this paper, without any loss of generality.

5.6.2 Decoupling the Stern and the diffuse layer

The ion distribution from a full simulation (type I) can be entirely reproduced by two separate simulations, one of the Stern layer (type II) and the other of the diffuse layer (type III) as diagramatically represented in Fig. 5.4(a). This was tested for both 1:1 and 2:1 electrolytes. The ion profile for a type II simulation (Fig. 5.4, blue), is in excellent agreement with the ion distribution of the Stern layer in the corresponding type IB simulation (Fig. 5.4, green). This implies that the counterion/lipid interaction is not affected by the ion distribution in the diffuse layer.

The results from a type III simulation (Fig. 5.4, red) show that a frozen Stern configuration with $\nu = \nu_{avg}$, is sufficient to reproduce the ion distribution observed in the diffuse layer for a full (type I) simulation. The dynamics of mobile ions within the Stern layer does not affect the ion distribution in the diffuse layer. This allows the Stern and the diffuse layer to be discussed independent of each other, sharing a common boundary at the Stern surface.

5.6.3 Stern layer analysis

The distribution of counterions in the Stern layer was further analyzed to identify the counterion binding sites. The number of binding sites per lipid (Fig. 5.5) were identified by counting the number of bound counterions per lipid at any instant. An ion within the Stern layer is considered bound to the i^{th} lipid at a given time if

$$-a_L/2 < x - x_{bi} < a_L/2 \; ; \; -a_L/2 < y - y_{bi} < a_L/2 \; ; \qquad z < Z_{stern} \quad (5.4)$$

where (x, y, z) are the coordinates of the counterion and (x_{bi}, y_{bi}) are the x and y coorindates of the base atom of the i^{th} lipid.

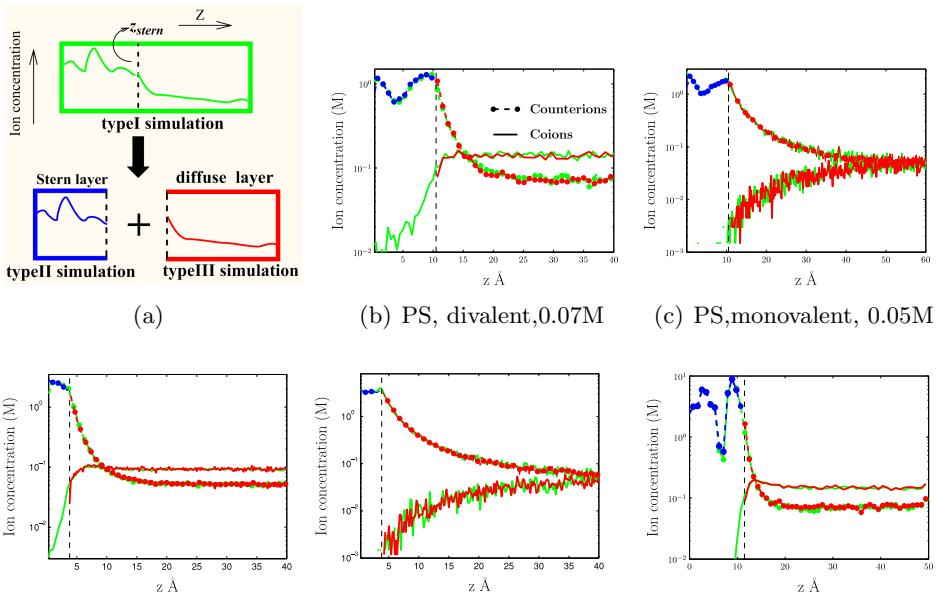

(a) (b) PS, divalent,0.07M (c) PS,monovalent, 0.05M

(d) PA,divalent,0.05M (e) PA,monovalent, 0.05M (f) PIP2, divalent,0.07M

Figure 5.4 (Color online) **(a)** Diagramatic representation of decoupling of Stern and diffuse layer. **(b)-(f)** Ion distribution comparison of the typeIB simulation (green) with the corresponding typeII (red) and typeIII simulations (blue) for Ac=70Å^2. The concentration of the electrolyte and Stern layer boundary (black dashed line) indicated in each case.

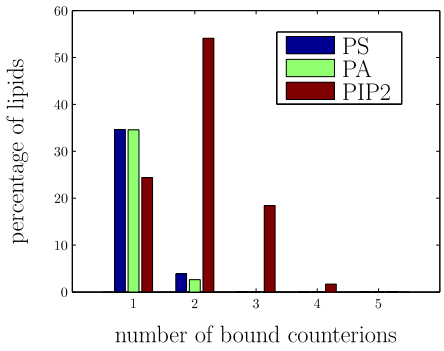

Figure 5.5 (Color online) Number of bound divalent counterions per lipid for Ac=70Å^2, 2:1 electrolyte (observed for bulk ion concentrations in range 0.02 to 0.1M).

The binding sites were then characterized based on the location of the bound counterion with respect to the associated lipid. Cylindrical coordinates are used to characterize the binding sites. The (ρ, z, θ) for the binding sites were determined as follows : (i) In each case the peaks in the $n_{cc}(z)$ distribution (z_{peak}) were used to identify possible z coordinates where counterions reside. These peaks correspond to the negative charge centers within the lipid headgroup. (ii) For all counterions in the band $z_{peak} \pm \delta z$, the ρ values are calculated with respect to a chosen reference atoms, with $\rho_{max} = a_L/2$ (beyond this point the counterion would be considered associated with the adjacent lipid). The reference atom in each case is chosen as an atom whose z coordinate is closest to the z_{peak}. (iii) The counterions which lie within $\rho_{peak} \pm \Delta\rho$ were then used to calculate the angle θ with respect to a reference bond. The chosen reference atom is at one end of the reference bond.

The results from type IB simulations for molecular area 70 and 100Å^2 were used to identify the binding sites for divalent counterions for each of the three phospholipids. The binding sites of divalent counterions, determined for each lipid are shown in Fig. 5.6. The reference atom (grey) and the reference bond (red) are marked in each case.

It has already been shown that the dynamics of the ions in the Stern layer does not affect the distribution within the diffuse layer (see section 5.6.2). Considering that the counterions reside in well defined binding sites, a Stern layer configuration built by placing the counterions at the binding sites should be equivalent to a frozen snapshot of the Stern layer obtained from a

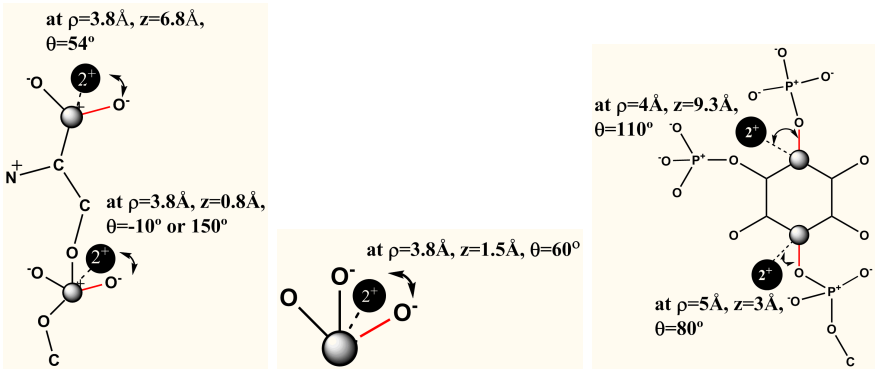

(a) PS (b) PA (c) PIP2

Figure 5.6 (Color online) Binding sites of divalent counterions identified for each lipid. The coordinates (ρ, z, θ) for each binding site with respect to the reference atom (grey sphere) and reference bond (red) is indicated in each case.

type IB simulation. To confirm this, a type IV simulation was set up such that the number of counterions in the Stern layer match the average number of counterions within the Stern layer for the corresponding type IB simulation. The ion distribution in the diffuse layer shows remarkable agreement to the corresponding type IB simulation (Fig. 5.7). No coions are placed in the Stern layer. This causes minor differences in the coion distribution close to the Stern surface, but does not have a significant effect on the overall ion distribution in the diffuse layer. Also the internal energy of the Stern layer configuration used for the type IV simulations matches the average Stern layer energy of the type IB simulation within error ($0.5 k_B T$).

5.6.4 Diffuse layer analysis

The diffuse layer starts at $z = Z_{stern}$. In case of monovalent counterions i.e. a 1:1 electrolyte, the ion distribution in the diffuse layer can be described using a Poisson Boltzmann (PB) distribution with a surface charge $\nu = \nu_{avg}$ (Fig. 5.8).

In case of systems with divalent counterions i.e. a 2:1 electrolyte, however, the diffuse layer distribution does not conform to the PB theory. At comparable surface charges, the exact ion distribution for a 2:1 electrolyte interacting with a uniformly charged interface showed relatively minor deviations from the PB theory (see supplementary material in Sect.6.3). The deviation

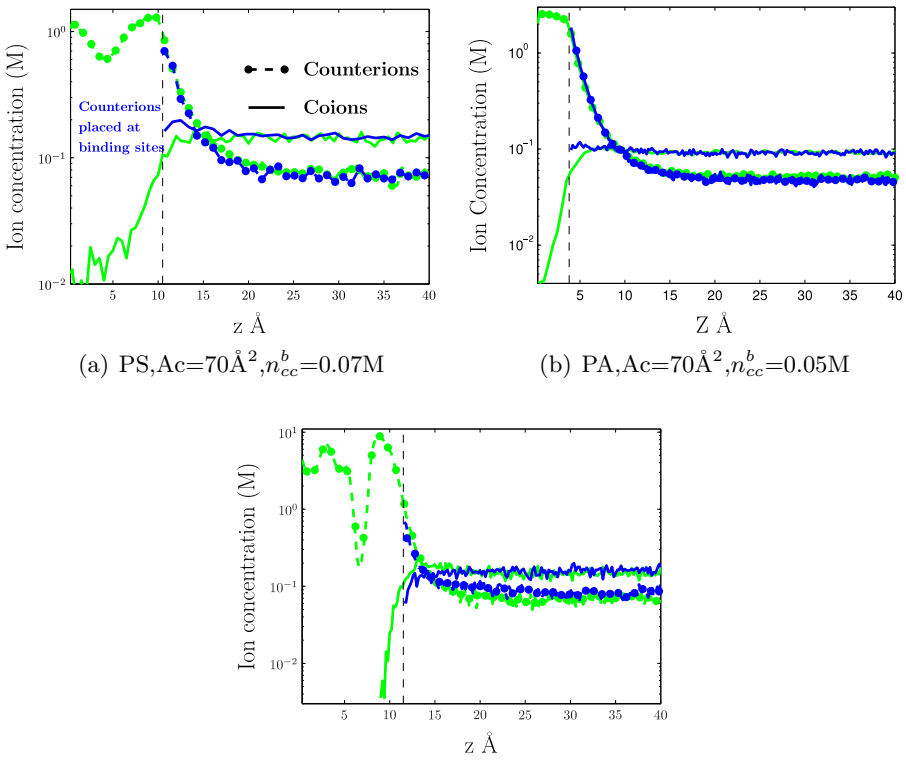

(a) PS,Ac=70Å^2,n^b_{cc}=0.07M (b) PA,Ac=70Å^2,n^b_{cc}=0.05M

(c) PIP2,Ac=70Å^2,n^b_{cc}=0.07M

Figure 5.7 (Color online) Plot of n_{cc}(z) and n_{co}(z),Ac=70Å^2. Ion distributions for full simulation (type IB) in green, and ion distribution for the case where the Stern layer was built by placing counterions at the binding sites (Type IV simulations) in blue. The Stern layer boundary is indicated by the black (dashed) line.

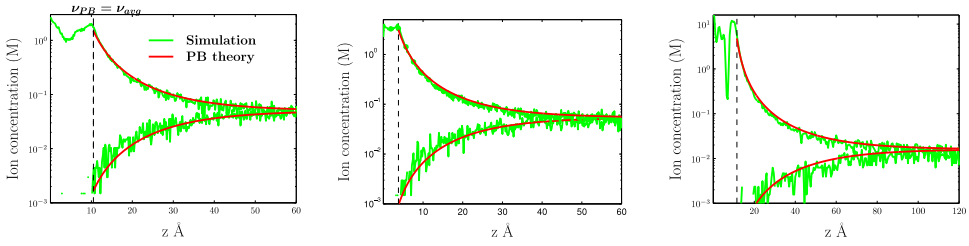

(a) PS,n^b_{cc}=0.05M (b) PA,n^b_{cc}=0.05M (c) PIP2,n^b_{cc}=0.02M

Figure 5.8 (Color online) Plot of n_{cc}(z) and n_{co}(z),Ac=70Å^2 for 1:1 electrolyte. Comparison of ion distribution in the diffuse layer for typeIB simulation (green) with Poisson Boltzmann distribution (red). The Stern surface is indicated by the black (dashed) line.

from PB theory for the diffuse layer distribution in the simulations should thus be attributed to the non-uniform surface charge density at the Stern surface. It was indeed found that the region of the diffuse layer in proximity of the Stern surface is decribed by a number distribution $n_{cc}(x, y, z)$, given by

$$n_{cc,calc}(x, y, z) = n_0 e^{-q_{cc}\phi_I(x,y,z)/\mathrm{k}_B\mathrm{T}} \tag{5.5}$$

where $\phi_I(x, y, z)$ is the bare potential at point (x, y, z), that is the potential due to the interfacial charges only. Interfacial charges include all charges within the Stern layer (i.e. charges on lipids and the bound counterions). The potential $\phi_I(x, y, z)$ and $n_{cc,calc}(z)$ were calculated as described in detail in the supplementary material in Sect.6.4. Results shown in Fig. 5.9. It was found that these calculations correctly predict ion distributions in the region Z_{Stern} to $Z_{Stern} + \Delta z$. Δz ranges from 1 or 1.5Å, depending on the molecular area Ac and the bulk ion concentration.

The trailing end of the diffuse layer is described well by the ion distribution from the SPEC model (as shown in Fig. 5.9, black markers). The results from SPEC simulations are shifted in each case, such that the surface charge $\nu_{avg}(Z_{Stern} + \Delta z)$ from the lipid monolayer simulations coincides with that of the SPEC model simulations. The charge on the SPEC particles interfacial charge in case of the SPEC simulations is $-1e/Ac$ for PS and PA, and $-4e/Ac$ for PIP2.

5.6.5 Mixed lipid monolayers

The effect of ionic concentration in clustering of PIP2 is studied by considering the number of bound counterions as a function of PIP2 concentration. A mixed lipid layer configuration of PS and PIP2 was generated by starting with a pure PS monolayer from type IB simulations. A specified percent of the molecules were then replaced by PIP2. Both clustered and dispersed arrangement of PIP2 molecules within the PS monolayer (Fig. 5.10(a)-(b)), were tested for different PIP2 and bulk ion concentrations. The decoupling of the Stern and diffuse layer as described for pure lipid monolayers also extends to mixed lipid layers as shown in Fig. 5.10(c)-

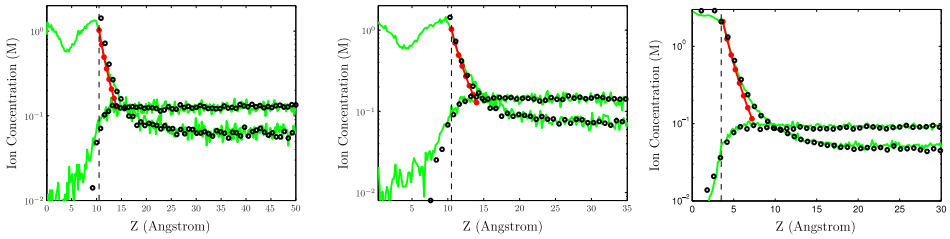

(a) PS,n^b_{cc}= 0.06M (b) PS,n^b_{cc}=0.07M (c) PA,n^b_{cc}=0.05M

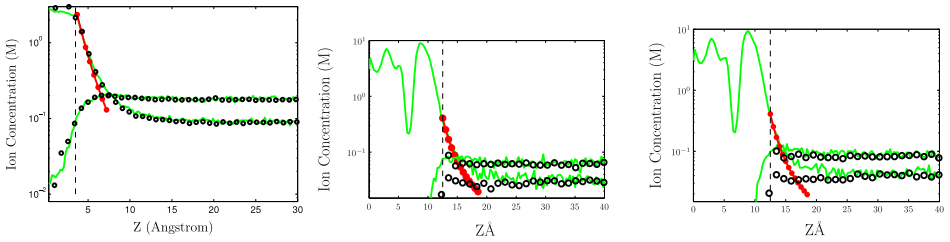

(d) PA,n^b_{cc}=0.09M (e) PIP2,n^b_{cc}=0.03M (f) PIP2,n^b_{cc}=0.05M

Figure 5.9 (Color online) Plot of n_{cc}(z) and n_{co}(z),Ac=70Å^2, 2:1 electrolyte. Comparison of ion distribution in the diffuse layer for typeIB simulation (green) with prediction from potential calculations (red) and ion distribution from the SPEC model (black markers). The Stern surface is indicated by the black (dashed) line

(d)).

The number of counterions bound to each lipid in the monolayer were identified using the criteria in Eq. 5.4. The fraction of counterions bound per lipid (for lipid type ν=all, PS or PIP2) is then calculated as :

$$f_{cc,\nu} = \frac{\int_{t=0}^{t_{sim}} N_{cc,\nu} dt}{t_{sim} N_{I,\nu}} \tag{5.6}$$

where $N_{cc,\nu}$ is the total number of counterions bound to lipid type ν, t_{sim} is the total time of simulation and $N_{I,\nu}$ is the total number of lipids in the monolayer of type ν.

The number of bound counterions does not show significant differences for bulk ion concentrations in the range 0.005-0.1M (refer supplementary material in 6.5). For a given value of PIP2 and bulk ion concentration, the total number of counterions in the Stern layer is the same for both a clustered or dispersed configuration. The binding location of counterions, however, is strongly influenced by the clustering of PIPs. As clear from Fig. 5.11(a)-(b), there is a coop-

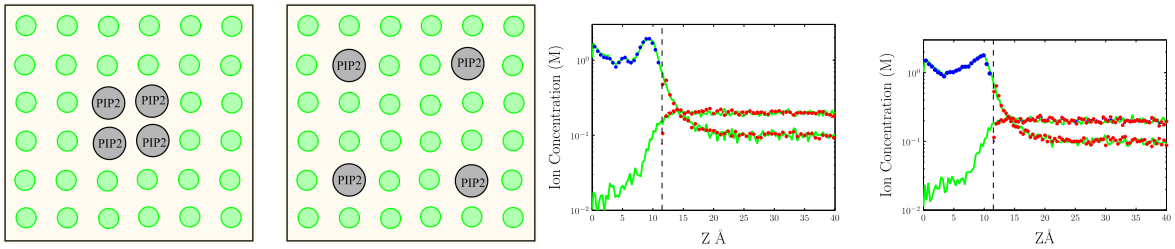

(a) PIP2 clustered configuration

(b) PIP2,dispersed configuration

(c)

(d)

Figure 5.10 (Color online) **(a)** Clustered and **(b)** dispersed configuration of mixed monolayers (PS (green), PIP2 (gray)). **(c) - (d)**: Ion distribution comparison of the full(type IB) simulation (green) with a corresponding frozen snapshot (typeIII) simulation (red) and (type II) simulation of the Stern layer (blue) for Ac=70Å^2. (10 % PIP2) for clustered and dispersed configurations respectively.

erative effect in enhancing binding of PIPs at the expense of PS when PIPs are clustered, while the binding fraction is approximately the same when PIPs are dispersed. The internal energy of the Stern layer is lower in case of the clustered configuration for a given PIP2 concentration (Fig. 5.11(c)), suggesting that the system prefers the clustered state over the dispersed state at this bulk ion concentration.

5.7 Conclusion

We have shown how to separate the Stern and diffuse layer into two independent entities that can be analyzed separately. We have provided a *minimal* coarse grained model for three anionic phospholipids, Phosphatidylserine (PS), Phosphatidic acid (PA) and Phosphatidylinositol(4,5)bisphosphate (PIP2), thus enabling a description of the Stern layer in terms of a Bjerrum pairing theory [59]. The diffuse layer is described by Poisson-Boltzmann (monovalent ions) [35] or by strong coupling theory [69] followed by a SPEC model [118] tail, as summarized in Fig. 5.12.

The description in terms of Bjerrum pairing allows to build the Stern layer by placing the counterions at the identified binding sites, without any error in the the ion distribution in the diffuse layer. The discreteness of the interfacial lipids becomes crucial for divalent counterions,

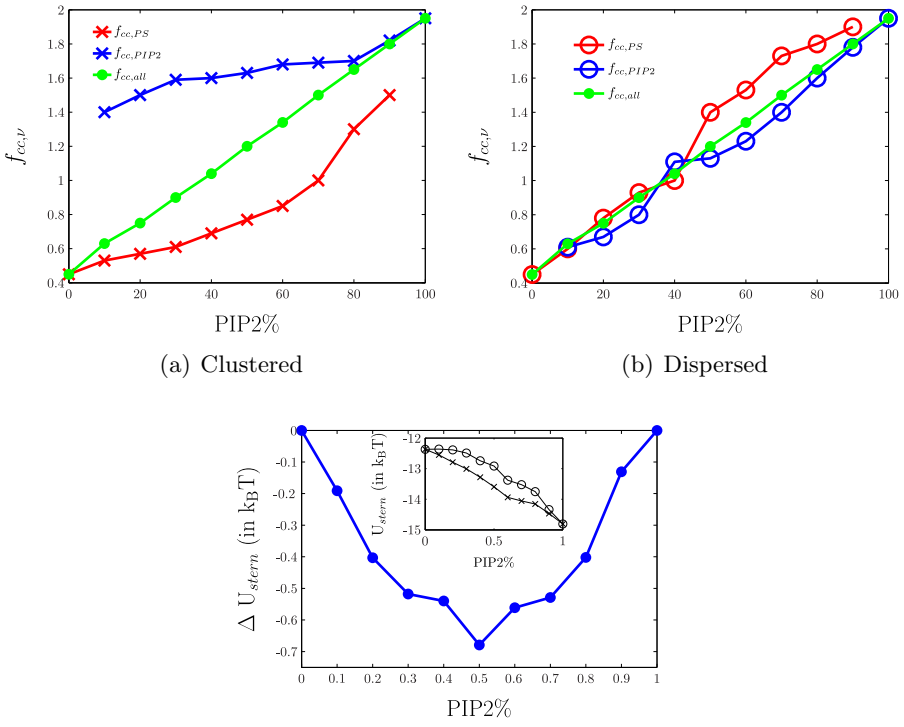

(a) Clustered (b) Dispersed

(c)

Figure 5.11 (Color online) **(a)-(b)** Number of bound ions per lipid as a function of PIP2 % for the same bulk ion concentration 0.02M. Results for (a) clustered configuration and (b) dispersed configuration. **(c)** Difference in internal energy of the Stern layer (U_{stern}) for the two configurations, $\Delta U_{stern}=U_{stern,cluster}-U_{stern,disperse}$. ($U_{stern}$ values for the clustered ($\times$) and dispersed ($\bigcirc$) configuration are shown in the inset plot.)

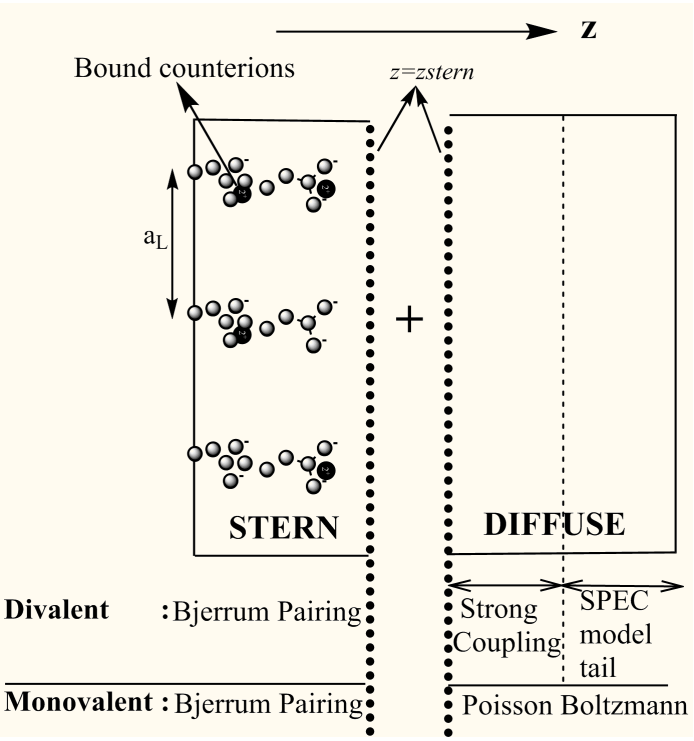

Figure 5.12 Summary of results

where PB breaks down and where clustering of PIPs results in preferential binding. The ion profiles in the region of the diffuse layer in close proximity of the Stern surface (1 to 1.5Å) for divalent counterions, depend on the bare potential of the surface as predicted by strong coupling theory [69], see Fig. 5.9. The predictions of strong coupling, however, do not extend to the remaining of the distribution, but rather, there is a tail, which is difficult to capture with analytical theories, as extensively described in Ref. [118]. The results presented are specific to three lipids, but extending these results to other lipids should be straightforward as long as the head group structure of the lipid is known.

Binding of Ca^{2+} to PS bilayers has been studied using all atom molecular dynamic simulations [123], showing site specific binding of the ions to PS head groups. The results from these all atom simulations show that calcium ions reside in the negative charge center created by the two carboxyl oxygens in the serine group, which is one of the binding sites predicted within the coarse-grained models presented here. For PIP2, the binding sites for Ca^{2+} ions have been analysed using all atom simulations in [124]. According to their simulations, the Ca^{2+} ions bind to the lipid at a distance of 2Å from the oxygens on the two phosphate groups on the inositol ring. The binding site as predicted from our coarse grained simulations is also equidistant from the two closest oxygen atoms on the phosphate groups (at a distance of $\approx$ 3.4Å). One of the reasons for the difference in binding distance could be the implicit solvent used in our model. Overall, the coarse-grained model presented in this paper represents very well the binding sites of lipid monolayers for small surface area per lipid.

Our studies show that ions within the Stern layer are described in terms of binding theory which is described by classical electrostatics, thus providing a more rigorous validation of our previous model, [111] where binding was described in terms of electrostatic binding constants that are predicted from Bjerrum theory [59]. In Ref. [111] the diffuse layer was described within PB theory, but the simulations reported in this paper show a more nuanced scenario in terms of strong coupling theory [69] and a SPEC [118] tail. Still, the very good agreement of the results in Ref.[111] with reported experimental binding constants such as [125, 91], shows

that PB theory may still provide an approximate description of the free energy of the diffuse layer that may be appropriate for semi-quantitative descriptions.

For divalent concentrations 0.005-0.1M, and PIP2 % in the range 10-80 %, the results within this model predict a preferential binding of divalent ions to clustered PIPs, with a decrease of internal energy of 0.4-0.7k_BT per site. Given that the total number of bound counterions is the same (and thus, it only depends on the overall surface charge of the Stern layer) in a clustered and dispersed configuration, the binding entropy of the bound ions is roughly the same, and therefore, there is a decrease of free energy given by 0.4-0.7k_BT per site.

In summary, our results report a rigorous way to separate the Stern and Diffuse layers so that they can be described independently. The Stern layer can be described simply in terms of Bjerrum pairing or with more sophisticated simulations, which could even include for example, all atom descriptions with explicit water or even polarizable models. Since those simulations are basically two dimensional, they are readily affordable with modern day computational resources. The diffuse layer can be described with simple electrostatic models with implicit solvent, or for qualitative or semi-quantitative analysis, can be described by PB theory, despite the limitations of this theory to accurately reproduce ionic distributions. As a concrete application, we have discussed the clustering of PIP2 depedending on calcium ion concentration. We will elaborate further in subsequent publications.

Acknowledgments We are indebted to Monica H. Lamm for discussions as well as for providing us with computer facilities. This work is supported by NSF through the grant CAREER DMR-0748475.

CHAPTER 6. SUPPLEMENTARY MATERIAL : SEPARATION OF THE STERN AND DIFFUSE LAYER IN COARSE-GRAINED MODELS ; THE CASE OF PHOSPHATIDYL SERINE, PHOSPHATIDIC ACID AND PIP2 MONOLAYERS

6.1 Simulation Variables and Parameters for Lipid Monolayers

The parameters used in the simulations are listed in Table 6.1. The interaction potential is implemented using the pair style $lj/cut/coul/long$.

Table 6.1 MD parameters simulation

	Parameter	Value
Lennard Jones	epsilon(ϵ_{LJ})	1 kcal/mol
	sigma(σ_{LJ})	3.0 Å
	rcut($rcut_{LJ}$)	3.3 Å
Coulomb (pppm)	cut-off	40 Å
	precision	$1e^{-5}$
Reflecting walls in z direction	zlo	-0.1 Å
	zhi (varying)	Lz+0.1Å
Ensemble	Integrator	nvt
	Temperature	300 K
	Relaxation Constant	100fs
Equilibration Run	# of steps @ time-step	3×10^5@$5.0fs$
Production Run	# of steps @ time-step	4×10^5@$5.0fs$

6.1.1 Phosphatidyl serine

Data table for full simulations of Phosphatidyl Serine (PS) monolayers for 1:1 and 2:1 electrolytes. (Table 6.2 & 6.3).

Table 6.2 Simulations for Phosphatidyl Serine (1:1 electrolyte)

A_c (Å^2)	N_{cc}	N_{ic}	zhiÅ7	c_BM
70	250	100	300	0.05
70	300	100	150	0.20

Table 6.3 Simulations for Phosphatidyl Serine (2:1 electrolyte)

A_c (Å^2)	N_{cc}	N_{ic}	zhiÅ	c_BM
70	120	100	200	0.026
70	200	100	400	0.063
70	200	100	350	0.071
100	150	100	300	0.030
100	150	100	215	0.044
100	160	100	150	0.073
361	200	100	200	0.025
361	300	100	200	0.047
361	400	100	200	0.071

6.1.2 Phosphatidic acid

Data table for full simulations of Phosphatidic Acis (PA) monolayers for 1:1 and 2:1 electrolytes. (Table 6.4 & 6.5)

Table 6.4 Simulations for Phosphatidic Acid (1:1 electrolyte)

A_c (Å^2)	N_{cc}	N_{ic}	zhiÅ7	c_BM
70	250	100	280	0.054

6.1.3 Phosphatidylinositol 4 5-bisphosphate

Data table for full simulations of Phosphatidylinositol 4 5-bisphosphate (PIP2) monolayers for 1:1 and 2:1 electrolytes. (Table 6.6 & 6.7)

6.1.4 Mixed lipid simulations (PS, PIP2)

Data table for full simulations of mixed lipid monolayers containing PS and PIP2 for 2:1 electrolytes (Table 6.8). The simulations were performed for different fractions of PIP2 in the monolayer both for dispersed and clustered configurations as explained in the main text.

Table 6.5 Simulations for Phosphatidic Acid (2:1 electrolyte)

A_c (Å^2)	N_{cc}	N_{ic}	zhiÅ7	c_BM
70	700	1259	120	0.033
70	800	1250	150	0.046
70	900	1250	120	0.093
100	700	1250	100	0.033
100	800	1250	100	0.050
100	1000	1250	110	0.096
361	1000	1250	75	0.042
361	400	100	200	0.071

Table 6.6 Simulations for PIP2 (1:1 electrolyte)

A_c (Å^2)	N_{cc}	N_{ic}	zhiÅ7	c_BM
70	850	100	800	0.023

6.2 Effect of Lipid Structure of Ion Distribution

Iion distributions for a 2:1 electrolyte interacting with a charged monolayer are compared for (i) A monolayer built using a single particle with equivalent charge (SPEC) model (ii) A monolayer built using the lipid headgroup structure (in this case PIP2). At the same bulk ion concentration the distributions are substantially different (refer Fig. 6.2).

Table 6.7 Simulations for PIP2 (2:1 electrolyte)

A_c (Å^2)	N_{cc}	N_{ic}	zhiÅ	c_BM
70	425	100	200	0.033
70	425	100	150	0.046
70	425	100	100	0.074
100	425	100	150	0.032
100	425	100	100	0.050
100	450	100	100	0.101
361	500	100	150	0.033
361	500	100	100	0.049
361	500	100	70	0.073

Table 6.8 Simulations for PS:PIP2 (2:1 electrolyte)

A_c (Å^2)	N_{cc}	N_{PIP2}	N_PS	zhiÅ	c_BM
70	250	10	90	300	0.10
70	150	10	90	300	0.02
70	165	20	80	300	0.005
70	175	20	80	300	0.01
70	180	20	80	300	0.02
70	250	20	80	300	0.088
70	210	30	70	300	0.02
70	240	40	60	300	0.02
70	270	50	50	300	0.02
70	300	60	40	300	0.02
70	330	70	30	300	0.02
70	345	80	20	300	0.005
70	350	80	20	300	0.01
70	370	80	20	300	0.02
70	450	80	20	300	0.1
70	390	90	10	300	0.02

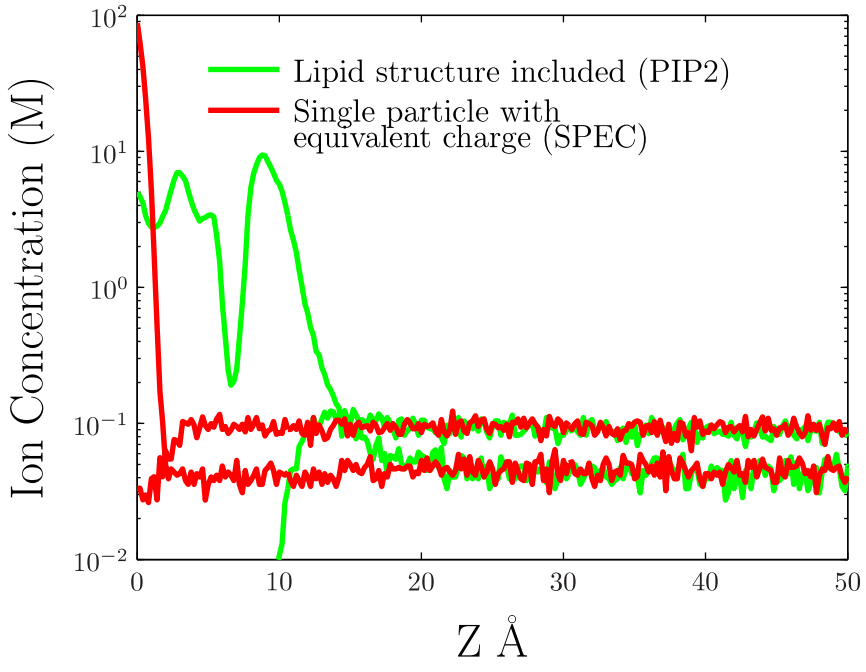

Figure 6.1 Ion distribution for SPEC and PIP2 compared for Ac=70Å^2 and bulk ion concentration 0.046M.

6.3 Comparison of Uniform Charge Simulations and Poisson Boltzmann

For a surface charge density $\sigma = -0.0029\text{Å}^2$, and bulk ion concentration 0.03M, the ion distribution from a uniformly charged interface agrees reasonably well with Poisson Boltzmann (PB) predictions for divalent counterions. Minor deviations can be attributed to ion-ion correlations, which are not incorporated in PB. (Fig. 6.3)

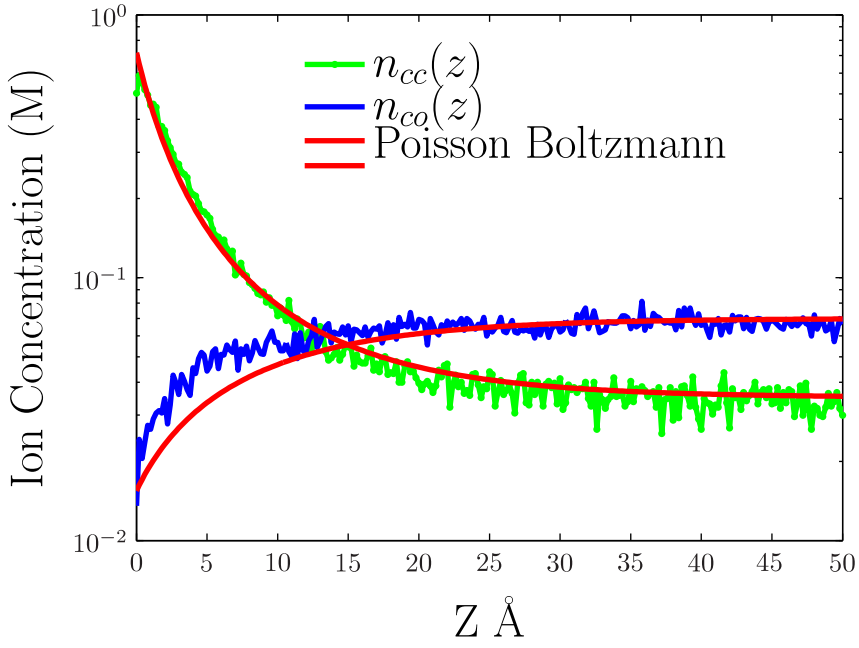

Figure 6.2

6.4 Interfacial Potential and Number Density Calculations

If the value of the electrostatic potential $\phi(x, y, z)$ is known at every point, a number density can be defined as

$$n_{\alpha,calc}(x, y, z) = n_{\alpha}^{b} e^{-q_{\alpha}\phi(x,y,z)/\mathrm{k}_B\mathrm{T}} \tag{6.1}$$

To compute the ion distribution in the diffuse layer for the lipid monolayer system using this method, a fixed Stern layer configuration was chosen. For each $z = Z_{stern}, Z_{stern} + \delta z, Z_{stern} + 2\delta z$ and so on, the xy plane was divided into grids (grid spacing= 2Å). The potential was calculated at every grid point ($\phi^{'}(x, y, z)$). The number distribution along the z direction was computed by averaging the same over the other two coordinates such that

$$n_{cc,calc}(z) = n_0 \frac{\int_{x=0}^{L_x}\int_{y=0}^{L_y} e^{-q_{cc}\phi^{'}(x,y,z)/\mathrm{k}_B\mathrm{T}}\mathrm{dx\ dy}}{\mathrm{L}_x\ \mathrm{L}_y} \tag{6.2}$$

where L_x,L_y are lengths of the system in the x and y dimensions. The normalization constant n_0 is chosen to match the calculated density to the observed density of ions at the Stern surface i.e. ($n_{cc,calc}(Z_{stern}) = n_{cc}(Z_{stern})$). A uniform background charge was added in each case to make the system charge neutral. This is done by placing a lattice of ions with appropriate charge to neutralize the Stern layer, sufficiently far from the Stern layer such that the generated electric field is uniform at the Stern surface. (If the baseatom of the lipid groups in the Stern layer are at $z = 0$, the lattice of ions is placed at $z \geq 4a_L$).

6.5 Number of Ions Bound as a Function of Concentration

The number of ions bound to PS and PIP2 as a function of bulk ion concentration. The results do not vary as a function of concentration as is evident from Fig. 6.5.

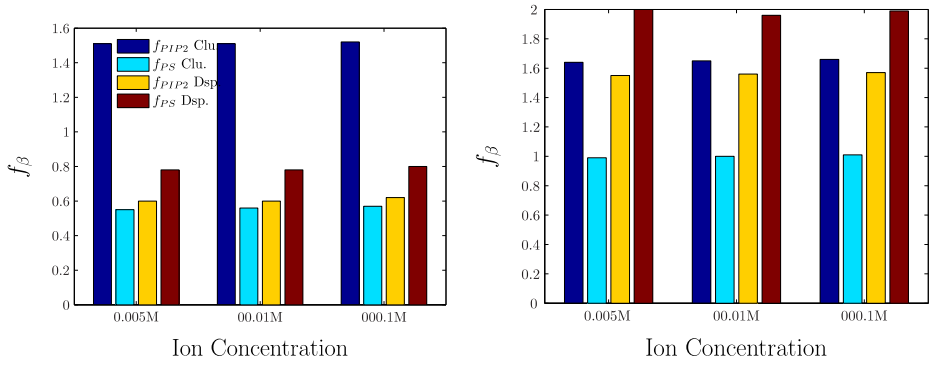

Figure 6.3 **(a)** PIP2 % = 20%. textbf(b) PIP2 % = 80%. For each value of concentration, the first two peaks are the number of bound ions per lipid for the clustered (Clu.) configuration (blue for PIP2, cyan for PS) and the next two peaks are number of bound ions per lipid for the dispersed configuration (yellow for PIP2 and brown for PS).

CHAPTER 7. CONCLUSION

The wide variety of vital cellular functions that membranes carry out by the lateral reorganization and compartmentalization of its components has made them the new target for understanding and treating the cause and propagation of several aging and metabolic disorders (like Alzheimer's, diabetes etc.) and viral and bacterial infections. Manipulating dietary cholesterol levels in animals has been linked to alterations in microdomain structure and composition thus influencing their functions [126]. Thus being able to narrow down and evaluate other parameters that affect microdomain structure would open the doors for several new targets that can be regulated to achieve the desired results. One such parameter is the interaction of positive divalent ions and basic polypeptides with the highly charged anionic lipid PIP2. Electrostatics induced clustering of anionic lipids has been identified as an important step in signal transduction [127, 14]. In this study we have developed a coarse grained model for lipids in order to study their interaction with surrounding electrolytes and predict the phase behavior of lipid monolayers in the light of electrostatics.

Starting with a simple model as described in chapter 2, where the headgroup of Phosphatidyl serine, an anionic phospholipid is approximated as a single particle with equivalent charge (SPEC model), it is shown that for monovalent and divalent ions like Na^+, K^+, Ca^{2+},Ba^{2+}, the interaction of electrolytes with the lipid monolayers can be described by electrostatics. Based on the free energy values of the system (calculated as described in chapter 2), the configuration of the system under different conditions like varying ion concentrations, pH and the counterion valence, is predicted. The configuration is determined by two variables - fraction of deprotonated lipids (f_{AL}) and the fraction of lipids with a bound counterion (f_b). Both these variables can be experimentally determined. The calculated values of f_{AL} and f_b,

show remarkable agreement with the experimental results. The most important consequence of this theoretical model is its ability to predict values of experimentally determined binding constants for ion-lipid association.

In systems where the charges on the interface are close to each other, counterion binding to the interfacial charges gives an accurate description of the Stern layer. This is the case for closely packed anionic lipid monolayers. Such systems are described by the theoretical model discussed above. However, when these anionic lipids are separated by membrane components like sterols, zwitterionic lipids like Phosphatidyl choline etc. the systems correspond to a case where the interfacial charges are separated by large distances leading to considerable movement of the counterions within the Stern layer. Molecular dynamic simulations were utilized to explore this regime in detail. The results from this set of simulations led to a general solution to the Planar Discrete Double Layer (PDDL) model, which comprises of fixed charges on a plane in contact with an electrolyte. The general approach when dealing with electric double layers is treating the system as a combination of a Stern layer and a diffuse layer. It was observed that the same approach could be extended to this system as well, with a displaced diffuse layer. Based on the area occupied per lipid Ac, the analysis was divided into different regimes. (i) Binding Regime : For small values of Ac, the picture that emerges from this study supports the one proposed in [111] where the Stern layer is described by binding of counterions to surface charges. In case of monovalent counterions the diffuse layer is described by the Poisson Boltzmann (PB) theory. (ii) Plasma Regime : In case of large values of Ac, i.e. when lipids are farther apart, counterion diffusion is evident within the Stern layer. The proposed solution in [118] provides an expression to calculate the ion distribution in the Stern layer for both monovalent and divalent counterions. In case of monovalent counterions, the diffuse layer starts at σ (the diameter of the counterions) and is accurately described by PB theory. For divalent counterions, the effect of discreteness of the interfacial charges extends the Stern layer to around $\sqrt{Ac}/3$. The ion distribution beyond this point i.e. in the diffuse layer can be represented by PB theory.

So far, Phosphatidyl serine which is a monovalent phospholipid was approximated as a single charge and we have a semi-analytical approach to predict ion distributions in such systems. In order to extend the analysis to multivalent lipids like Phosphatidic acid and PIP2, for exam-

ple, where subtleties arise from the higher valence and multiple binding sites, the effects of an extended structure of the lipids would have to be examined.The final part of this study focused on analyzing such systems by replacing SPEC with headgroup structures of different lipids (chapter 5). It was observed that the structure and the charge on the headgroup together dictate (i) the amount of charge in the Stern layer in equilibrium (ii) the extent to which the diffuse layer is displaced from the impenetrable hydrophobic boundary of cell membranes. The Stern layer and diffuse layer can be decoupled and treated independent of each other sharing a common surface at the Stern boundary. The binding sites of divalent counterions predicted from the results of these simulations to a good extent match those derived from experimental studies. Further, simulation results from mixed lipid monolayers of PS and PIP2 show that divalent cations favor clustered PIP2 over dispersed PIP2 configurations. The internal energy calculations indicate that, in the presence of divalent ions, same number of PIP2s when grouped together in the monolayer form a more stable system than when they are farther apart.

In summary we have provided through this study a general solution for studying the interaction of discretely charged interfaces with electrolytes, keeping anionic phospholipids as the primary focus. In both cases (SPEC and phospholipid monolayers) we have provided means to predict the ion distribution in the Stern layer (an analytical expression in case of the SPEC model and binding sites in case of phospholipid monolayers). The decoupling of the Stern and the diffuse layer allows one to use the desired level of coarse-graining or detailing in each layer to study a target process. As for the interactions governing the clustering of PIP2s, our model supports the experimental findings - electrostatic interactions of PIP2 clusters with divalent ions leads to a more stable system compared to the electrostatic interactions of dispersed PIP2s with divalent ions.

BIBLIOGRAPHY

[1] Garcia, Z., Kumar, A., Marques, M., Cortes, I., Carrera, A.C.: Phosphoinositide 3-kinase controls early and late events in mammalian cell division. EMBO J **25**(4) (February 2006) 655–661

[2] Saiardi, A., Resnick, A.C., Snowman, A.M., Wendland, B., Snyder, S.H.: Inositol pyrophosphates regulate cell death and telomere length through phosphoinositide 3-kinase-related protein kinases. Proceedings of the National Academy of Sciences of the United States of America **102**(6) (2005) 1911–1914

[3] Gorter, E., Grendel, F.: On biomolecular layers of lipoids on the chromocytes of the blood. The Journal of experimental medicine **41** (1925) 439443

[4] Danielli, J., Davson, H.: A contribution to the theory of permeability of thin films. Journal of Cellular and Comparative Physiology **5** (1935) 495

[5] Singer, S.J., Nicolson, G.L.: The fluid mosaic model of the structure of cell membranes. Science **175**(4023) (1972) 720–731

[6] Brewis, I.A., Turner, A.J., Hooper, N.M.: Activation of the glycosyl-phosphatidylinositol-anchored membrane dipeptidase upon release from pig kidney membranes by phospholipase c. Biochem. J. **303**(2) (1994) 633–638

[7] Stryer, L.: Biochemistry. W.H. Freeman and Company, New York (1988)

[8] David l. Nelson, M.M.C.: Lehninger Principles of Biochemistry,4th ed. W.H. Freeman and Company, New York (2004)

[9] Simons, K., Vaz, W.L.: Model systems, lipid rafts, and cell membranes1. Annual Review of Biophysics and Biomolecular Structure **33**(1) (2004) 269–295

[10] Rajendran, L., Simons, K.: Lipid rafts and membrane dynamics. Journal of Cell Science **118**(6) (2005) 1099–1102

[11] Eyster, K.M.: The membrane and lipids as integral participants in signal transduction: lipid signal transduction for the non-lipid biochemist. Advances in Physiology Education **31**(1) (2007) 5–16

[12] Weidong Zheng, Zhenya Li, K.S., Crooke, E.: Mutations in dnaa protein suppress the growth arrest of acidic phospholipid-deficient escherichia coli cells. The EMBO Journal **20** (2001) 11164–1172

[13] Esposti, M.D.: Lipids, cardiolipin and apoptosis: a greasy licence to kill. Cell Death & Differentiation **9**(3) (2002) 234

[14] McLaughlin, S., Wang, J., Gambhir, A., Murray, D.: Pip2 and proteins: Interactions, organization, and information flow. Annual Review of Biophysics and Biomolecular Structure **31**(1) (2002) 151–175

[15] Wang, X., Devaiah, S.P., Zhang, W., Welti, R.: Signaling functions of phosphatidic acid. Progress in Lipid Research **45**(3) (2006) 250 – 278

[16] KARNOVSKY, M., KLEINFELD, A., HOOVER, R., DAWIDOWICZ, E., MCINTYRE, D., SALZMAN, E., KLAUSNER, R.: Lipid domains in membranes. ANNALS OF THE NEW YORK ACADEMY OF SCIENCES **401**(DEC) (1982) 61–75

[17] Simons, K., Ikonen, E.: Functional rafts in cell membranes. Nature **387**(6633) (1997) 569–572 10.1038/42408.

[18] Pike, L.J.: Rafts defined: a report on the Keystone Symposium on Lipid Rafts and Cell Function. JOURNAL OF LIPID RESEARCH **47**(7) (JUL 2006) 1597–1598

[19] Schmitz, G., Grandl, M.: Update on lipid membrane microdomains. CURRENT OPINION IN CLINICAL NUTRITION AND METABOLIC CARE **11**(2) (MAR 2008) 106–112

[20] Morrow, I.C., Parton, R.G.: Flotillins and the phb domain protein family: Rafts, worms and anaesthetics. Traffic **6**(9) (2005) 725–740

[21] Wang, Y.H., Collins, A., Guo, L., Smith-Dupont, K.B., Gai, F., Svitkina, T., Janmey, P.A.: Divalent cation-induced cluster formation by polyphosphoinositides in model membranes. Journal of American Chemical Society **134** (2012) 3387–3395

[22] van den Bogaart, G., Meyenberg, K., Risselada, H.J., Amin, H., Willig, K.I., Hubrich, B.E., Dier, M., Hell, S.W., Grubmueller, H., Diederichsen, U., Jahn, R.: Membrane protein sequestering by ionic protein-lipid interactions. NATURE **479**(7374) (NOV 24 2011) 552–555

[23] Wang, J., Gambhir, A., Hangyas-Mihalyne, G., Murray, D., Golebiewska, U., McLaughlin, S.: Lateral sequestration of phosphatidylinositol 4,5-bisphosphate by the basic effector domain of myristoylated alanine-rich c kinase substrate is due to nonspecific electrostatic interactions. J Biol Chem **277** (2002) 34401

[24] Gambhir, A., Hangys-Mihlyn, G., Zaitseva, I., Cafiso, D.S., Wang, J., Murray, D., Pentyala, S.N., Smith, S.O., McLaughlin, S.: Electrostatic sequestration of {PIP2} on phospholipid membranes by basic/aromatic regions of proteins. Biophysical Journal **86**(4) (2004) 2188 – 2207

[25] Mbamala, E.C., Ben-Shaul, A., May, S.: Domain formation induced by the adsorption of charged proteins on mixed lipid membranes. Biophysical Journal **88**(3) (2006) 1702–1714

[26] Heo, W.D., Inoue, T., Park, W.S., Kim, M.L., Park, B.O., Wandless, T.J., Meyer, T.: Pi(3,4,5)p-3 and pi(4,5)p-2 lipids target proteins with polybasic clusters to the plasma membrane. Science **314** (2006) 1458–1461

[27] Laux, T., Fukami, K., Thelen, M., Golub, T., Frey, D., Caroni, P.: Gap43, marcks, and cap23 modulate pi(4,5)p2 at plasmalemmal rafts, and regulate cell cortex actin dynamics through a common mechanism. The Journal of Cell Biology **149** (2000) 1455–1472

[28] McLaughlin, S., Murray, D.: Plasma membrane phosphoinositide organization by protein electrostatics. Nature **438**(7068) (December 2005) 605–611

[29] Mbamala, E.C., Fahr, A., May, S.: Electrostatic model for mixed cationic-zwitterionic lipid bilayers. Langmuir **22**(11) (2006) 5129–5136 PMID: 16700604.

[30] Lorenz, C.D., Faraudo, J., Travesset, A.: Hydrogen bonding and binding of polybasic residues with negatively charged mixed lipid monolayers. Langmuir **24**(5) (2008) 1654–1658

[31] Duan, X., Li, Y., Zhang, R., Shi, T., An, L., Huang, Q.: Regulation of anionic lipids in binary membrane upon the adsorption of polyelectrolyte: A monte carlo simulation. AIP Advances **3**(6) (2013)

[32] Levental, I., Christian, D.A., Wang, Y.H., Madara, J.J., Discher, D.E., Janmey, P.A.: Calcium-dependent lateral organization in phosphatidylinositol 4,5-bisphosphate (pip2)-and cholesterol-containing monolayers. Biochemistry **48**(34) (2009) 8241–8248

[33] Sarmento, M.J., Coutinho, A., Fedorov, A., Prieto, M., Fernandes, F.: Ca2+ induces pi(4,5)p2 clusters on lipid bilayers at physiological pi(4,5)p2 and ca2+ concentrations. Biochimica et Biophysica Acta (BBA) - Biomembranes **1838**(3) (2014) 822 – 830

[34] Bedzyk, M., Bommarito, G., Caffrey, M., Penner, T.: Diffuse-double layer at a membrane-aqueous interface measured with x-ray standing waves. Science **248**(4951) (1990) 52–56

[35] Bu, W., Vaknin, D., Travesset, A.: How accurate is poisson boltzmann theory for monovalent ions near highly charged interfaces? Langmuir **22**(13) (2006) 5673–5681 PMID: 16768493.

[36] Winiski, A.P., McLaughlin, A.C., McDaniel, R.V., Eisenberg, M., McLaughlin, S.: An experimental test of the discreteness-of-charge effect in positive and negative lipid bilayers. Biochemistry **25**(25) (1986) 8206–8214

[37] Tanizaki, S., Feig, M.: A generalized born formalism for heterogeneous dielectric environments: Application to the implicit modeling of biological membranes. **122**(12) (2005) 124706

[38] Marrink, S.J., Risselada, H.J., Yefimov, S., Tieleman, D.P., de Vries, A.H.: The martini force field: A coarse grained model for biomolecular simulations. The Journal of Physical Chemistry B **111**(27) (2007) 7812–7824 PMID: 17569554.

[39] Wang, Z.J., Deserno, M.: A systematically coarse-grained solvent-free model for quantitative phospholipid bilayer simulations. The Journal of Physical Chemistry B **114**(34) (2010) 11207–11220

[40] Noguchi, H., Takasu, M.: Self-assembly of amphiphiles into vesicles: A brownian dynamics simulation. Phys. Rev. E **64** (Sep 2001) 041913

[41] Lyklema, J.: Fundamentals of Interface and Colloidal Science. Volume 1-2. Academic Press, New York (1991)

[42] Fennell Evans, D., Wennerstrom, H.: The Colloidal Domain, Where Physics, Chemistry, and Biology meet. Wiley-VCH (1999)

[43] Bu, W., Vaknin, D., Travesset, A.: Monovalent counterion distributions at highly charged water interfaces: Proton-transfer and poisson-boltzmann theory. Physical Review E (Statistical, Nonlinear, and Soft Matter Physics) **72**(6) (2005) 060501–4

[44] Grosberg, A.Y., Nguyen, T.T., Shklovskii, B.I.: Colloquium: The physics of charge inversion in chemical and biological systems. Rev. Mod. Phys. **74**(2) (April 2002) 329–

[45] Boroudjerdi, H., Kim, Y.W., Naji, A., Netz, R.R., Schlagberger, X., Serr, A.: Statics and dynamics of strongly charged soft matter. Physics Reports **416**(3-4) (2005) 129–199

[46] Lyklema, J.: Overcharging, charge reversal: Chemistry or physics? Colloids and Surfaces A: Physicochemical and Engineering Aspects **291**(1-3) (2006) 3 – 12 Special Issue in Honor of Professor Jarl B. Rosenholm on the Occasion of his 60th Birthday.

[47] Messina, R.: Electrostatics in soft matter. Journal of Physics: Condensed Matter **21**(11) (2009) 113102

[48] Kjellander, R.: Intricate coupling between ion-ion and ion-surface correlations in double layers as illustrated by charge inversion combined effects of strong coulomb correlations and excluded volume. Journal of Physics: Condensed Matter **21**(42) (2009) 424101

[49] Kaganer, V.M., Mohwald, H., Dutta, P.: Structure and phase transitions in langmuir monolayers. Rev. Mod. Phys. **71**(3) (April 1999) 779–819

[50] McLaughlin, S.: The electrostatic properties of membranes. Annual Review of Biophysics and Biophysical Chemistry **18**(1) (1989) 113–136

[51] Bu, W., Flores, K., Pleasants, J., Vaknin, D.: Preferential affinity of calcium ions to charged phosphatidic acid surface from a mixed calcium/barium solution: X-ray reflectivity and fluorescence studies. Langmuir **25**(2) (2009) 1068–1073

[52] Nelson, A., McQuarrie, D.: The effect of discrete charges on the electrical properties of a membrane. i. Journal of Theoretical Biology **55**(1) (1975) 13 – 27

[53] Moreira, A.G., Netz, R.R.: Counterions at charge-modulated substrates. EPL (Europhysics Letters) **57**(6) (2002) 911

[54] Lukatsky, D.B., Safran, S.A.: Universal reduction of pressure between charged surfaces by long-wavelength surface charge modulation. EPL (Europhysics Letters) **60**(4) (2002) 629

[55] Travesset, A.: Salty solutions near a charged modulated interface. Eur. Phys. J E **17** (2005) 435–446

[56] Henle, M., Santangelo, C., Patel, D., Pincus, P.: Distribution of counterions near discretely charged planes and rods. Europhys. Lett. **66** (2004) 284

[57] Madurga, S., Martín-Molina, A., Vilaseca, E., Mas, F., Quesada-Pérez, M.: Effect of the surface charge discretization on electric double layers: A monte carlo simulation study. The Journal of Chemical Physics **126**(23) (2007) 234703

[58] Calero, C., Faraudo, J.: The interaction between electrolyte and surfaces decorated with charged groups: A molecular dynamics simulation study. The Journal of Chemical Physics **132**(2) (2010) 024704

[59] Travesset, A., Vaknin, D.: Bjerrum pairing correlations at charged interfaces. Europhys. Lett. **74** (2006) 181–187

[60] Faraudo, J., Travesset, A.: The many origins of charge inversion in electrolyte solutions: Effects of discrete interfacial charges. Journal of Physical Chemistry C **111**(2) (2007) 987 1932-7447.

[61] Outhwaite, C.: Modified poisson-boltzmann equation in electric double layer theory based on the bogoliubov-born-green-yvon integral equations. J. C. S. Faraday **74** (1978) 1214

[62] Outhwaite, C., Bhuiyan, L., Levine, S.: Theory of the electric double layer using a modified poisson-boltzmann equation. J.C.S. Faraday II **76** (1980) 1388

[63] Kjellander, R., Marcelja, S.: Inhomogeneus coulomb fluids with image interactions between planar surfaces i. The Journal of Chemical Physics. **82** (1984) 2122

[64] Kjellander, R., Marcelja, S.: Double-layer interaction in the primitive model and the corresponding poisson-boltzmann description. The Journal of Chemical Physics **90**(7) (1986) 1230–1232

[65] Kjellander, R., Marcelja, S.: Inhomogeneus coulomb fluids with image interactions between planar surfaces iii: Distribution functions. The Journal of Chemical Physics **82** (1988) 7138

[66] Totsuji, H.: Numerical experiment on two-dimensional electron liquids. thermodynamic properties and onset of short-range order. Phys. Rev. A **17**(1) (January 1978) 399–406

[67] Martin-Molina, A., Maroto-Centeno, J., Hidalgo-Alvarez, R., Quesada-Pérez, M.: Testing one component plasma models on colloidal overcharging phenomena. The Journal of Chemical Physics **125**(14) (2006) 144906 journal article.

[68] Trulsson, M., Jönsson, B., Akesson, T., Forsman, J., Labbez, C.: Repulsion between oppositely charged surfaces in multivalent electrolytes. Physical Review Letters **97**(6) (2006) 068302

[69] Moreira, A., Netz, R.: Strong-coupling theory for counter-ion distributions. EPL (Europhysics Letters) **52** (2001) 705

[70] Wang, W., Park, R.Y., Travesset, A., Vaknin, D.: Ion-specific induced charges at aqueous soft interfaces. Phys. Rev. Lett. **106**(5) (February 2011) 056102–

[71] Faraudo, J., Bresme, F.: Anomalous dielectric behavior of water in ionic newton black films. Phys. Rev. Lett. **92** (2004) 236102

[72] Ninham, B.W., Parsegian, V.A.: Electrostatic potential between surfaces bearing ionizable groups in ionic equilibrium with physiologic saline solution. Journal of Theoretical Biology **31**(3) (1971) 405 – 428

[73] Nikas, Y., Puvvada, S., Blankschtein, D.: Surface tensions of aqueous nonionic surfactant mixtures. Langmuir **8** (1992) 2680

[74] Bloch, J., Yun, W.: Condensation of monovalent and divalent metal ions on a langmuir monolayer. Phys. Rev. A. **41** (1990) 844

[75] Kjellander, R., Mitchell, D.J.: Dressed ion theory for electrolyte solutions: A debye-hckel like reformulation of the exact theory for the primitive model. The Journal of Chemical Physics **101**(1) (1994) 603–626 journal article.

[76] Attard, P.: Asymptotic analysis of primitive model electrolytes and the electrical double layer. Phys. Rev. E **48**(5) (November 1993) 3604–3621

[77] Lozada, C.M.: Fundamentals of Inhomogeneus Fluids. Dekker, New York (1992)

[78] Healy, T.W., White, L.R.: Ionizable surface group models of aqueous interfaces. Advances in Colloid and Interface Science **9**(4) (1978) 303 – 345

[79] Levin, Y.: Electrostatic correlations: from plasma to biology. Reports on Progress in Physics **65**(11) (2002) 1577

[80] Lyklema, J.: Quest for ion-ion correlations in electric double layers and overcharging phenomena. Advances in Colloid and Interface Science **147-148** (2009) 205 – 213 Colloids, polymers and surfactants.Special Issue in honour of Brian Vincent.

[81] Besteman, K., Zevenbergen, M., Heering, H., Lemay, S.: Direct observation by multivalent ions as a universal electrostatic phenomena. Phys. Rev. Lett. **90** (2004) 178102

[82] Besteman, K., Zevenbergen, M.A.G., Lemay, S.G.: Charge inversion by multivalent ions: Dependence on dielectric constant and surface-charge density. Phys. Rev. E **72** (Dec 2005) 061501

[83] van der Heyden, F.H.J., Stein, D., Besteman, K., Lemay, S.G., Dekker, C.: Charge inversion at high ionic strength studied by streaming currents. Phys. Rev. Lett. **96** (Jun 2006) 224502

[84] Di Paolo, G., De Camilli, P.: Phosphoinositides in cell regulation and membrane dynamics. Nature **443**(7112) (October 2006) 651–657

[85] Labbez, C., Jonsson, B., Skarba, M., Borkovec, M.: Ionion correlation and charge reversal at titrating solid interfaces. Langmuir **25**(13) (2009) 7209–7213 PMID: 19514750.

[86] Martin-Molina, A., Maroto-Centeno, J.A., Hidalgo-Alvarez, R., Quesada-Perez, M.: Charge reversal in real colloids: Experiments, theory and simulations. Colloids and Surfaces A: Physicochemical and Engineering Aspects **319**(1-3) (2008) 103 – 108 Colloids and Interfaces for Nanoscience and Nanotechnology Selected papers from the 20th European Colloid and Interface Society (ECIS) Conference jointly organized with 18th European Chemistry at Interfaces Conference (ECIC) held on 17-22 September, 2006 in Budapest, Hungary.

[87] Israels, R., Leermakers, F.A.M., Fleer, G.J., Zhulina, E.B.: Charged polymeric brushes: Structure and scaling relations. Macromolecules **27**(12) (1994) 3249–3261

[88] Nap, R., Gong, P., Szleifer, I.: Weak polyelectrolytes tethered to surfaces: Effect of geometry, acidbase equilibrium and electrical permittivity. Journal of Polymer Science Part B: Polymer Physics **44**(18) (2006) 2638–2662

[89] Gong, P., Wu, T., Genzer, J., Szleifer, I.: Behavior of surface-anchored poly(acrylic acid) brushes with grafting density gradients on solid substrates: 2. theory. Macromolecules **40**(24) (2007) 8765–8773

[90] Hehmeyer, O.J., Arya, G., Panagiotopoulos, A.Z., Szleifer, I.: Monte carlo simulation and molecular theory of tethered polyelectrolytes. The Journal of Chemical Physics **126**(24) (2007) 244902 journal article.

[91] McLaughlin, S., Mulrine, N., Gresalfi, T., Vaio, G., McLaughlin, A.: Adsorption of divalent cations to bilayer membranes containing phosphatidylserine. The Journal of General Physiology **77**(4) (1981) 445–473

[92] Tsui, F., Ojcius, D., Hubbell, W.: The intrinsic pka values for phosphatidylserine and phosphatidylethanolamine in phosphatidylcholine host bilayers. Biophysical Journal **49**(2) (1986) 459 – 468

[93] Huster, D., Arnold, K., Klaus, G.: Strength of ca2+ binding to retinal lipid membranes: Consequences for lipid organization. Biophysical Journal **78**(6) (2000) 3011–3018

[94] Levental, I., Janmey, P., Cbers, A.: Electrostatic contribution to the surface pressure of charged monolayers containing polyphosphoinositides (2008)

[95] Pandit, S.A., Berkowitz, M.L.: Molecular dynamics simulation of dipalmitoylphosphatidylserine bilayer with na+ counterions (2002)

[96] Yi, M., Nymeyer, H., Zhou, H.X.: Test of the gouy-chapman theory for a charged lipid membrane against explicit-solvent molecular dynamics simulations. Phys. Rev. Lett. **101** (Jul 2008) 038103

[97] Vaknin, D., Krugger, P., Loesche, M.: Anomalous x-ray reflectivity characterization of ion distribution at biomimetic membranes. Phys. Rev. Lett. **90**(17) (May 2003) 178102–178105

[98] Pittler, J., Bu, W., Vaknin, D., Travesset, A., McGillivray, D.J., Lösche, M.: Charge inversion at minute electrolyte concentrations. Phys. Rev. Lett. **97** (Jul 2006) 046102

[99] Seok, S., Kim, T.J., Hwang, S.Y., Kim, Y.D., Vaknin, D., Kim, D.: Imaging of collapsed fatty acid films at airwater interfaces. Langmuir **25**(16) (2009) 9262–9269 PMID: 19627076.

[100] Martell, A.E., Smith, R.M.: Critical Stability Constants. Volume 2-3. Plenum, New York (1977)

[101] Robinson, R., Stokes, R.: Electrolyte Solutions. Butterworth & Co. (2002)

[102] Loverde, S.M., de la Cruz, M.O.: Asymmetric charge patterning on surfaces and interfaces: Formation of hexagonal domains. The Journal of Chemical Physics **127**(16) (2007) 164707 journal article.

[103] Grzybowski, A., Gwóźdź, E., Bródka, A.: Ewald summation of electrostatic interactions in molecular dynamics of a three-dimensional system with periodicity in two directions. Phys. Rev. B **61** (Mar 2000) 6706–6712

[104] Levin, Y., Fisher, M.E.: Criticality in the hard-sphere ionic fluid. Physica A: Statistical and Theoretical Physics **225**(2) (1996) 164 – 220

[105] Pianegonda, S., Barbosa, M.C., Levin, Y.: Charge reversal of colloidal particles. EPL (Europhysics Letters) **71**(5) (2005) 831

[106] González-Amezcua, O., Hernández-Contreras, M., Pincus, P.: Electrostatic correlation force of discretely charged membranes. Phys. Rev. E **64** (Sep 2001) 041603–041607

[107] Khan, M.O., Petris, S., Chan, D.Y.C.: The influence of discrete surface charges on the force between charged surfaces. The Journal of Chemical Physics **122**(10) (2005) 104705–104710

[108] Plischke, M., Henderson, D.: The primitive model of the electric double layer: Nonsymmetric electrolytes. The Journal of Chemical Physics **90**(10) (1989) 5738–5741

[109] Plimpton, S.: Fast parallel algorithms for short-range molecular dynamics. Journal of Computational Physics **117**(1) (1995) 1–19

[110] Samaj, L., Trizac, E.: Ground state of classical bilayer wigner crystals. EPL (Europhysics Letters) **98**(3) (2012) 36004

[111] Travesset, A., Vangaveti, S.: Electrostatic correlations at the stern layer: Physics or chemistry?. Journal of Chemical Physics **131**(18) (2009) 185102

[112] Christa T, T.M.: Molecular, cellular, and physiological responses to phosphatidic acid formation in plants. Journal of Experimental Botany **175** (2011) 1–13

[113] Liu, Y., Su, Y., Wang, X.: Phosphatidic acid-mediated signaling. In Capelluto, D.G., ed.: Lipid-mediated Protein Signaling. Volume 991 of Advances in Experimental Medicine and Biology. Springer Netherlands (2013) 159–176

[114] Vance, J.E., Tasseva, G.: Formation and function of phosphatidylserine and phosphatidylethanolamine in mammalian cells. Biochimica et Biophysica Acta (BBA) - Molecular and Cell Biology of Lipids **1831**(3) (2013) 543 – 554

[115] Berridge MJ, I.R.: Inositol phosphates and cell signalling. Nature **341** (1989) 197–205

[116] Suh, B.C., Hille, B.: Regulation of ion channels by phosphatidylinositol 4,5-bisphosphate. Current Opinion in Neurobiology **15**(3) (2005) 370 – 378

[117] Epand, R.M.: Proteins and cholesterol-rich domains. Biochimica et Biophysica Acta (BBA) - Biomembranes **1778** (2008) 1576 – 1582

[118] Vangaveti, S., Travesset, A.: General solution to the electric double layer with discrete interfacial charges. The Journal of Chemical Physics **137**(6) (2012) 30–40

[119] Ellenbroek, W.G., Wang, Y.H., Christian, D.A., Discher, D.E., Janmey, P.A., Liu, A.J.: Divalent cation-dependent formation of electrostatic pip2 clusters in lipid monolayers. Biophys J **101**(9) (November 2011) 2178–2184

[120] John JH Shin, C.J.L.: Putting the ph into phosphatidic acid signaling. BMC Biology **9** (December 2011) 1912–1925

[121] Toner, M., Vaio, G., McLaughlin, A., McLaughlin, S.: Adsorption of cations to phosphatidylinositol 4,5-bisphosphate. Biochemistry **27**(19) (1988) 7435–7443

[122] Martinez, L., Andrade, R., Birgin, E.G., Martinez, J.M.: Packmol: A package for building initial configurations for molecular dynamics simulations. Journal of Computational Chemistry **30**(13) (2009) 2157–2164

[123] Boettcher, J.M., Davis-Harrison, R.L., Clay, M.C., Nieuwkoop, A.J., Ohkubo, Y.Z., Tajkhorshid, E., Morrissey, J.H., Rienstra, C.M.: Atomic view of calcium-induced clustering of phosphatidylserine in mixed lipid bilayers. Biochemistry **50**(12) (2011) 2264–2273

[124] Slochower, D.R., Huwe, P.J., Radhakrishnan, R., Janmey, P.A.: Quantum and all-atom molecular dynamics simulations of protonation and divalent ion binding to phosphatidylinositol 4,5-bisphosphate (pip2). The Journal of Physical Chemistry B **117**(28) (2013) 8322–8329

[125] Eisenberg, M., Gresalfi, T., Riccio, T., McLaughlin, S.: Adsorption of monovalent cations to bilayer membranes containing negative phospholipids. Biochemistry **18**(23) (1979) 5213–5223

[126] Yaqoob, P., Shaikh, S.R.: The nutritional and clinical significance of lipid rafts. CURRENT OPINION IN CLINICAL NUTRITION AND METABOLIC CARE **13**(2) (MAR 2010) 156–166

[127] Martin, T.F.: Pi(4,5)p2 regulation of surface membrane traffic. Current Opinion in Cell Biology **13**(4) (2001) 493 – 499